Cape Peninsula University of Technology

Design optimisation of pillar-mounted sun tracking solar-water purifiers for large households

by

JEREMIA NDESHIPANDA PETER

Thesis submitted in fulfilment of the requirements for the degree

Master of Engineering: Mechanical Engineering

in the Faculty of Engineering

at the Cape Peninsula University of Technology

Supervisor: Dr K.E Kanyarusoke

Bellville

September 2019

DECLARATION

I, Jeremia Ndeshipanda Peter, declare that the contents of this dissertation/thesis represent my own unaided work, and that the dissertation/thesis has not previously been submitted for academic examination towards any qualification. Furthermore, it represents my own opinions and not necessarily those of the Cape Peninsula University of Technology.

01/09/19

Signed **Date**

ABSTRACT

This study was conducted to design a pillar-mounted sun tracker for solar-water purifiers for large households. The main reason for doing this research was to reduce the ground space taken up by solar-water purifiers when used by large households and increase yields. No previous work has been done by researchers to address this problem. Moreover, most people in sub-Saharan Africa and in other developing countries do not have access to clean water. There is need for a solar water purification method to be used by households to purify water for human consumption. Research on the following four different types of solar water purification methods was conducted: Solar-water disinfection, Solar-water pasteurization, Solar-water distillation and Solar-water reverse osmosis. At the university, research work has been done by two students on water purifiers by distillation for small households in rural areas. Their work focused on ground-mounted single basin type design solar water purifiers units that do not track the sun. Larger families would need multiple units of the type developed by these students. These would occupy much space in the compounds, and therefore necessitate to look upward without having to compromise performance or effort to refill the purifiers., Additionally, the effectiveness of the purifiers is to be improved increasing its yields by allowing them to rotate to track the sun since they will all be mounted off the ground. A single axis pillar sun tracker was designed, constructed and tested at the roof top of the Mechanical Engineering at the Cape Peninsula University of Technology. The tracking system consists of a compound gearbox and a stepper motor driven by an Arduino Uno powered by 2 DC 12V batteries. The stepper motor was programmed to rotate intermittently at 15 degrees per hour in the East-West direction. Four Engohang-Kanyarusoke solar water purifier's were mounted on the tracking system and another unit was ground-mounted. Experiments were performed from the 29th of May 2018 to the 07th of June 2018 for 10 connective days at Bellville; Cape Town; South Africa. An area of 30 m^2 was saved by mounting four purifiers on the pillar this could however go up to 35 m^2 if the full potential of the designed pillar is utilised. The pillar-mounted tracking solar water purifies out-performed the ground mounted still by about 31% in terms of daily water yield.

ACKNOWLEDGEMENTS

I wish to thank and express my gratitude to:

- The almighty God, for giving me the strength, power and the intelligence to undertake this masters study.
- My supervisor Dr Kant Kanyarusoke for his encouragement, excellent guidance and support. This thesis would not have been possible without his input and constant support.
- My parents William Peter, Hileni Nghimwena for their love, support, for their encouragement for me to study up to this level and complete my masters.

The financial assistance of the National Research Foundation towards this research is acknowledged. Opinions expressed in this thesis and the conclusions arrived at, are those of the author, and are not necessarily to be attributed to the National Research Foundation.

DEDICATION

I dedicate this thesis to my African brothers and sisters.

TABLE OF CONTENTS

Contents **Page**

LIST OF FIGURES

Figures **Page**

LIST OF TABLES

Tables **Page**

GLOSSARY

Terms/Acronyms/Abbreviations	Definition/Explanation
A	Surface area
RO	Reverse osmosis
SOPAS	Solar water pasteurization
CPC	Parabolic collector
°C	Degrees Celsius
UV	Ultraviolet radiation
PET	Polyethene terephthalate
SODIS	Solar water disinfection
β	Slope angle
i	Incidence angle of the sun
Z_θ	Zenith angle
α_{noon}	Solar angle at noon
L	Latitude
I_{oa}	Actual exterrastrial radiation
$t_{day:}$	Time of the day
CPUT	Cape Peninsula University of Technology
o	Degrees
µ	Micro
m/s	Metres per second
m^2	Square meter
η	Efficiency
W/m^2	Watts per square metres

CHAPTER ONE
INTRODUCTION

1.1 PROBLEM STATEMENT

Solar water purification is a natural way of making water safe for human consupamtion that has been used for many years. A great deal of research has been done on the different types of solar water purification methods in the previous years (Zhang et al., 2018a). The different types of solar water purification technologies that had been studied over the previous years are; solar water disinfection, solar water reverse osmosis, solar water pasteurization and solar water distillation.

Although research has been conducted on different types of solar water purification methods, a large number of households in developing countries still do not have sufficient drinking water suitable for human consumption. Often, the water that is available is contaminated with microbes and chemicals, making it unsafe for human consumption. Furthermore, the past research conducted by scholars and two students at CPUT did not address the challenge of space taken up by the solar water purification systems in large households. It only addressed the water shortage problem in small households. The major concern of this research is to address the space problem. A pillar is designed for multiple stills mounting to conserve space. Additionally, it enables the purifiers to track the sun so that more distilled water is produced than would have been the case if they were ground mounted. Figure 1.1 shows four typical solar water distillation purifiers, each taking 2 m^2 of ground area which is able to produce 5 Litres that can be mounted on the pillar.

Figure 1.1 Solar water purifiers
(Kanyarusoke, 2018)

1.2 BACKGROUND TO THE RESEARCH PROBLEM

Many families, especially in sub-Saharan Africa countries and developing countries, do not have access to clean water that can be used for drinking purposes. The water that is available is often not purified and it contains salt, metals, waterborne bacteria, viruses and other organisms. The most affected areas are rural areas which often get their water from boreholes, rivers, lakes, wells, streams, etc. The contaminated water that comes from these sources, when consumed without being purified, causes diseases characterised by vomiting, diarrhoea, headaches, stomach cramps, etc. This is a greater risk to people who have severely weak immune systems according to (Manchanda & Kumar, 2018; DH et al., 2016).

The water might be available in some areas from the taps but it is often not pure and it needs purification. The tap water contaminations are caused by water pipes which burst especially when not noticed and fixed in time. According to File, (2018) water contaminants in taps can also be caused by water outages. When the water pipes are empty there is always a high risk of soil contaminating the water by entering the pipes. He further stated that contamination can also result when source dam water levels are running low since the water at the bottom is of poor quality, and is difficult to treat.

These water problems force people to buy bottled mineral water from shops which in the long run, is not economical. Moreover, most African communities are poor. So, they cannot keep on buying water and some can not afford it. Furthermore, the people also travel long distances to access clean safe water for drinking. This is time-consuming.

A more sustainable solution is the use of solar energy to purify the water. Solar energy is an abundant, free resource, especially in Africa where the sun shines 365 days a year and can easily be used to purify large volumes of water. Currently, solar-purification systems would have to be very large and to occupy a lot of space, especially in large households where more then one solar water purifier unit is needed. This is the main concern of this research: to provide a solution to the large space occupied in compounds by the stills.

1.3 OBJECTIVES

The main objective of this research is to increase the distilled water yield of solar stills per unit ground area in large homesteads. This is done by designing and optimising a pillar-mounted sun tracking solar-water purifier system.
Accordingly, the two sub-objectives are:

a) Minimize the area ground space used per purifier.
b) Increase daily production much beyond the Engohang-Kanyarusoke values to cater for large homesteads.

1.4 DELIMITATION OF THE RESEARCH

This thesis will be delimitated to the following areas;

- The study will consider only domestic home applications.
- No new designs of solar water purifiers units will be used. Instead, existing Kanyarusoke-Engohang designs will be used, since they have already been tested in smaller homes on the continent.
- Filling of the stills will be manual, since they are meant to be used in areas with limited supply of water and with limited technical skills.

1.5 THESIS SCOPE

The remainder of the thesis is organised as follows:
Chapter two presents a literature review, showing the lack of water and looking at other different types of solar water purification methods. It also looks at solar tracking systems.

Chapter three considers different designs for a solar tracking system to be used in the new system. Structural 3D drawings, geometry, material selections, Autodesk Fusion360 simulation and the pillar design will be presented. The different types of drive systems are also shown in this section. The chapter further presents the construction of the tracking system and the different steps that were followed to build the structure and the electro-mechanism of the system.

Chapter four presents the experimentation and the methodology of determining space saving and yield improvements. The penultimate chapter gives test results and their discussion. The thesis concludes in chapter six with recommendations for further improvements.

CHAPTER TWO
LITERATURE REVIEW

This literature review looks at the lack of potable water problems especially in the sub-Saharan African countries. Then, it surveys the four most common types of solar water purification methods and their limitations. These are: Solar water disinfection, Solar water pasteurization, Solar water distillation and Solar water reverse osmosis. Solar tracking systems are also reviewed in fair detail because this is the main focus of this study.

2.1 LACK OF CLEAN WATER

Developing countries, especially the African countries, are economically poor. In them, there is a high percentage of people who do not have access to safe clean water for drinking. According to Water (2017), an estimate of 1.1 billion people do not have access to safe managed clean water for drinking. Over half of these (58%) live in sub-Saharan Africa. The available water in these countries is from boreholes, lakes and rivers and it is contaminated. According to Orisaleye et al., (2018) even the protected sources of water in developing countries in urban areas can also be contaminated with the microbiological water contaminants. This makes the water unsafe for drinking. Even areas with access to tap water can suffer the same fate because, the water is often not properly treated. It is contaminated by the industrial wastewater and municipal discharges (Zhang et al., 2018a).

A survey was carried out by the World Health Organization (WHO) in 2017 to find statistics of how many people had safe clean water for drinking. The survey found that far too many people in the world had experienced health problems that were caused by drinking unsafe water (Water, 2017). This survey also found that people in developing countries travel long distances just to get access to safe water for drinking. The figure on the next page shows the percentage of people that had access to clean fresh drinking water in 2017. It is clear that sub-Saharan African countries had a very low percentage of people with access to safe clean water.

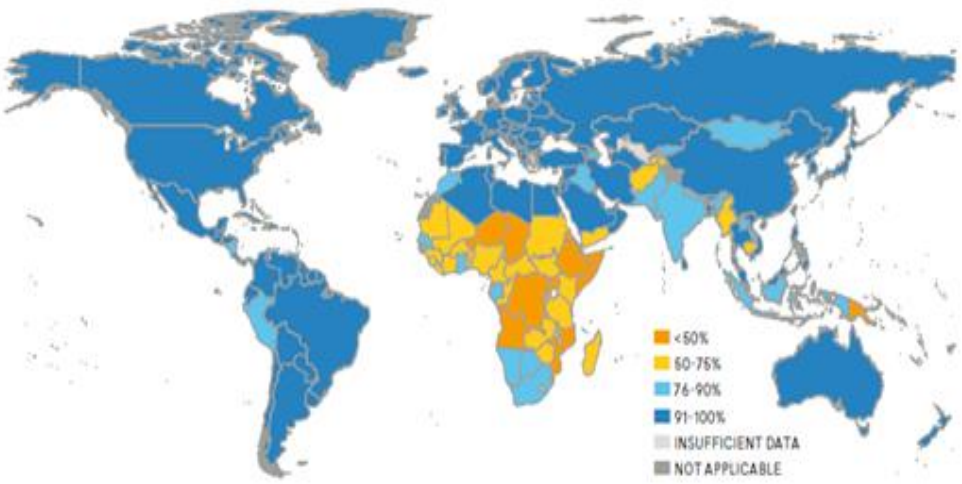

Figure 2.1: Population percentage with basic drinking water
(Water, 2017)

The contaminated water contains waterborne diseases which cause about 46% of 50200 deaths every year. This results from diarrheal and hepatitis E (Reyneke et al., 2018). The numerous contaminants that are found in the water are chemical and microbial in nature. Chemical contaminants are partly caused by the nitrogen and sulphur oxides, which are released into the atmosphere. These dissolve in rain water, forming what is commonly called 'acid rain'. The gases are caused by burning firewood, fossil fuels in automobiles, power plants and in mining and metallurgical industries. The problem in developing countries is that there is no or very little control over these processes, and therefore large volumes of the gases are released into the atmosphere. Figure 2.2 shows how acid rain is formed.

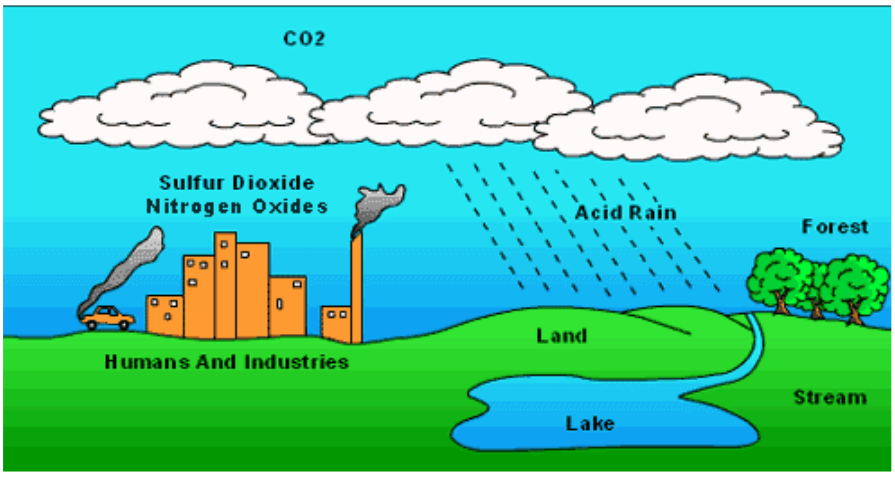

Figure 2.2: Acid rain formation
(Mustafa, 2015)

2.2 SOLAR WATER PURIFICATION METHODS

2.2.1 Solar water disinfection

Solar water disinfection (SODIS) is an ancient technology that is used for water purification. This solar water technique was first studied in 1980 by researchers (Helali et al., 2013). It is the simplest technique of water purification and is a low form of technology of making the water pure by using the sun's UV radiation. It consists of clear plastic polyethylene terephthalate (PET) bottles that are exposed to the direct sunlight for at least 6 hours during the day. This destroys the bacteria in the water (Mac Mahon & Gill, 2018). According to Samrath (2011), "PET bottles are considered to be best for SODIS as they contain fewer UV stabilizers". Figure 2.3 shows the schematic of the solar water disinfection.

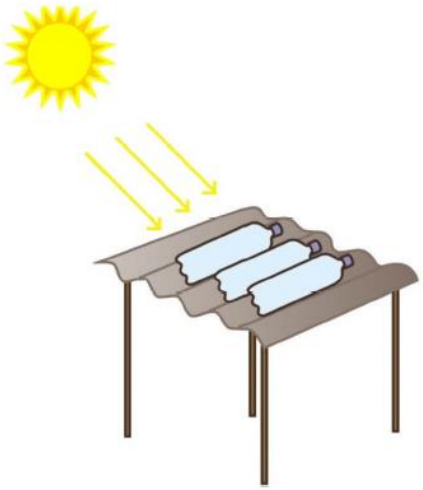

Figure 2.3: Solar water disinfection schematic
(Zhang et al., 2018)

According to Zhang et al., (2018) the SODIS is a suitable method of water purification for developing countries that do not have access to safely managed water supply for drinking but get high amounts of sunlight. They further state that the SODIS has been proved to be effective against waterborne microbial species. SODIS reduces the rate of childhood dysentery and diarrhoea (Zhang et al., 2018b). In addition, this method of water purification is economical in developing countries, especially in poor rural areas.

SODIS has shortcomings. It cannot purify high amounts of water per day. Also, it does not purify water against chemical contaminants. It is only suitable for microbial contaminants. When there is no clear sky with enough sunlight the water takes longer to be purified.

A continuous solar water disinfection system has been developed in some countries. It was built in Kenya's Mutomo District (Mac Mahon & Gill, 2018). It is suitable in places where there is a continuous supply of water, such as on a lake-side or along a river. It could also be used

where there are boreholes, dams and other permanent water source. This system consists of a Concentrated Power Collector (CPC) which reflects sunlight on the bottles that are joined together continuously (Mac Mahon & Gill, 2018). As the sunlight UV radiation reflects on the rector it is directed on the continuous bottles which purify the water. This system is ideal for large communities but it is expensive to set up. It also requires suitable weather conditions to purify a high amount of water. Figure 2.4 shows schematic photograph of such a system.

Figure 2.4: Solar water continuous disinfection
(Mac Mahon & Gill, 2018)

2.2.2 Solar water pasteurization

Solar water pasteurization (SOPAS) is a water purification method process whereby the water is heated to a specific minimum temperature of 65 °C to kill the organisms in the water to make it safe for human consumption (Reyneke et al., 2018). This system consists of a water tank used to store untreated water and connected to the borosilicate glass tubes in which the water passes as it is heated by the sun's UV rays. The bacteria species in the water are killed, and the water is stored in the storage tank of the system. According to Carielo et al., (2017) the flow of the water in the pasteurization system is based on the density difference. Furthermore, the system is also painted black so that it absorbs more radiation and generates more heat to kill the organisms in the water. Figure 2.5 shows the SOPAS system.

Figure 2.5: SOPAS system
(Reyneke et al., 2018)

The solar water pasteurization is a reliable method of water purification and it is considered a suitable method for areas where large volumes of water are required (Reyneke et al., 2016). Reyneke, et al., (2018) state that solar water pasteurization is an effective method of destroying bacteria, viruses and other microbials. The water does not need to boil at 100 °C for the bacteria's to be killed. Solar water pasteurization (SOPAS) is an easy system to install. It operates automatically as the flow is continuous. The user only has to ensure that the storage tank of the contaminated water is full. The main drawback of SOPAS is that a temperature of 65 °C is required for the system to be effective. This is not always possible especially when there is no clear sky. Also, the purification method is not economical for poor communities, as it requires a high investment and maintenance costs. Additionally, the method requires some technical skill and occupies large amounts of space for the tanks and tubes.

2.2.3 Solar water distillation

Solar water distillation is a process used for water purification, very much similar to the natural phenomenon of rain formation (Aybar, 2006). This method of water purification is the most used method (Aybar, 2006). According to Zarzo & Prats (2018), solar distillation has become one of the world's most important water purification method in recent years, especially in places where the water is scarce.

The solar water distillation works on the same principle as the water cycle that is used for the formation of the rain (Shatat et al., 2013). The distillation purification systems are built with a transparent glass where the sun heats the water through the glazing where the solar radiation enters the still. The water in a basin heats up, evaporates, rises and condenses on the glazing.

It then flows downward into a channel which channels the purified water out of the basin into a collecting container outside. According to Shatat et al., (2013), “In a solar still, the temperature difference between the water and glass cover is the driving force of the pure water yield”. As the water surface evaporates the vapour is trapped in the unit where it condenses on the transparent glass, slides down and it’s collected through the channel and it is ready for drinking. In 2015 a single basin solar water purifier unit was developed at CPUT at the mechanical engineering department which was developed. Mbadinga, (2015) carried out experiments where she was measuring the yield of the unit which only produced a small amount of water. More work was further carried out by Engohang in 2018. She tried to improve on Mbadinga’s solar still to increase yields, reduce solar still sizes and weights. Figure 2.6 shows a schematic of the solar water machines designed by Mbadinga and Engohang.

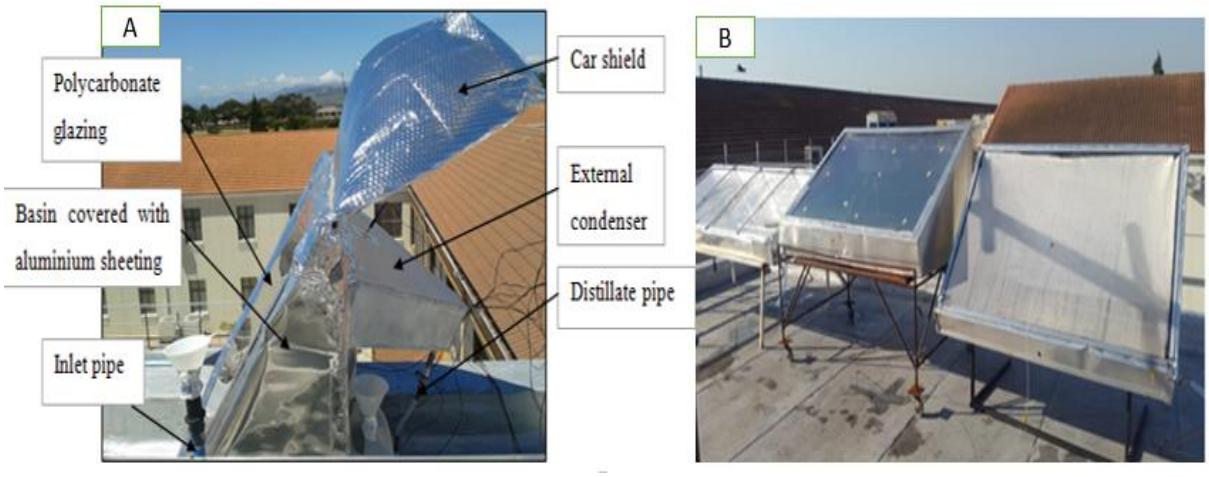

Figure 2.6: Solar water machines schematic (A Mbadinga still, B Engohang-Kanyarusoke stills) (Engohang & Kanyarusoke, 2018)

Solar distillation can purify the water against both chemical and microbiological contaminants. It is also economical for the poor households where there is a need of purification as it requires minimum initial investment cost (Chafidz et al., 2016). Al-harahsheh et al., (2018) also state that a solar water distillation purification unit can be designed from using abundant local materials. However, there are limitations to this purification method in places with tropical rain patterns. For example in the equatorial regions of Uganda, experiments done by Kanyarusoke early 2018 yielded less than the 5 Litres per day in a purifier that was producing that quantity in Cape Town’s summer season. The obtained yields were between 3 and 4 Litres due to cloud cover (Engohang & Kanyarusoke, 2018). To increase the daily yields to the 5 Litre mark it would necessitate increasing glazing and ground area occupied by the stills.

2.2.4 Solar water reverse osmosis

Solar water reverse Osmosis (RO) is a water purification process whereby the water is permeated through a membrane from a concentrated salt solution. Joyce et al., (2001), state that the membrane must be semi-permeable in order for it to reject all kinds of solutes in the water. The solar water RO operates by passing the contaminated water through two filters as is shown in Figure 2.7. Primary water is pre-filtered, and then it is filtered a final time where the water is ready for human consumption. Figure 2.7 shows the RO system.

Figure 2.7: Solar water RO system
(Chafidz et al., 2016)

The solar water RO method of purifying water was proved to be the most reliable, cost-effective and efficient in producing water that is suitable for human consumption (Shaaban & Yahya, 2017). This method of water purification removes all the two types of contamination chemical and microbiological contaminants from the water. The solar water RO method has the major disadvantage of being high energy intensive (Shaaban & Yahya, 2017). It also requires a lot of space for setting up the whole unit. Additionally, a lot of maintenance and a technically trained person are required to keep it in good operating condition. It is neither economical nor technically appropriate for many households.

2.3 SOLAR TRACKING

The first solar tracking system was introduced in 1927 by Finster. This system was only mechanical as it did not consist of electrical parts. It was then improved by Saavedra in 1963 where he used an automatic electronic control unit on the tracking system (Nsengiyumva et al., 2018). Over the years, solar tracking systems have been studied by researchers to find a way on how they can be improved to increase the energy output from the units and if they are feasible.

Solar tracking (ST) is technology that is used to track the sun from sunrise till sunset for maximizing energy output from a system (Eldin et al., 2016). The ST systems are used to increase efficiencies of different systems - for example: solar panels and solar water purifiers by making their surfaces change orientations with the apparent movement of the sun which then keeps the solar radiation perpendicular to the systems surface (Hafez et al., 2018; Kanyarusoke, 2017a). Kanyarusoke et al., (2015) reported that solar tracking improves energy yields and it is not debatable. Solar tracking is also important when it is cloudy and it is difficult to obtain a maximum amount of energy. Solar tracking places the panel to be perpendicular to the solar radiation. Eldin et al., (2016) state that 30% of power increase to the solar units could be achieved by applying a solar tracker to the solar systems or units if the tracker is more optimized. According to Sumathi et al., (2017) there are two motion of solar tracking technologies that could be used for tracking solar radiation: single axis tracker (SATS) or dual axis tracker (DATS). The DATS`s follow the direction of the sun`s solar radiation beam for it to be able to get the perpendicular cadence over the module, and the SATS units are aligned from North to South and also have the freedom of rotating from east to west (Sumathi et al., 2017). Sumathi et al., (2017) states that there are two methods that are used for tracking the sunlight; active solar tracking and passive solar tracking.

2.3.1 Active solar tracking

According to Nsengiyumva et al., (2018) active solar trackers (ST) which are also known as continuous trackers, use sensors, programmes, gear mechanisms and motors for their operation. There are five different types of active drive systems: sensors drive system, microprocessor drive system, open-closed loop drive system, intelligent drive system and the combination of two or more of the stayed driving systems. (AL-Rousan et al., 2018). When designed with sensors, two of the sensors are used to determine the position of the sun in the sky so that the system can continuously be adjusted by the electrical motor to face the sun (Nsengiyumva et al., 2018). Figure 2.8 shows the schematic layout block of the active solar tracking design. Nsengiyumva et al., (2018) states that the active ST is made with two sensors that are used to generate composite signals which trigger the electrical motor to move or orientated the beam. At the point when the sun radiation beam and tracker's PV board are not typically adjusted these sensors are struck by an alternate brightening making a differential signal that is then used to decide the course in which the tracker must be coordinated. “The tracker's movement stops when the two sensors are equally illuminated i.e. the solar radiation beam is perpendicular to the PV module” (Nsengiyumva et al., 2018). The active solar tracking systems are accurate and they are the most used. However, the electrical motor of the tracking system needs to be powered for the operation of the whole system (Sumathi et al., 2017).

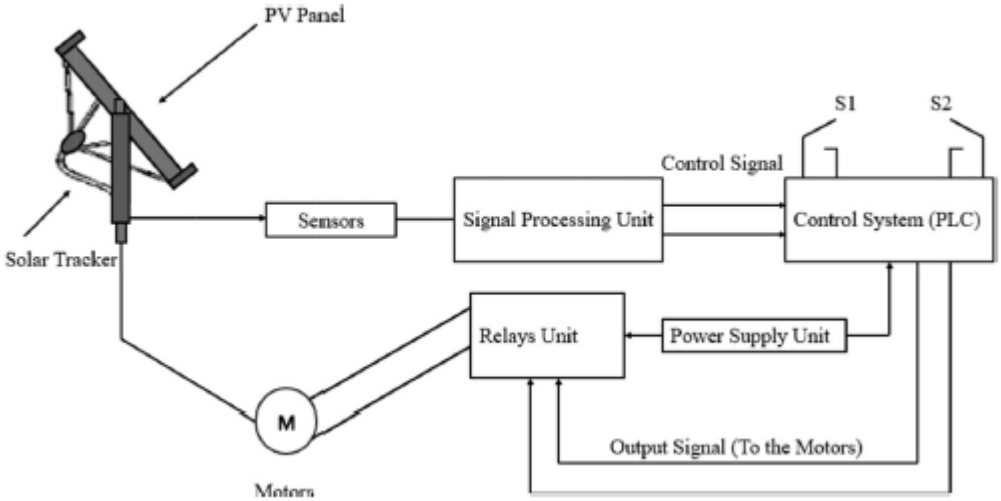

Figure 2.8: Active solar tracking system block diagram
(Nsengiyumva et al., 2018)

2.3.1.1 Active solar trackers with a single axis

Active solar trackers with single axis are tracking systems that only provide one degree of rotation in one direction from east to west following the direction of the sun. The Active single-axis solar tracking systems are designed with a single motor which is used to rotate the panel which is mounted on the tracking system. According to Kanyarusoke et al., (2015) the single active solar tracking system has only one set of the control system. Figure 2.9 shows the active single-axis tracking system which was designed at the Cape Peninsula University of Technology (CPUT) this tracking system was designed with a single motor and it also consists of a set of gears which rotates the solar collector from east to west by tracking the sunlight from sunrise to sunset. This system is designed by using a hollow pipe fixed on the ground which is used as a pillar. The motor is supported underneath by a round bar which is connected to the pillar on the ground and the motor is bolted on a square plate on top of the round bar.

Figure 2.9: Active solar tracker with a single axis

2.3.1.2 Active solar trackers with dual axes

The active dual solar trackers are tracking systems that have two degrees of freedom of movement (motion) about two axes which are mostly perpendicular to one another (Sumathi et al., 2017). The dual axis tracking system consists of two motors which rotate the tracking system into two different directions to the two motors is a chain which transfers the motion to the tracking system. Kanyarusoke et al., (2015) stated two sets of LDR sensors can be used to drive one motor from the east to east-west direction and a second smaller motor can be used to rotate about a perpendicular axis. He further stated that this type of system has an electromechanical drive which employing four relays it consists of two electronic circuits one on each motor which are connected to the computer. The second motor rotates the pillar which is positioned vertically where the first tracking system is mounted on as is shown in Figure 2.10. The vertical and horizontal pillars are held in position by sets of bearings.

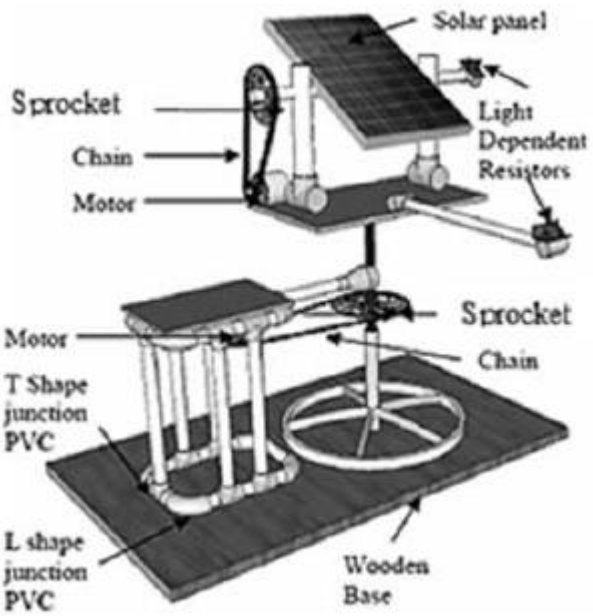

Figure 2.10: Active solar tracker with dual axis

(Kanyarusoke, Gryzagoridis, et al., 2015)

2.3.2 Passive solar tracking single axis

Passive solar tracking is the process whereby the sun is tracked without the use of any mechanical drives and electrical power systems (Nsengiyumva et al., 2018). The passive tracking system has a less complex structure and does not have any hardware implementations compared to the active tracking method. According to Nsengiyumva et al., (2018) the passive method of tracking has a simple operation and contains a pair of actuators which are usually filled with expansible gas. These expansible gas actuators work against each other by causing unbalanced forces in the actuator. When the gas is heated by the sun it expands then it causes an unbalanced gravitational which the heated liquid follows to one direction, hence the passive tracker panel tilts towards the direction of the sun. According to Kanyarusoke et al., (2015) a passive single-axis tracking system was built by Zomeworks which is shown in figure 2.11 this tracking system is made of two cylinders which are linked together by a tube. This tracking system has only one direction of movement and a rugged support frame which is vertical where the cylinder is pivoted on in the centre. Kanyarusoke et al., (2015) further stated that the Zomeworks tracker had problems which are: alack of a mechanism to return to its original position, and a slow response in the morning because of the limitation of the inclination surface angle.

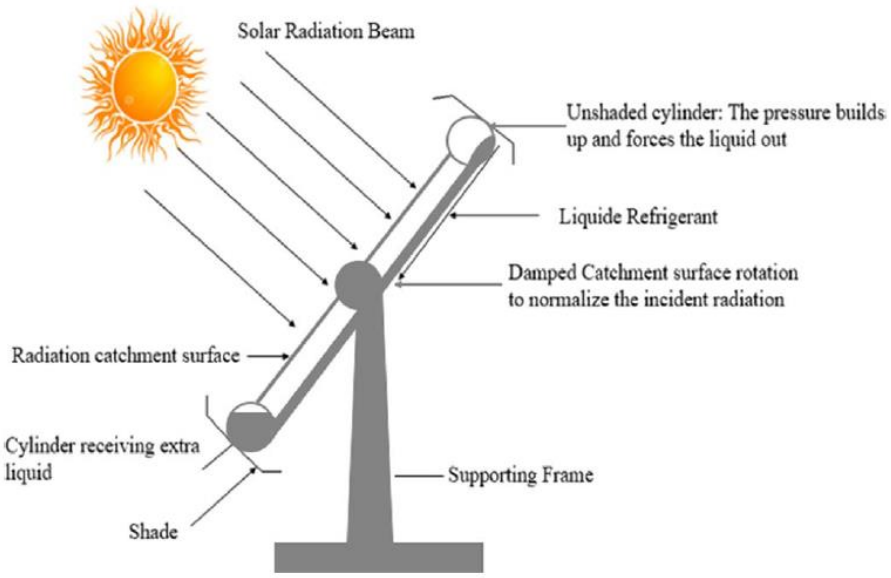

Figure 2.11. Passive single axis tracker

(Nsengiyumva et al., 2018)

2.3.3 Passive solar trackers with dual axes

According to Kanyarusoke et al., (2015) single axis trackers can be changed to dual axis tracking by providing an independent axis perpendicular to the main one or the first axis. A dual passive tracker for a solar concentrator 3-D visualisation was studied by (Kanyarusoke, Gryzagoridis, et al., 2015). This dual passive tracker was designed with a reflecting system that focuses the radiation to the fixed collector. Solar energy that has been received by the system is reflected in the control plane that is used for the balancing purposes. According to Kanyarusoke et al., (2015) “One Gimbal rotates about an N-S axis and carries the optical system – with its balancing subsystem”. The second Gimbal rotates about the east-west axis and the point of intersection of the two axes is about the fixed energy collection surface. The fluid or refrigerant is contained in the canisters at the two ends of the Gimbals. Figure 2.12 shows a dual axis tracker.

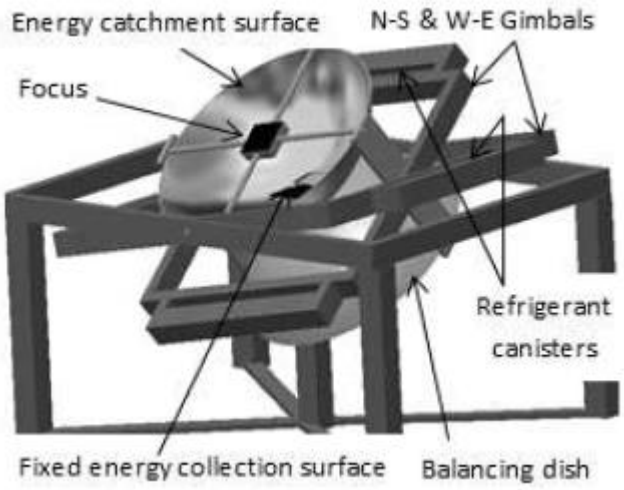

Figure 2.12: Passive dual axis tracker

(Kanyarusoke, Gryzagoridis, et al., 2015)

2.4 Concluding the chapter

In this, chapter a brief review of the literature review of the lack of clean water, different types solar water purification and solar tracking has been presented as follows; the first section covered the lack of clean water for human consumption in the world especially developing countries and Sub-Saharan African countries. Whereby it was found that high number of people who live in the Sub-Saharan African countries still lack clean water for drinking. The second section covered the four different types of solar water purification which are solar water disinfection, solar water pasteurization, solar water distillation and the solar water reverse osmosis. After a careful consideration study it was then considered that Engohang-Kanyarusoke standard size solar water purifiers will be used discussed in section 2.2.3. The third section covered the two types of solar tracking methods: active tracking and passive tracking. By following the limitation from chapter one and literature review it was then considered that active single axis tracking system method will be used. The findings from the literature review therefore forms a foundation on which the next chapter is built on.

CHAPTER THREE
DESIGN AND CONSTRUCTION OF THE TRACKING SYSTEM

3.1 Number Of purifiers

In this chapter, two designs are presented and the final concept, six solar water purifiers on a single axis drive system is selected. The number is limited to 6 because of manual filling height considerations.

3.2 Solar water purifier concepts

The purifiers have to be arranged in a way that they do not shade each other during the day especially between mid-morning and early afternoon when the radiation intensity is highest. Furthermore, the solar stills have to be arranged such that they can be able to purify large amounts of water during the solar noon period. Two different types of concepts are presented in the following sub-sections.

3.2.1 Concept one

The first concept consists of two solar water purifiers. The first solar still is mounted at the top of the pillar on the left-hand side and the second purifier is mounted below the first one but on the right side of the pillar. This arrangement does not have to consider the shading or the solar noon angle of the sun because it only consists of the two solar water purifiers which even if they are arranged on the same level, they will not shade each other. As this concept consists of only two solar water purifiers, less water will be obtained from system. This does not satisfy the main objectives of the thesis. Figure 3.1 shows the first concept with the two solar water purifier’s structure and assembly.

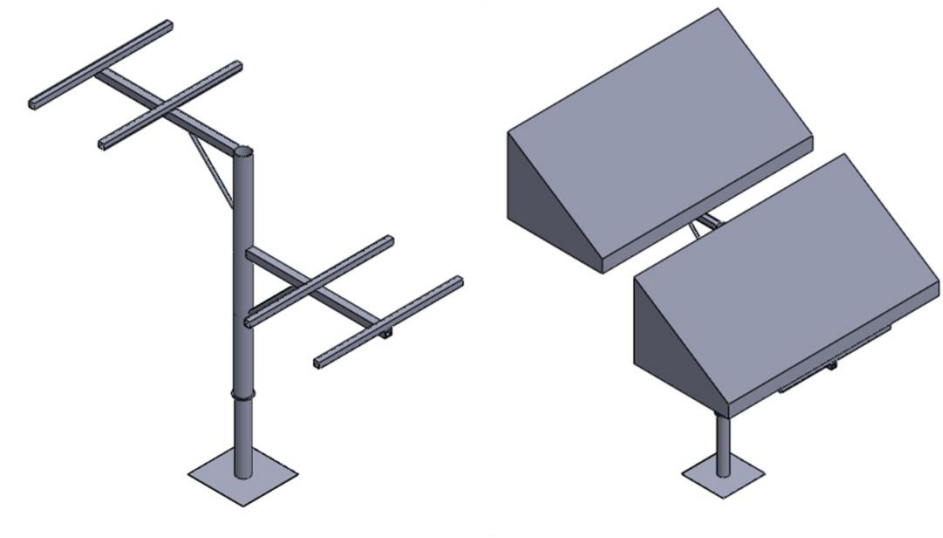

Figure 3.1: Concept one (Structure left and assembly right)

3.2.2 Concept two

Concept two consists of four solar purifiers. The stills are placed around the pillar in a way that the forces exerted by the stills are balanced out while also avoiding shading at the same time. This concept consists of two levels whereby one unit is placed on level one and the other three units are placed on the same level on top of the pillar. The two stills at level two are placed side by side one on the right and another one on the left of the pillar while the fourth unit is placed at the back of the two units making sure that there is no shading on the unit. Figure 3.2 shows concept two with the structure design on the left and the assembly of the system on the right.

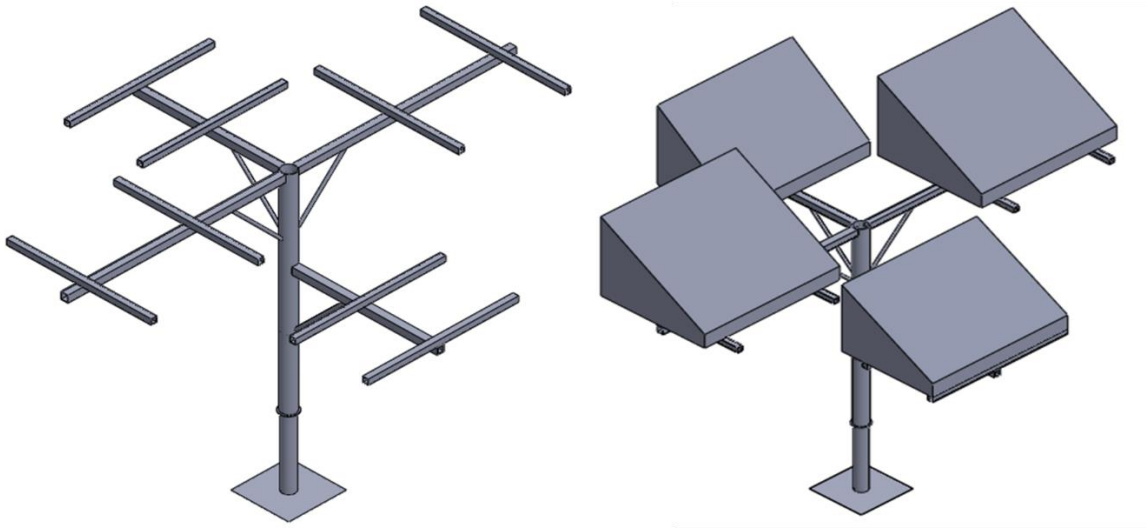

Figure 3.2: Concept two (Structure left and assembly right)

3.3 FINAL CONCEPT

This concept consists of three levels where each level was designed in such a way that it can carry two purifiers. This concept was the most suitable one because it can carry a maximum of six purifiers which will not shade each other. Furthermore, this concept will provide a high yield of water that is needed in large households. This concept was also selected because it meets the objectives of this thesis as they are stated in chapter one. It is also simple to design, construct and maintain as it only consists of a simple structure.

3.3.1 Final design

3.3.1.1 Structure

The final design structure consists of four straight square tubes which are to be bolted on the brackets with two bolts on each tube which are to be welded on the pillar or shaft. Two square sections are attached to each straight square tube horizontal which supports the solar water purifiers when placed on top of the structure. Each straight square tube section is supported by one round hollow bar that prevents the structure from bending. The round bars are joined to the pillar and structure by using one bolt on each end. Figure 3.3 shows the structure design.

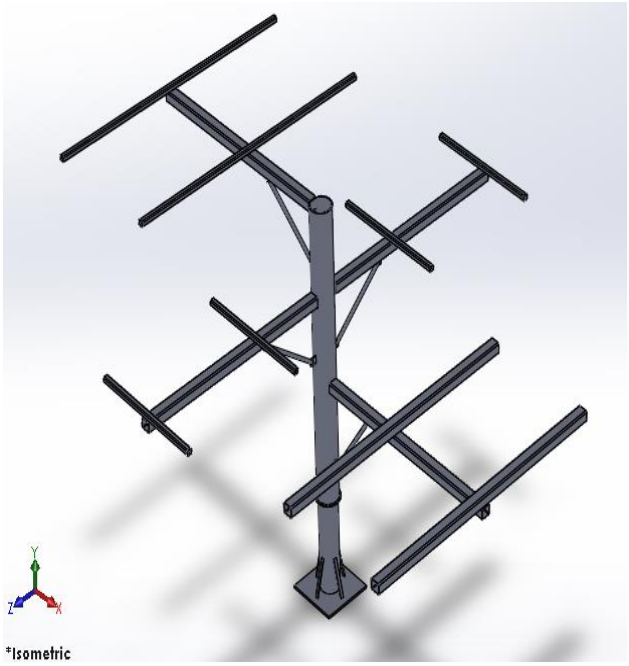

Figure 3.3: Structure design

3.3.1.2 Geometry

The tracking system consists of stainless steel round hollow bars, structure square tubes that are welded together and bolted on the pillar. It also consists of a pillar with a small diameter of

147mm x 1600mm and a big pillar with a diameter of 150mm x 2100mm. Further dimensions are shown in table 3.1 below. Detail drawings with dimensions are shown in appendix A.

Table 3.1: Solar tracker geometry

Part	Quantity	Dimensions (mm)
Pillar	1	Ø 150 x 1400 x 4.5
Pillar	1	Ø 147 x 1100 x 4.5
Flange	2	Ø 165.10 x 3
Support arms	2	Square tubing 70 x 70 t = 8 l = 1610
	2	Square tubing 70 x 70 t = 8 l = 1600
Solar panel brace	4	Square tubing 50 x 50 t = 2 l = 2111
	4	Square tubing 50 x 50 t = 2 l = 910
Side supports plates	8	50 x 50 x 2
Gussets	4	40 x 280
Base plate	1	400 x 400 x 8
Round hollow section	4	Dia=110 l = 700
Bolts	4	Roll bolts
	8	M12
	8	M15

3.3.1.3 Area occupied by the tracking system

The standard Engohang-Kanyarusoke tracking solar water purifiers mounted around the pillar will cover an effective ground footprint of a rectangle measuring 3.7m X 1.5m or an effective area of 5.55 m^2. While the ground mounted purifiers arranged in a way that they avoid shading and provide enough room around each purifier for filling and emptying will require an effective area of 39m^2 (9.2m X 4.2m). This means that an effective ground area of about 33.45 m^2 was saved up by mounting the purifiers on the pillar. Furthermore, as the purifiers are mounted off the ground space under the purifiers can be used for another purpose, for example, it can be

used to grow crops in village home steads. Figure 3.4 shows the area that is covered by solar water purifiers when they are mounted on the pillar.

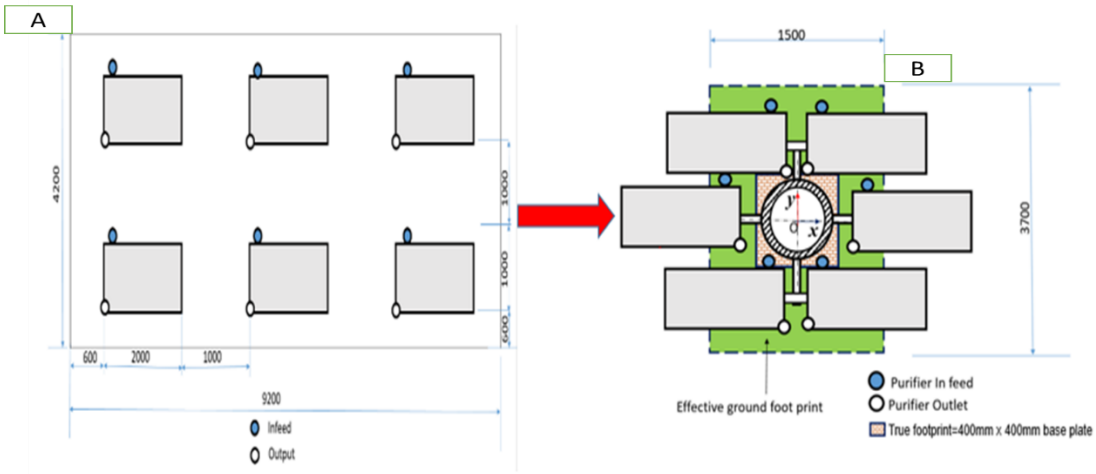

Figure 3.4: Areas occupied by the purifiers (A- Ground mounted purifiers, B- Purifiers mounted around the tracking pillar)

3.3.1.4 Assembly

The solar water purifiers are placed facing the northern direction. The top structure which is the third level carries two solar water purifiers that are placed next to each other. The second level consists of two purifiers with one on the right, and the other, on the left side. The first level also consists of two purifiers which are placed side by side next to each other. Figure 3.5 shows the assembly of the final design;

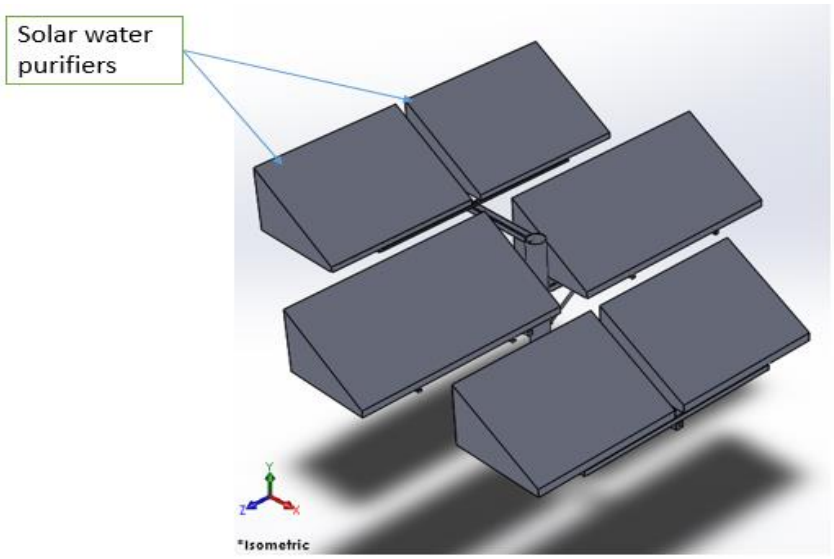

Figure 3.5: Assembly with purifiers

3.3.2 Material selection

Three types of materials were considered as possible choices to be used in this design. Their physical and mechanical properties are shown in Table 3.2. Carbon steel was a suitable chosen material.

Table 3.2: Material properties

Aluminium	Stainless steel	Plain Carbon steel
Mechanical properties		
E=71.7GPa	E=190GPa	E=207GPa
G=26.9GPa	G=73.1GPa	G=79.9GPa
n=0.333	n=0.305	n=0.292
Physical properties		
Corrosion resistant	Corrosion resistant	Corrosion risk
Lightweight	Heavy	Heavy
Difficult to weld	Difficult to weld	Easy to weld
Easy to machine or cut	Difficult to machine or cut	Difficult to machine or cut

3.3.3 Structural mechanics of the final design

A uniformly distributed load of 40kg was applied to the square tube beams, this weight was taken as the maximum weight of each purifier that are to be placed on top of the structure when filled with water to the design overflow level.

Carbon steel was the selected material for the square tubes, stainless steel for the round hollow section which supports the structure as it was explained before in the previous section and which was used in the simulation. The yield strengths of the materials were selected in the software as the references for the design to see if it can withstand the applied weights to it. The structure was then simulated whereby a comment stating that the design can easily withstand the applied loads without failing was made which showed a blue box with two white ticks in it. A maximum static safety factor of 15 was obtained in both structures with the first level structure acting at the joint where the round hollow section is joined to the square section as is shown in figure 3.6 on the left side structure. The maximum safety factor of level two structure was at the end of the structure this was due to the fact that the structure had a long structure arm.

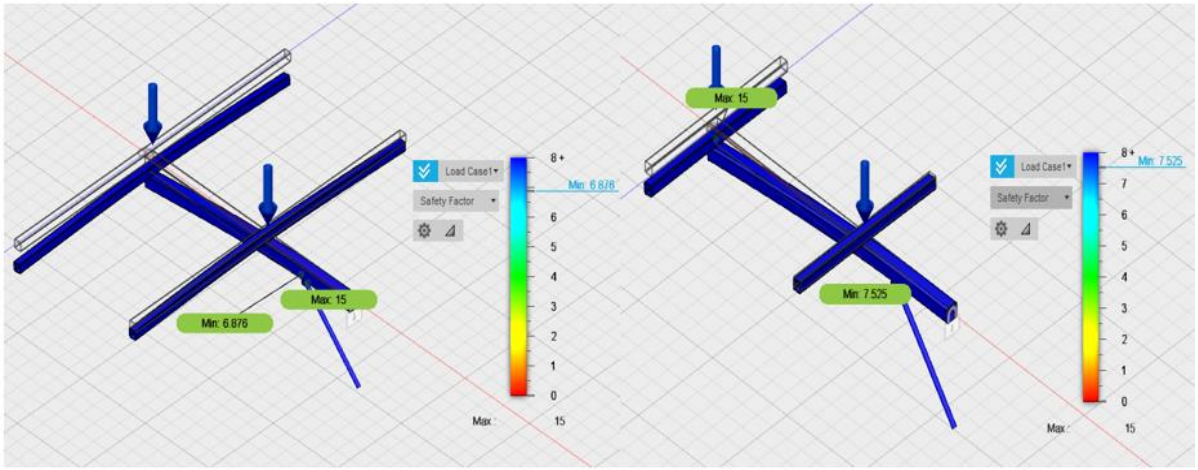

Figure 3.6: Safety factors

Von Mises stresses were obtained to determine if the material will yield under the applied loads on the structure. They were found to be less than the yield limit of the material which shows that the material was safe to be used in the design. Figure 3.7 shows Von Mises stresses of the two different structures..

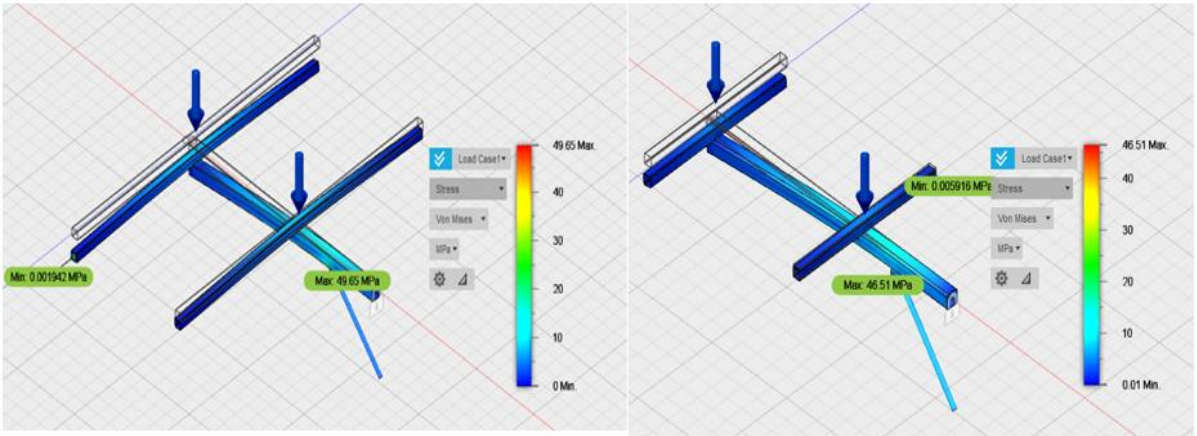

Figure 3.7: Von Mises stress

The maximum displacement of the two structures was found to be high at the ends where they were not fixed - with displacements of 1.587 mm and 1.26 mm. Having a high displacement can lead to the structure to bend at the ends which then causes the water in the still not be levelled this then affects the evaporation of the water to the glazing. See Figure 3.8 for the displacement values obtained.

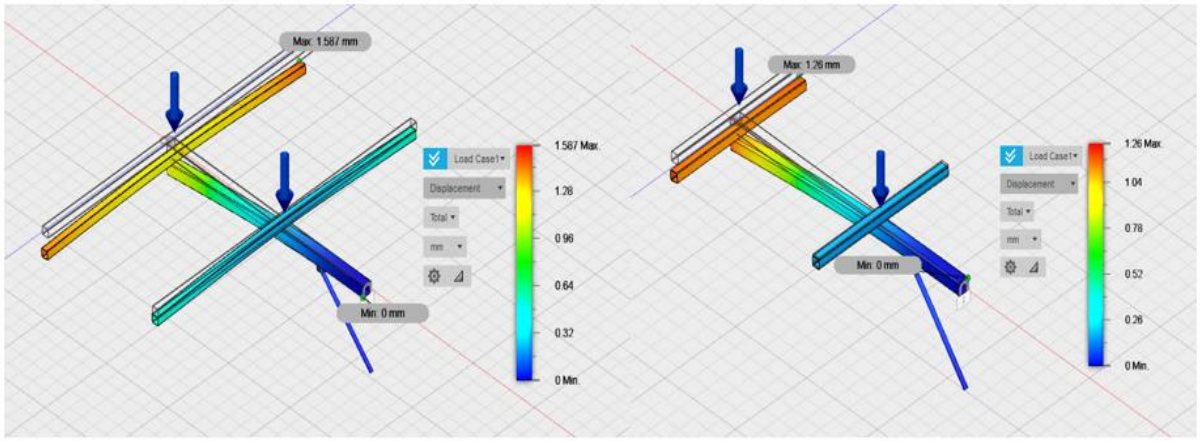

Figure 3.8: Displacement

As the round hollow sections were used to support the structures they had to carry all the weight of the structure with a high reaction force obtained at the fixed end where the hollow section joins the pillar in both structures. Figure 3.9 shows the reaction forces where they are acting on the structures.

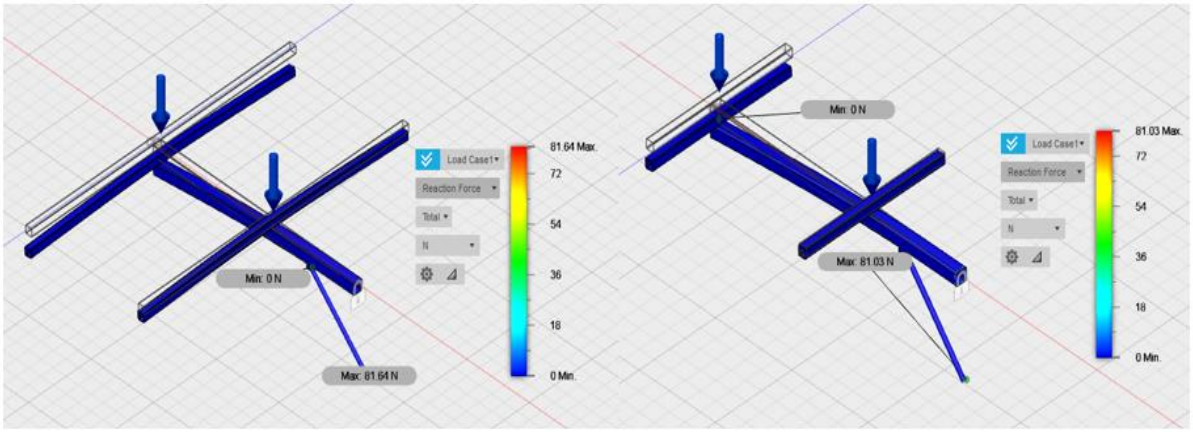

Figure 3.9: Reaction force

Figure 3.10 shows the strain that the structure had. Deflections were small towards the pillar where it is fixed while they were big at the end of the structure due to the cantilevering effect.

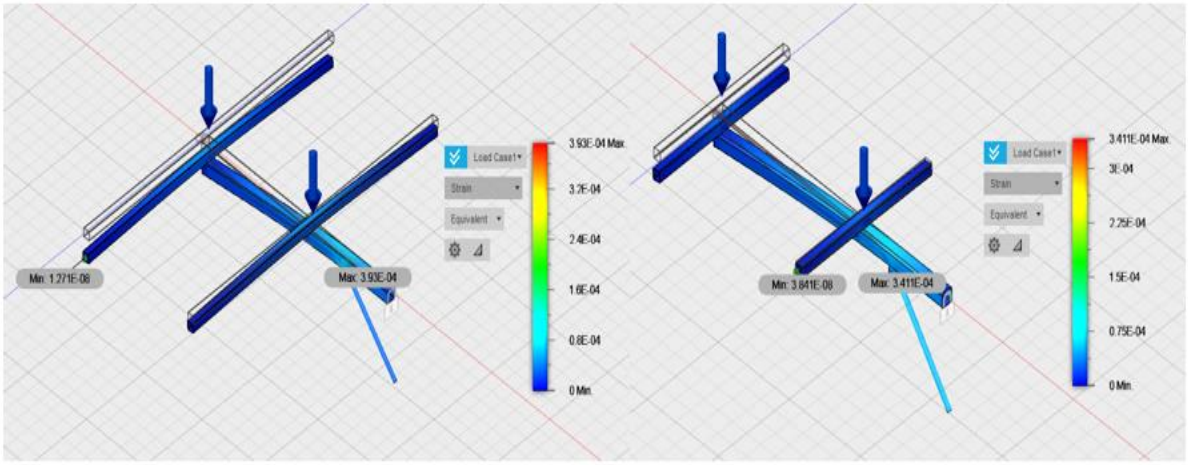

Figure 3.10: Strain

3.3.4 Pillar design and bending stress

The drag force that is caused by the wind that is exerted on the back area of the purifiers causes bending stresses at the bottom of the pillar. It was calculated in an excel spreadsheet whereby the selected diameter pillar was simulated in Autodesk Fusion360 in this section. Cape Town was taken as the reference point for the standard weather conditions where by the density of the air is 1.225 kg/m^3, drag coefficient 1.02, wind velocity 33.333 m/s (Wright & Grab, 2017). The back areas of purifiers are uniform with an area of 1.5 m^2 each still. Whereby the drag force acting on each purifier was found to be 1.041 kN by using equation 3.1. The wind forces which are acting on the pillar from the purifiers that are mounted on each level of the structure were calculated and used to find the maximum bending stress at the fixed bottom end of the pillar. Figure 3.11 shows the schematic of the typical beam of the wind acting on the back of the purifiers;

$$D_{Force} = C_D A \frac{\rho V^2}{2} \qquad 3.1$$

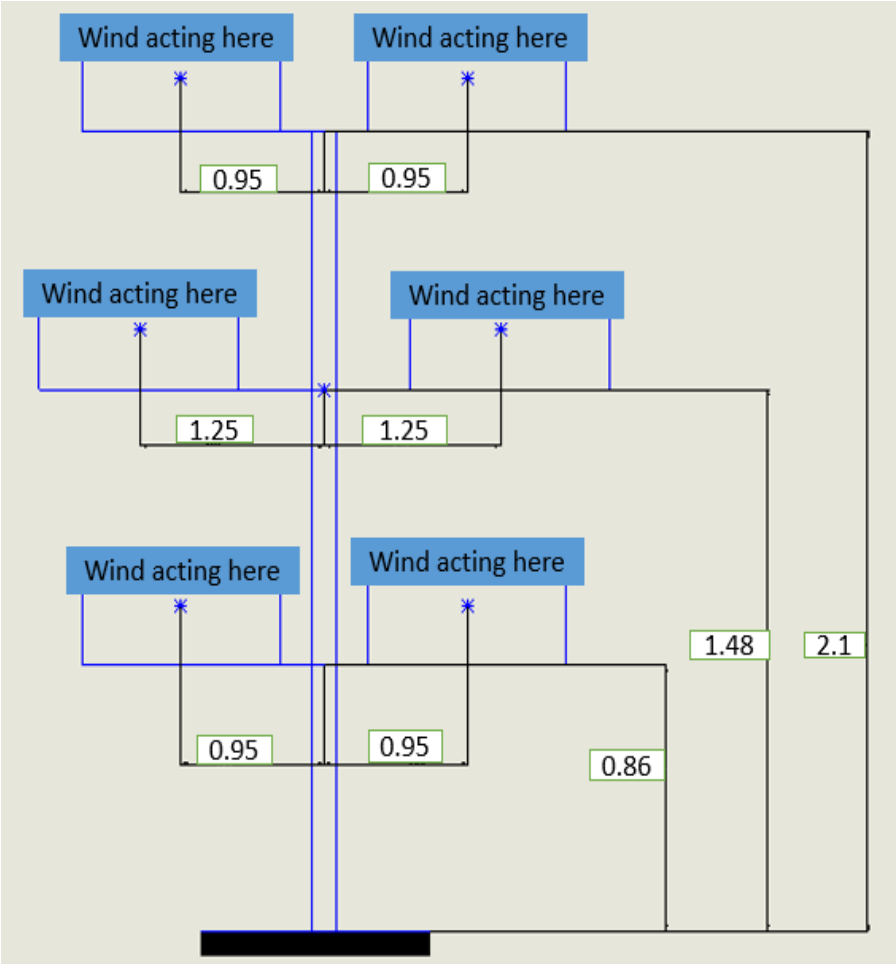

Figure 3.11: Wind acting on the back of the purifiers beam

The reaction at level A due to drag force (Third level) was found to be 1.978 kN which is the same reaction as it is on level C/ point C on these two levels two purifiers are to be mounted on each level. Level B (Second level) also consists of two purifiers which had a big area than the other four purifiers on point C & A. The reaction force at B was found to be 2.602 kN. A free body diagram was drawn as it is shown in figure 3.12 to show where the different forces are acting on the pillar which is considered as a cantilever;

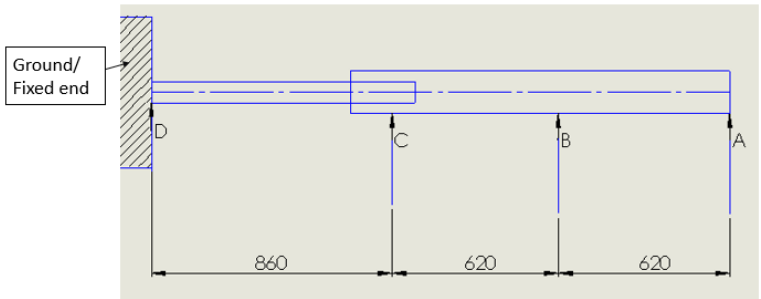

Figure 3.12: Pillar considered as a beam

The bending moment due to wind force taking the bending moment from point D where the cantilever is fixed on the ground.

$$M_{DA} = 1.978 \times 2.1 = 4.154\ \text{kNm}$$
$$M_{DB} = 2.602 \times 1.48 = 3.851\ \text{kNm}$$
$$M_{DC} = 1.978 \times 0.86 = 1.701\ \text{kNm}$$

The resultant bending moment was found as follows; $M_{DA}+M_{DB}+M_{DC}$= 4.154 + 3.851 + 1.701 = 9.706 kNm

This is the reversed loading on the pillar hence the endurance limit in the next part of the calculations is used.

The pilar was designed for fatigue loading as follows with the working stress of the pillar was found by;

$$\sigma_{working} = \frac{32.M}{\pi(D^3 - d^3)}$$

$$\sigma_{working} = \frac{32\times(9.706\times10^3)}{\pi(0.147^3 - 0.138^3)} = 10984.95\ \text{Pa}$$

Endurance limit for the pillar;

$$S`_e = 0.5S_{ut}$$
$$S`_e = 0.5 \times 168.4803 = 84.24015\text{Pa}$$

Endurance limit-Limit modifying factors;

$$S_e = k_a \times k_b \times k_c \times k_d \times k_e \times k_f \times S`_e$$
$$S_e = 1.58 \times (1.189 \times 150^{-0.097}) \times 0.868 \times 1 \times 0.514 \times 1.945 \times 84.24015 = 16476\text{Pa}$$

Factor of safety;

FOS=Endurance Limit/ Working stress

$$\text{FOS} = \frac{16476}{10984.95} = 1.5$$

3.3.5 Solar tracking single axis drive system design and stepper motor

3.3.5.1 Thrust bearing

A Thrust bearing was required to support the load of the whole system and also to provide a smooth rotation between the two moving parts (Pillars). However, the size of 150 mm thrust bearing was not available. As this is not a standard size, special arrangements had to be made with a local company (Bearing man) where it had to source the bearing of the size of dia 150 mm. Figure 3.13 shows the thrust bearing.

Figure 3.13: Thrust bearing

3.3.5.2 Electrical motor (Stepper motor 24V DC)

3.3.5.2.1 Power requirements

The power requirements of the system were calculated through experiment and measurement. The unloaded frame assembly without the water weighed roughly 94 kg. The torque required to turn the frame was then measured using a scale, the scale hook was attached at one end of the structure arms which was then pulled at a distance of 1.6 m from the axis rotation which resulted with a torque of 26.478N of force at a distance of 1.6 m from the axis of rotation.

$m = 94\ kg \qquad p = 2.7\ kg \qquad R = 1.6\ m \qquad r = 0.0725\ m\ (Radius\ at\ contact\ faces)$

$T = p \times R = 4.8\ kg.m \qquad \mu = \frac{T}{m.r} = 0.704$

From this it is possible to calculate the torque when the system is loaded as well as the power requirements since the rotational speed was already found. The total load when the entire system is working at capacity is 394 kg.

$m = 394\ kg \qquad At\ 0.0725m: p = m.\mu\ = 394 \times 0.02 = 7.88kg \qquad T = p.g.r\ = 5.604453\ Nm$

Power required was calculated by using the following gear schematic specifications below:

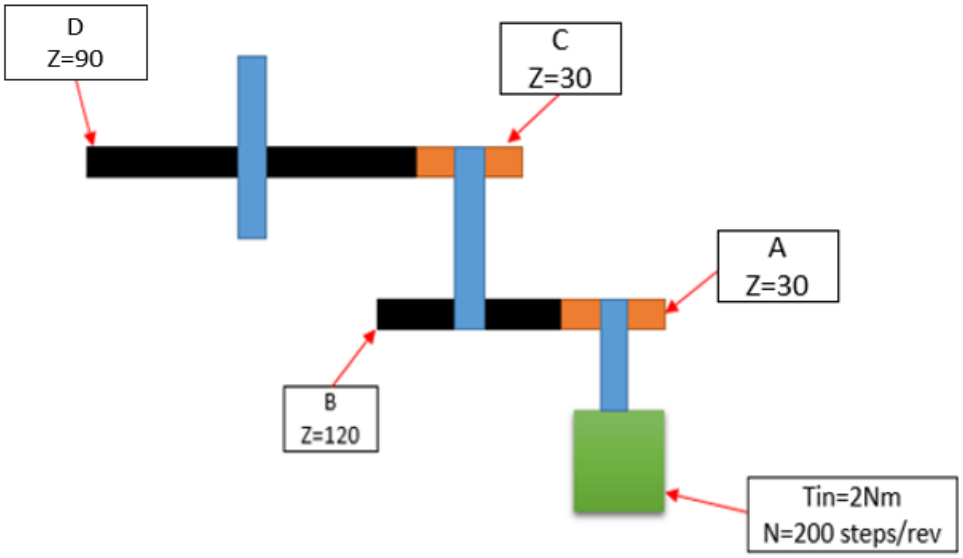

Figure 3.14: Gear system schematic

$$\frac{1\ step}{pulse} \times \frac{200\ pulse}{1\ sec} \times \frac{1.8\ degree}{1\ s} \times \frac{1\ revolution}{360\ degrees} \times \frac{60\ sec}{1\ min} = 60\ rev/min$$

$$G_{R1} = \frac{Z_B}{Z_A} = \frac{120}{30} = 4$$

$$G_{R2} = \frac{Z_D}{Z_C} = \frac{90}{30} = 3$$

$$T_B = T_C = G_{R2} \times T_B = 2 \times 4 = 8\ Nm$$

$$T_D = G_{R2} \times T_C = 3 \times 8 = 24\ Nm$$

$$N_B = N_C = \frac{rpm\ of\ A}{ratio} = \frac{60}{4} = 15\ rpm$$

$$N_D = \frac{rpm\ of\ C}{ratio} = \frac{15}{3} = 5\ rpm$$

3.3.5.2.2 Stepper motor

A stepper motor NEMA23 was used - as it was the only available motor at the time of the design from the supplier. The motor had the following specifications, holding torque 2.0Nm and a 1.8º step angle (200 steps/revolution). As the torque was less than the initial 5.60 Nm required to turn the system a compound gearbox was designed to step-up the torque to drive the vertical pillar.

3.3.5.3 Solar tracking drive system design

The many numbers of different types of power transmission systems offered a vast array of options from which feasible concepts could be created. Systems like the worm and wheel gear trains, simple, compound spur gear trains, bevel gear trains and chain drives were considered for the tracking system. Some of these types of systems were employed in the concept phase and were chosen based on their simplicity to manufacture or acquire, their cost, simplicity of their mechanism and their reliability. Below is a brief breakdown of the various concept of drive design systems, which includes the final concept drive design system, design 3.

3.3.5.3.1 Drive system concept one

The first concept made use of the bevel type gearing system. With a small gear ratio and pitch line velocity than a simple spur gear, this type of power transmission at first seemed to be an attractive one as the necessity for a sample gear trains well as simplicity were required in order to work with the small capacity stepper motor employed to power the movement. Figure 3.15 shows the bevel type gearing system. Table 3.3 gives merits and demerits of the system.

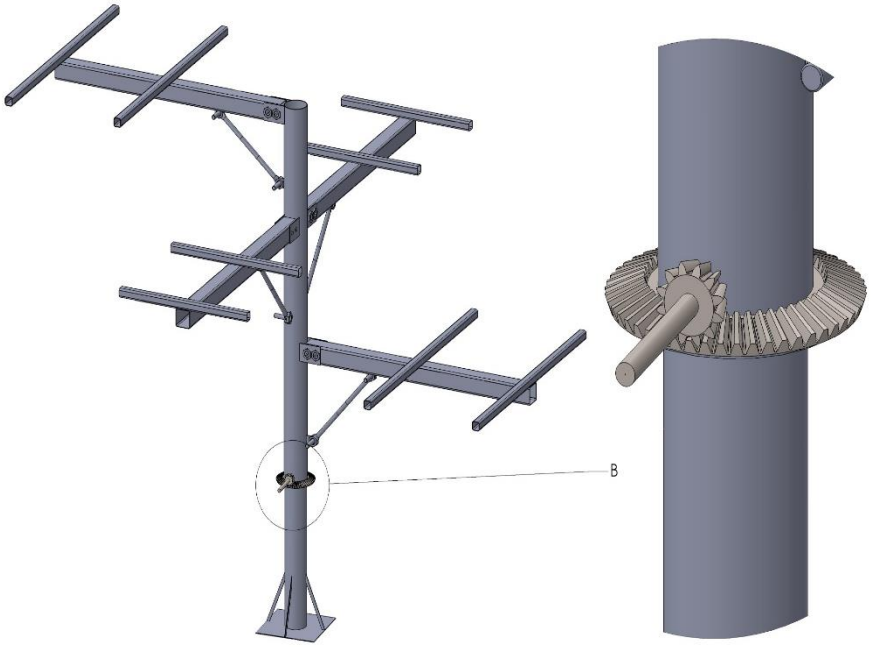

Figure 3.15: Bevel type gearing system

Table 3.3: Positive and negative attributes of the bevel gear system

Positive attributes	Negative attributes
Relatively simple mechanism	Gears are relatively expensive to purchase
Easy to install and operate	Gears are difficult to manufacture

Little maintenance required for optimum function	The difficulty in manufacturing leads costs to rise, so increasing the cost of the system

3.3.5.3.2 Drive system concept two

The second concept is of the chain drive variety of power transmission systems. Their ease of manufacture and wide availability of parts within the Cape Town area made this concept a strong contender for the final design. However, further investigation found that the system cannot produce the required gear ratio to enable the stepper motor to perform normally without the introduction of a compound chain type system. The compound chain type system would dramatically increase the build and design complexity and could have led to too many unforeseen problems in assembly. The design can be seen in figure 3.16 along with table 3.4 of its merits and demerits.

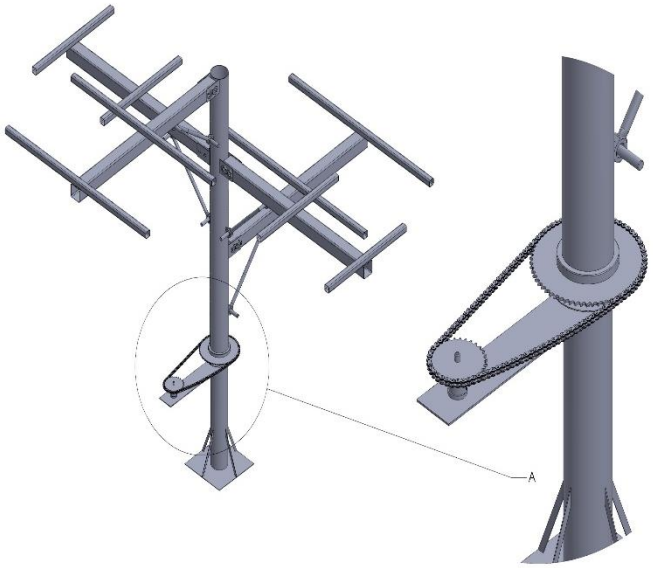

Figure 3.16: Chain drive system

Table 2.4: Positive and negative attributes of the chain drive system

Positive attributes	Negative attributes
The operating mechanism is simple and easy to install	The greater number of moving parts (chain links) creates a greater possibility of failure
Parts are relatively affordable compared to gear type transmissions	It is unknown as to whether the system can withstand the fluctuating Cape climate over extended periods
The system is lighter than traditional steel gears	Compound chain drives are too complex for this project's purpose

3.3.5.3.3 Final drive system concept

The final concept is of the compound spur gear type. The torque required to rotate the pillar exceeds the torque limit of the motor even with a simple 1:6 gear reduction. It was therefore necessary to produce a solution that would allow the motor to function properly. This led to the development of compound gear train concept illustrated below. The readily available gears meant that procurement of critical parts was easy, while the sturdy design of the gears meant that longevity of the transmission would not be a great concern. This concept seemed to address all the aims and limitations of the design. Figure 3.17, 3.18 shows the final drive system and the final concept detail view. Table 3.5 shows the gears geometry.

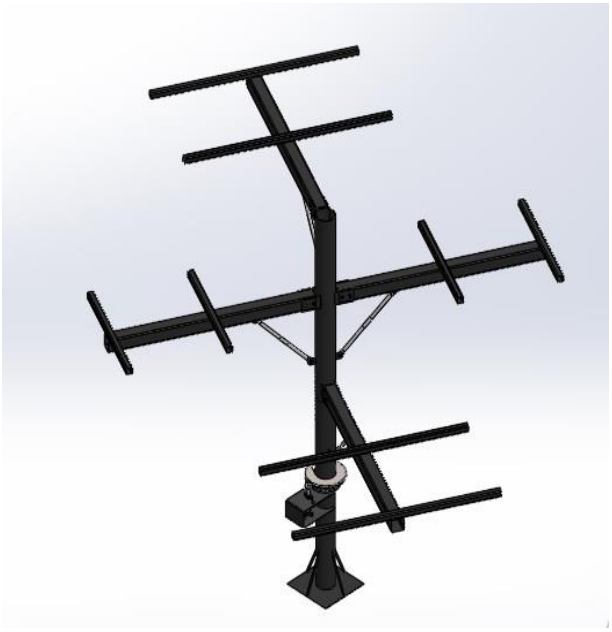

Figure 3.17: Final drive system

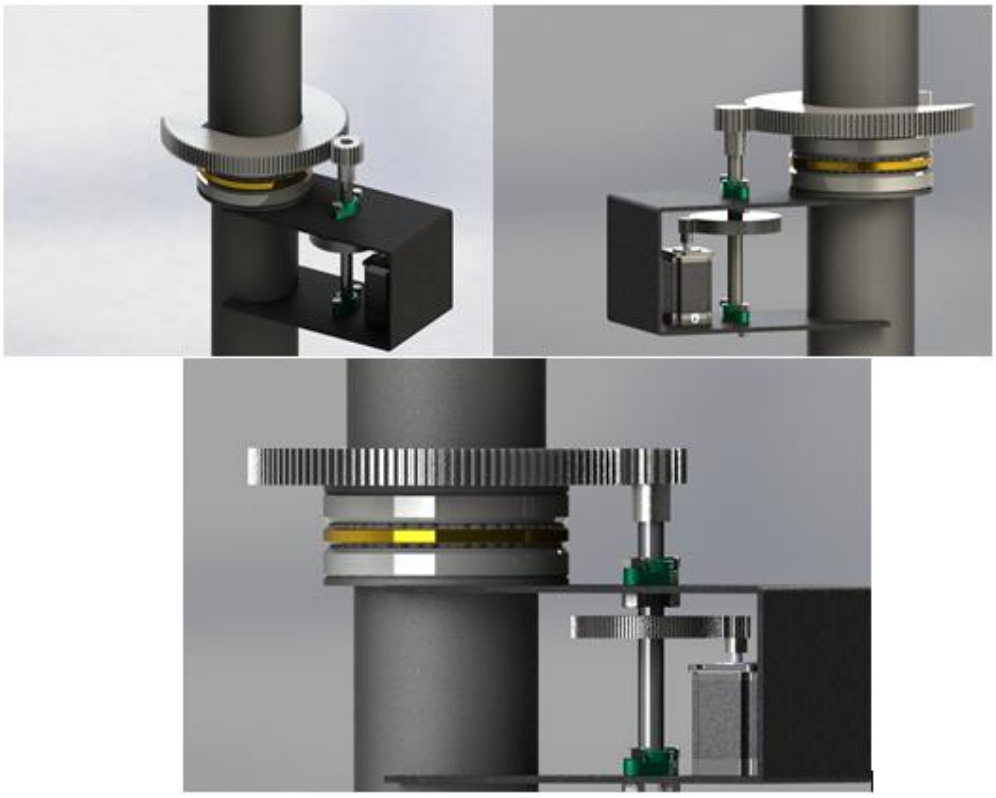

Figure 3.18: Final concept detailed view

Table 3.5: Gear geometry

Motor pinion	MS z = 30; m = 2.5 mm
Motor gear	MS z = 120; m = 2.5 mm
Pillar drive pinion	MS z = 30; m = 4 mm
Pillar drive gear	MS z = 100; m = 4 mm

3.3.5.3.3.1 Forces and stress analysis on gears

Analysis of the forces and stresses on each of the gear components were conducted in order to understand the operating limits of each component. Mechanical Engineering Design 3 gear design spreadsheets by Kanyarusoke were used to analyse the gears. Table 3.6 illustrates the key stresses and forces acting on each gear as well as the factors for operating safety. Also included below are the mathematical theories used in the calculation of forces and stresses from Kanyarusoke Machine Design course notes. Also, see Appendix A for the gear design spreadsheets.

$$Modified\ Lewis\ Bending\ Equation: \sigma_B = \frac{F_T.K_v.K_o.K_m}{m.w.J} \quad 3.2$$

$$Pitting\ Stress\ Equation: \sigma_C = C_p\sqrt{\frac{F_T K_v.K_o.K_m}{w.I.d_p}} \quad 3.3$$

Table 3.6: Gear specifications

	Gear 1	Gear 2	Gear 3	Gear 4
Bending Fatigue Strength (MPa)	237.675	237.675	237.675	237.675
Pitting Fatigue Strength (MPa)	808.414139	808.414139	808.414139	808.414139
Corrected Tangential Force (N)	23.352	23.352	56.04453	56.04453
Bending Stress (MPa)	7.328	5.794	4.22	3.337
Pitting Stress (MPa)	180.072	180.072	136.66	136.66
Bending Safety Factor	32.4	41.02	56.316	71.224
Pitting Safety Factor	4.489	4.489	5.915	5.915

3.3.6 Project cost

Table 3.7 shows the project cost of all the materials that were used for building the project;

Table 3.7: Project cost

Material	Quantity	Cost
Square tubes 50 x 50	8	Sponsored by Progressive Africa Solar Engineering
Square tubs 70 x 70	4	Sponsored by Progressive Africa Solar Engineering
140mm diameter hollow pipe	1	Sponsored by Progressive Africa Solar Engineering
160mm diameter hollow pipe	1	Sponsored by Progressive Africa Solar Engineering
Round hollow pipes bar	8	Sponsored by Progressive Africa Solar Engineering
M12 bolts and nuts	25	R 150
Flate plate	1	R 200
Paint	1	R 100
Solar purifiers	5	Provided by the supervisor
Stepper motor DC	1	R 1744.55
Ball bearing	1	R 1100.00
Flange bearings	2	R 169
Gears	4	R 1500
Batteries 12V	2	Provided by the supervisor

Total cost	**R 4963.55**

3.4 CONSTRUCTION OF THE TRACKING SYSTEM

3.4.1 Pillar and Base construction

The hollow pipe was first marked out to the right size as is shown in the pillar design section above. After the marking out the hollow pipe was then cut to the right size to form a pillar. A round flange plate was welded on the right side of the pillar is shown in figure 3.25 were the thrust bearing will be. Eight brackets were also welded on the pillar where the four structures (rectangle tubes) of the pillar were attached. Furthermore, four other plates were welded underneath each main bracket of the structure. These plates were to be used to attach a round bar that supported the structure at each level. Figure 3.19 illustrates the fully constructed pillar.

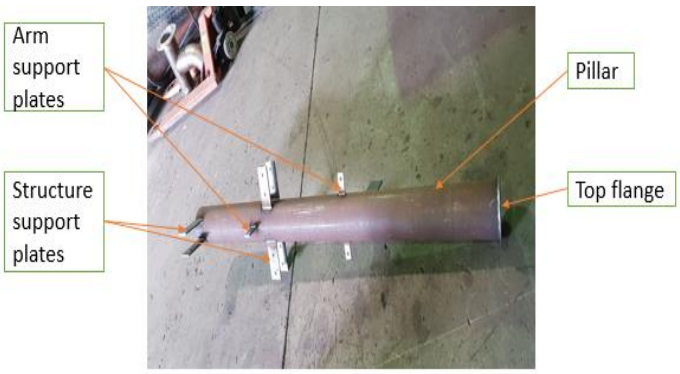

Figure 3.19: Constructed pillar

A hollow internal pipe was welded all round in the middle of the flat base plate the internal pipe goes into the main pipe. This flat plate is bolted on the floor with four rawl bolts to hold the pillar. Four gussets flat plates were also welded at an angle of 45º on the sides of the shaft, these gussets were used to strengthen the base of the pillar. A round flat flange plate was welded on the internal shaft. This flange acts as the rotating point of the two pillars the internal and the external where the bearing will be placed. The constructed internal pillar is demonstrated in figure 3.20;

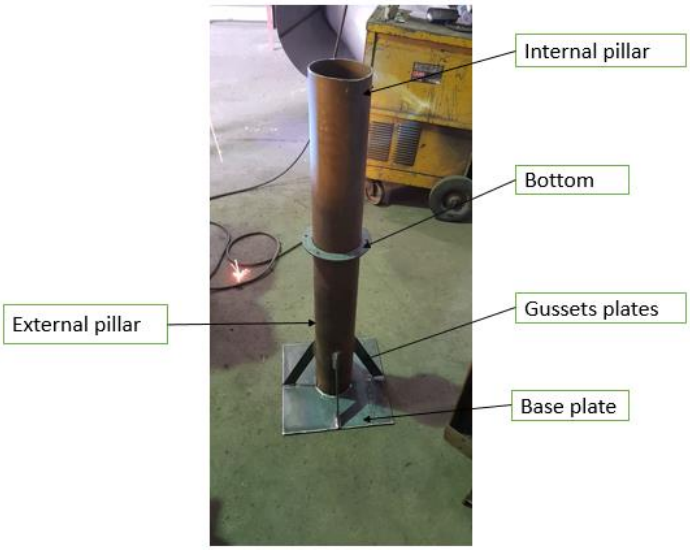

Figure 3.20: Constructed pillar

3.4.2 Structure construction

The structure square tube arms were welded on the main rectangle angle tube. A small flat plate was also welded under the rectangle tube with a hole drilled in the welded plate where it was bolted to the round tube attached to the pillar. This member is used to support the structure. Furthermore, two holes were also drilled in the rectangle tube which these holes are used to bolt the rectangle tube to the pillar. Figure 3.21 shows the structural members that were constructed.

Figure 3.21: Structure arms

3.4.3 Assembly of the tracking system

The ground floor atop of the Mechanical Engineering department where the assembling of the tracking system was to be fixed was first marked out. Four holes were drilled at each corner of

the base plate into the floor 100 millimetres deep with a 10 millimetres drill bit. After then the four rawl bolts of 111 millimetres long were inserted in the holes to hold the base plate where the pillar is mounted on - as can be seen figure 3.22. The rawl bolts nuts were then tightened until the base plate was properly fixed on the floor and making sure that there is no any kind of movement on the pillar or base plate.

The rawl bolts were were used because they have a locking sleeve which expands when they are tightened, thus occupying the whole diameter area in the hole and then making the attached object firm.

Figure 3.22: Fixed base

The thrust bearing bottom round plate was inserted on its resting point on the bottom flange after which, it was aligned 90° to prevent any wear on the bearing. The top flange pillar was then inserted to set on the bearing where it was fixed on and further, the structure arms were also attached/blotted on the top pillar. Figure 3.23 shows the thrust bearing installation.

Figure 3.23: Bearing installation

The next step was to customise the gears that were bought and begin assembling the gearbox. This involved welding a solid shaft between gears 2 and 3, and CNC cutting a section out of gear 4 so that it could be installed on the rotating pillar. The gearbox housing itself was then

made from 5mm thick Mild steel, bent to form a box shape, with a profile cut out of the one side so that it could be fitted neatly to the stationary pillar tube. Holes were then drilled through the box to allow the connecting shaft gears protrude out the box, this allowed for two bearings to be fitted to either side of the connecting shaft. Lastly, holes for bolts were drilled which would allow the secure fitting of the motor within the gearbox. Figure 3.24 shows the gearbox being assembled.

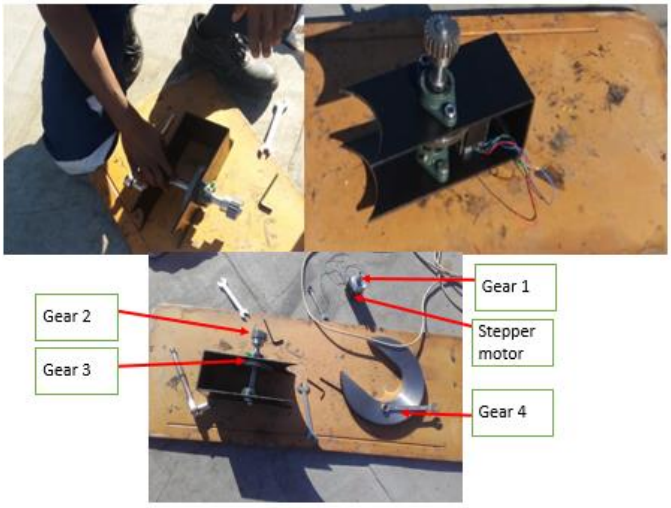

Figure 3.24: Assembly of the gearbox

The main gear was then attached on to the rotating/top pillar. Following the assembly and alignment of the gears, the gearbox was then installed by welding it to the stationary pillar tube, illustrated in figure 3.25.

Figure 3.25: Welding gearbox to the stationary pillar

Before attaching the motor it was necessary to triple check the gears alignment between gears 4 and 3, and 1 and 2. Misalignment can lead to early gear failure and excessive wear, as well as incorrect operation. Adjustments were made accordingly and are pictured in figure 3.26.

Figure 3.26: Gear alignment and inspection

Figure 3.27 shows the assembly drawing of the tracking pillar at the roof-top of the mechanical engineering department with the left side showing the gearbox of the system, and the right side showing the full assembly of the tracking pillar.

Figure 3.27: Assembly drawing (Gearbox left and full assembly right)

3.5 Concluding the chapter

This chapter presented three different types of arrangements of the solar water stills, whereby the third arrangement was the most suitable concept. The final design could take up to six solar water stills without them shading each other. The simulation of the structure arms of the final design was done by using Autodesk Fusion 360 and mild-steel was the selected material for the simulation to see if the selected materials will fail or not. The construction of the tracking system and programming of the stepper motor was done at the roof-top of the mechanical engineering department. The next chapter deals with testing of the assembly.

CHAPTER FOUR
EXPERIMENTAL SETUP AND METHODOLOGY

This chapter gives the experimentation that was done to test the performance of the designed system. The testing apparatus, the setup and the procedure that was used to record results are given. The tracking system was assembled on the roof of the mechanical engineering department where the experiments were performed. After assembling the system, it was first tested without purifiers on it, after which, the Engohang-Kanyarusoke solar water purifiers were mounted on it, and then the experiments were performed. Only four Engohang-Kanyarusoke solar water purifiers were available to be mounted on the pillar although the tracking system was designed to take up to six solar water purifiers. A fifth one was used as a control non-tracking purifier and was ground-mounted. All experiments were performed at Bellville campus of CPUT, Cape Town South Africa on 10 consecutive days.

Optical and thermodynamic analyses were done and comparisons made. In this modelling, use is made of solar radiation, ambient temperature and wind speeds data from the weather station at the top of the Mechanical Engineering building. The Perez model of diffuse radiation as used by Kanyarusoke, (2017) in his doctoral thesis is used to determine the total solar radiation actually entering the water purifiers at any one time during the day. The main comparison parameters here are the thermodynamic efficiencies of the tracking and non-tracking systems.

4.1 TESTING APPARATUS AND MEASURED DATA

The following apparatus were used to carry out the experiment.

a) The pillar solar tracking system was used as the main apparatus where the four Engohang-Kanyarusoke solar water purifiers were mounted. The tracking system was

then set to rotate intermittently 15° every hour following the sun throughout the day, and then moving back to its initial position at the end of the day.

Figure 4.1: Pillar solar tracking system

b) Weather station

A Campbell-Scientific weather station installed at the department was used to monitor and log solar radiation and other weather data during the experiments. The weather data recorded during the experimental period consisted of: wind speed, total solar radiation on a horizontal plane, diffuse radiation and the ambient temperature. The weather station (figure 4.2) consists of a pyranometer to measure the total solar radiation (diffuse and beam), a pyranometer with a shading ring to measure the diffuse radiation and the cup anemometer to measure wind speed. All these equipment were connected to a Data logger.

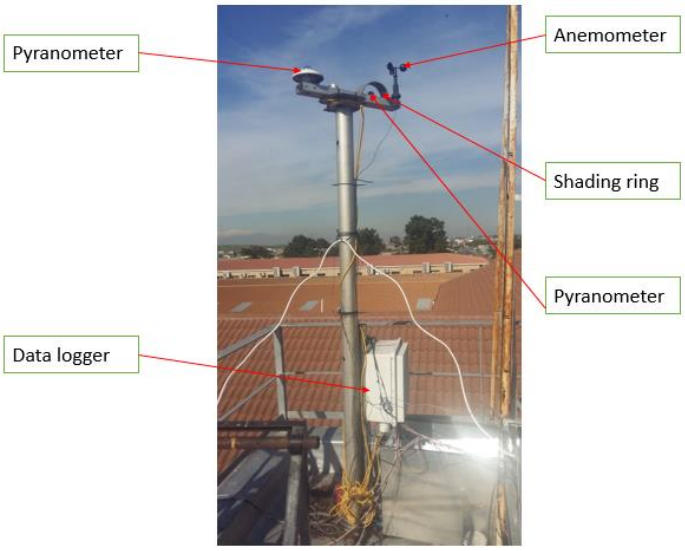

Figure 4.2: Scientific Campbell weather station

❖ Wind speed

The wind speed was measured by using the 030101 R.M young three cup anemometer which measures the horizontal speed of the wind. As the wind is blowing it rotates the three cups on the anemometer which then produces the AC sine wave voltage with a frequency that is proportional to the wind speed. The data logger shown in figure 4.2 is connected to the cup anemometer as in figure 4.3. It measures the pulse signal and then converts it to speed in m/s. Detailed technical specifications of the 03101 R.M cup anemometer are given in Appendix B.

Figure 4.3: Cup anemometer
(Wind et al., 2017)

❖ Solar radiation measurement

Diffuse solar radiation was measured using a Kipp & Zonen SP-LITE silicon Pyranometer integrated with a shading ring to shade the instrument from beam radiation. It consists of a of a photodiode complete with housing and cable. The circuit includes a shunt resistor for the photodiode in order to generate a voltage output. The SP-LITE has a spectral range of 400 to

range of 400 to 1100 nm. See appendix B for technical specification of the pyranometer. Figure 4.4 shows the Kipp & Zonen SP-LITE silicon Pyranometer.

Figure 4.4: Kipp & Zonen SP-LITE silicon pyranometer

https://www.campbellsci.com.au/splite2

Total solar radiation intensity was measured using a Kipp & Zonen CMP06 type pyranometer. The pyranometer consists of a series of 64 thermocouples junctions connected in series of sensing element and has a high quality blackened thermopile (detector) protected by a double glass dome. Its flat spectral sensitivity, from 285 to 2800 nm, makes it ideal for measuring natural sunlight and it is most usually used to measure solar radiation being received on the horizontal plane. This pyranometer produces a millivolt signal that is measured directly by a Campbell Scientific control data logger. Figure 4.5 shows the Kipp & Zonen CMP6 Pyranometer.

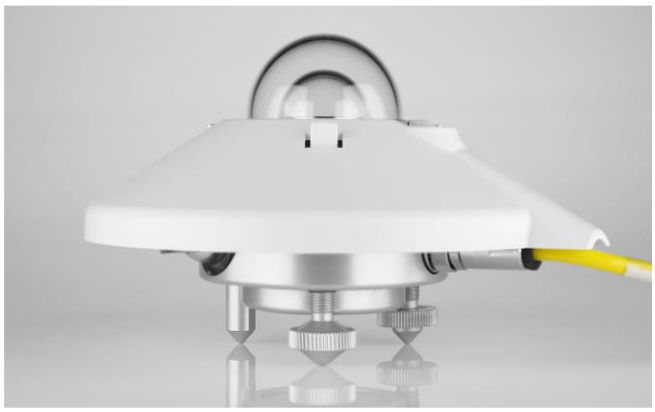

Figure 4.5: Kipp & Zonen CMP6 Pyranometer

https://www.campbellsci.com.au/splite2

- Ambient temperature

Ambient temperature was measured with air temperature sensor (109 Temperature Probe) mounted on the scientific Campbell weather station on the top. The 109 Temperature

Probe consists of thermistor encapsulated in an epoxy-filled aluminium housing. The sensor`s wires are connected to the data logger where the data is logged in.

e) Stills temperatures

The Reed TP-01 K Thermocouples wire probe were used to measure the vapour and the glass temperature of the solar water purifiers. The data were read with the center 307/308 min thermometer that has a range of -200`C to 1370`C which is shown in figure 4.7. Figure 4.6 shows the Reed TP-01 K Thermocouple wire probe;

Figure 4.6: Reed TP-01 K Thermocouple wire probe

https://www.staples.ca/en/Reed-TP-01-Type-K-Thermocouple-Wire- Probe/product_992084_1-CA_1_20001

Figure 4.7: Center 307/308 mini thermometer

http://www.dpstar.com.my/our-products/instrument-control-cables-and-heating-cables/center/mini-thermometer-center-307308/

An Analog thermometer was inserted into the water where the reading of the temperature of the water was read directly from the Analog thermometer which is shown in figure 4.8.

Figure 4.8: Analog water thermometer

a) Yield

A 300mm ruler and five measuring cylinders were used to measure the yields from the solar water purifiers after every hour during the period of the experiment.

4.2 EXPERIMENTAL SET-UP

The following points were followed to set-up the experiments;

- Two Reed TP-01 K Thermocouples wire probe were fixed on glazing of each of the five purifiers that were used for the experiments, the two thermocouples were used to measure the temperature of the glass and the vapour/ steam as shown in figure 4.9 on the fixed ground mounted solar water purifier/ non-tracking solar water purifier. The Analog thermometers were also inserted in each of the purifiers to measure the temperature of the water.

Figure 4.9: Non-tracking (Control) solar water purifier

- The solar purifier in figure 4.9 was ground-mounted on a stand facing north throughout the experimental period.
- Four Engohang-Kanyarusoke solar water purifiers sizes where mounted on the pillar with all the thermocouples attached on the purifiers as explained for the fixed one.

Figure 4.10 shows the Engohang-Kanyarusoke solar water purifiers mounted on the pillar;

Figure 4.10: Solar purifiers mounted on the pillar

- On each purifier a two litter battle was placed were the water will be collected and measured from the purifiers.

4.3 TESTING PROCEDURE

The experiments where performed at CPUT, Bellville, Cape Town, South Africa from 29th May to 7th June 2018. This experiment data were recorded for 10 consecutive days with the tracking system set to rotate automatically in an East-West at steps of 15 degrees every hour and the data recorded hourly.

The five solar water purifiers were fed with 15 litres of tap water each on the first day of the experiment on the 29th of May 2018. After which, two litres of water was been fed in the solar stills from the 30th of May 2018 every day until the last day of the experiment. This was done every morning before sunrise. The tap water was the only water used as the study did not concern the type of water that was being fed into the solar stills, since this had already been accomplished by the previous researchers (Mbadinga, 2015, Engohang 2018). This study's main concern was only about the amount of yields from and the amount of space taken up by the solar purifiers.

4.4 Solar incidence and radiation entering the glass/glazing

The weather data that was obtained during the experimental period from the weather station only shows the solar radiation on the horizontal surface. The total incident solar radiation on a sloped/ titled panel is represented by $\mathbf{G_{panel}}$**.** The incident radiation equation was developed by Perez, which consists of three different spatial distributions according to Duffie & Beckman

(2013), which are beam radiation, diffuse radiation, and the ground reflected radiation. The solar incident radiation calculations were done on Matlab®. The solar incident radiation is found by the following equation;

$$G_{panel} = G_{bh}R_b + G_d(1-F)\left(\frac{1+COS\beta}{2}\right) + G_d F_1 \frac{a}{b} + G_d F_2 \sin(\beta) + G_h \rho_g \left(\frac{1-COS\beta}{2}\right) \quad 4.1$$

a and b in equation 4.1 are the terms that account for angles of incidence of the sun tilted on a horizontal surface. The unknown terms of a and b are found by the equations below;

$$a = \max(0, cos\theta_i) \quad 4.2$$

$$b = \max(cos85°, cos\theta z \quad 4.3$$

F_1 and F_2 in equation 4.1 are brightness coefficients factors and according to Duffie & Beckman (2013), "the factors are functions of three parameters that describe the sky conditions, zenith angle, clearance ε, and brightness Δ". G_d is the diffuse radiation and the normal incidence beam radiation is represented by $G_{b,n}$. The equation below shows how the clearance parameter is found;

$$\epsilon = \frac{\frac{G_d+G_{b,n}}{G_d}+5.535\times10^{-6}{\theta_z}^3}{1+(5.535\times10^{-6}{\theta_z}^3)} \quad 4.4$$

The incidence beam radiation is given by the following equation;

$$G_{b,n} = \frac{G_b}{cos\theta_z} \quad 4.5$$

The brightness factor, air mass, G_{on} extraterrestrial normal-incidence radiation and brightness coefficients F_1 & F_2 factors are computed as follows;

$$\Delta = m\frac{G_d}{G_{on}} \quad 4.6$$

$$m = \frac{1}{cos\theta_z} \quad 4.7$$

$$G_{on} = G_{sc}(1 + 0.3cos\frac{360n}{365}) \times cos\theta_z \quad 4.8$$

$$F_1 = \max\left[0.\left(f_{11} + f_{12}\Delta + \frac{\pi\theta_z}{180}f_{13}\right)\right] \quad 4.9$$

$$F_2 = \left(f_{21} + f_{22}\Delta + \frac{\pi\theta_z}{180}f_{23}\right) \quad 4.10$$

The beam radiation on a tilted surface is determined by multiplying direct horizontal radiation by the geometric factor R_b ($G_{Tb}=G_bR_b$). The beam radiation ratio on a titled surface is shown by symbol R_b which is shown by equation 4.2 were by $G_{b`}$ is the flux beam radiation incident on the tilted surface and G_b is flux beam radiation on the horizontal surface.

$$R_b = \frac{G_{b`}}{G_b} = \frac{cos\theta_i}{cos\theta_z} \quad 4.11$$

$cos\theta_i$ and $cos\theta_z$ are determined by the following two equations;

$$COS_{\theta_i} = \cos(L+\beta)COS\delta COS\omega + \sin(L+\beta)sin\delta \quad 4.12$$

$$COS_{\theta_z} = \cos Lcos\delta cos\omega + sinLsin\delta \quad 4.13$$

Were by L is the latitude of the location and β is the tilt angle

The δ declination angle is calculated by using the following equation;

$$\delta = 23.45\sin(360\frac{284+n}{365}) \quad 4.14$$

Were n is the number of the day of the month that can be found in table 4.3 and ω is the angle hour which is found by equation 4.15.

$$\omega = 15(t - t_{noon}) \quad 4.15$$

$$Equation\ on\ time = 9.87sinB - 7.53cosB - 1.5sinB \quad 4.16$$

$$B = (n-81)(\frac{360}{365}) \quad 4.17$$

Table 4.3: Average days of different months with the values of n (Duffie & Beckman, 2013)

Month	*n* for *i*th Day of Month	For Average Day of Month		
		Date	*n*	δ
January	i	17	17	−20.9
February	$31 + i$	16	47	−13.0
March	$59 + i$	16	75	−2.4
April	$90 + i$	15	105	9.4
May	$120 + i$	15	135	18.8
June	$151 + i$	11	162	23.1
July	$181 + i$	17	198	21.2
August	$212 + i$	16	228	13.5
September	$243 + i$	15	258	2.2
October	$273 + i$	15	288	−9.6
November	$304 + i$	14	318	−18.9
December	$334 + i$	10	344	−23.0

Figure 4.11 shows the different types of solar radiation that enter the glazing that were shown on the previse page and the energy transfers that will be discussed in section 4.5.

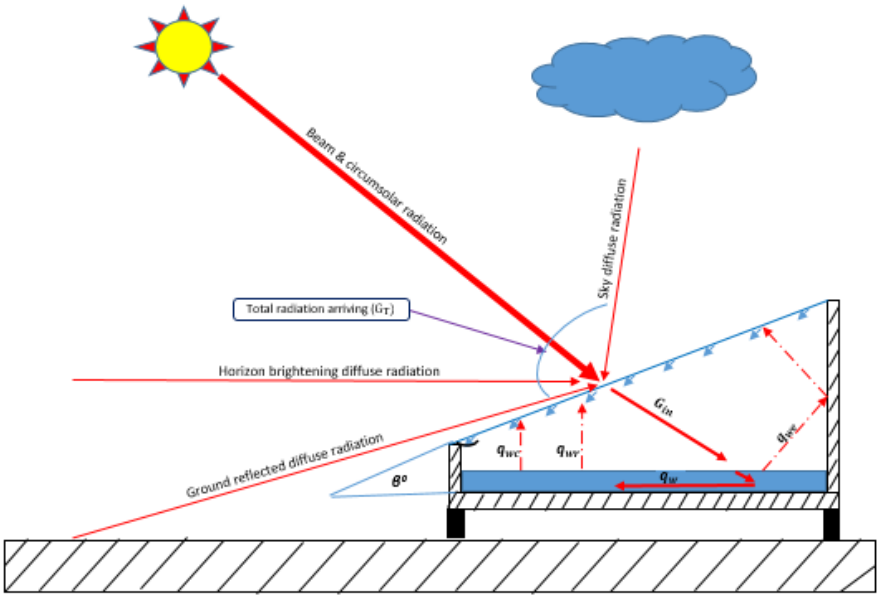

Figure 4.11: Solar radiation entering the still from the outside and energy transfer inside the still

4.5 Solar purifiers efficiencies of the tracking and non-tracking systems

The solar purifiers efficiencies were calculated by using the efficiency formulas as they are used by (Kanyarusoke., 2018)

The optical efficiency was calculated by using the following equation 4.18, whereby the G_{gl} is the total solar radiation entering the glazing of the solar purifier and G_{in} is the total solar radiation entering the solar purifier from the glazing.

$$\eta_{optical} = \frac{G_{in}}{G_{gl}} \quad 4.18$$

The sensible heat efficiency is the amount of heat obtained to heat up the water, it was calculated by using equation 4.19 below, whereby the m_w is the amount of water that was in the solar purifier in the morning at beginning of the experiment; *h* is the enthalpy of the water. The energy incident was found by integrating the area (from 8 am to the time were the water attains its maximum temperature) under the AG_{gal} vs time graph.

$$\eta_{sensible} = \frac{m_w(h_{max} - h_{8am})}{Energy\ incident\ up\ 11am} \quad 4.19$$

The efficiency of the solar purifiers were found by using equation 4.20 whereby m is the mass of water collected, h_{fg} is the latent heat of evaporation of the water in the basin of the still and the energy incident on the glazing is A_gIG_{gl} were by A_{gl} is the area of the glazing and G_{gl} is the total solar radiation coming on to the tilted solar purifier glazing.

$$\eta_{solar\ still} = \frac{mxh_{fg}}{Energy\ incident\ on\ glazing} \quad 4.20$$

$$h_{fg} = 2.4965 \times 10^6 \times [1 - 9.4779 \times 10^{-4}T + 1.3132 \times 10^{-7}T^2 - 4.7979 \times 10^{-9}T^3] \quad 4.21$$

CHAPTER FIVE
TEST RESULTS AND DISCUSSION OF RESULTS

5.1 INTRODUCTION

This chapter gives and discusses the results obtained from the experiments of chapter 4. The results are: The distillate yields obtained from the ground-mounted (control) still with a glazing area of 1.5 m^2 (slope β=30º), tracking still one & four with the glazing area of 1.5 m^2 (slope β=36.8º), tracking still two 1.5 m^2 (slope β=30º), tracking still three 1.5 m^2 (slope β=45º) and the weather data obtained from the weather station.

5.2 SOLAR PURIFIER'S PERFORMANCE

The ground-mounted solar water still and the pillar-mounted purifiers were tested from 29 May to 07 June 2018. The experiments were perfumed for 10 consecutive days with the data logger switched on from the 29th May 2018 at 11:00 due to battery changing. The 31st of May and 3thd of June were selected as the typical good days that are discussed in detail while the other data are presented in Excel graphs.

5.2.1 Experimental data on 31 May 2018

5.2.1.1 Meteorological conditions

Figure 5.1 shows the variations of the weather conditions with respect to time on 31 May 2018 (day 3), it can be observed that higher ambient temperature occurred peaking from noon (12:00) reaching the maximum of 19.06 ºC with a wind speed of 6.445 m/s at 14:00. The maximum wind speed was 7.683 m/s, observed at 13:00. It can also be seen that the wind speed was fluctuating throughout the day. The ambient temperature started decreasing from 14:00 with the wind speed starting to decrease from 15:00 to 16:00 and increasing from 17:00. Furthermore, it can be observed that the total horizontal solar radiation increased with ambient temperature. The maximum radiation was at noon. Further, the horizontal plane solar radiation had the same trend as the beam solar radiation with its peak observed at noon, with the maximum total horizontal solar radiation of 387.2 W/m^2 and the solar beam radiation of 332.59 W/m^2. It was further seen that during the day the solar beam radiation was higher than the solar radiation diffuse throughout the day. This can only be true because when it is sunny most of the solar radiation is beam and the diffuse solar radiation only consists of about five to twenty per-cent of the horizontal solar radiation (Kanyarusoke, 2017a). See Appendix C for the meteorological conditions readings obtained from the weather station.

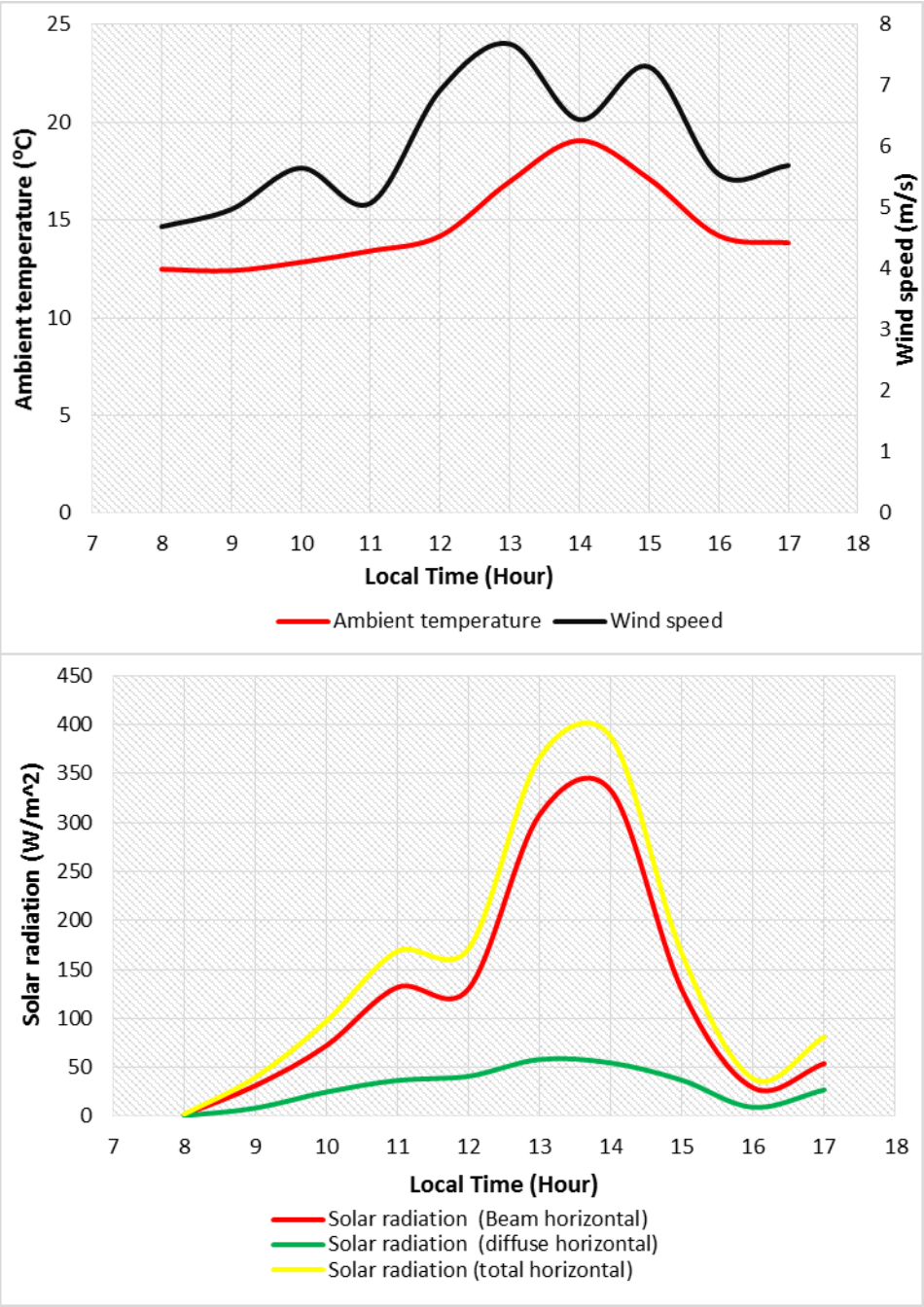

Figure 5.1: Variation of weather condition on 31 May 2018 at Cape Peninsula University of Technology, Bellville, Cape Town South Africa

5.2.1.2 Solar stills performance

The total solar radiation obtained on the glazing on ground-mounted still and the tracking stills were computed by using the formulas in chapter four by using the Perez model equation, programmed in Matlab®. The variation of the total horizontal solar radiation, ground-mounted still and tracking stills are shown in figure 5.2. It can be seen that the total horizontal solar radiation was low throughout the day compared to that on the tilted surfaces as earlier computed by Kanyarusoke etal. (2012). It can be observed that the tracking stills obtained a

high amount of solar radiation throughout the day compared to the ground-mounted still. It was also observed that stills peaked at 14:00, peak of solar radiation on the ground-mounted still 619.08 W/m^2, still no. one & four 656.73 W/m^2, still no. two 622.92 W/m^2 and still no. three 686.2 W/m^2.

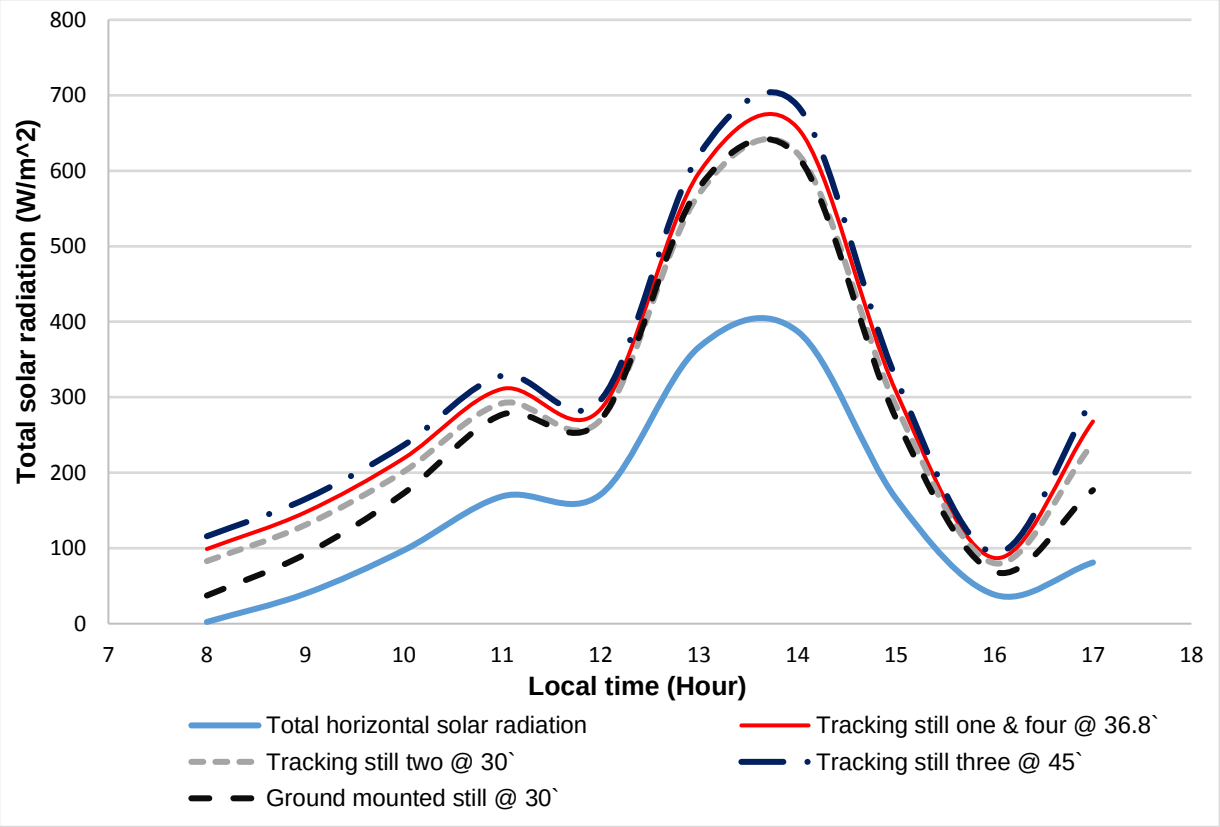

Figure 5.2: Variation of solar radiation on ground-mounted still and tracking stills on 31 May 2018

The water temperatures of the ground-mounted still and tracking stills were measured on the hourly basis as it is shown in figure 5.3. It can be observed that the water temperatures started peaking from 11:00 with the ground-mounted still with 33.5 ºC maximum obtained, still no. one 33.5 ºC, still no. two 37.25 ºC, still no. four 35.23 ºC and still no. three with 40 ºC during noon at 14:00. It can also further be seen that the ground-mounted still had lower water temperature throughout the day compared to the tracking stills this was because tracking stills were following the sun throughout the day while the ground-mounted still was fixed on one position. Which makes the solar tracking stills to have a high water temperature compared to the ground-mounted still.

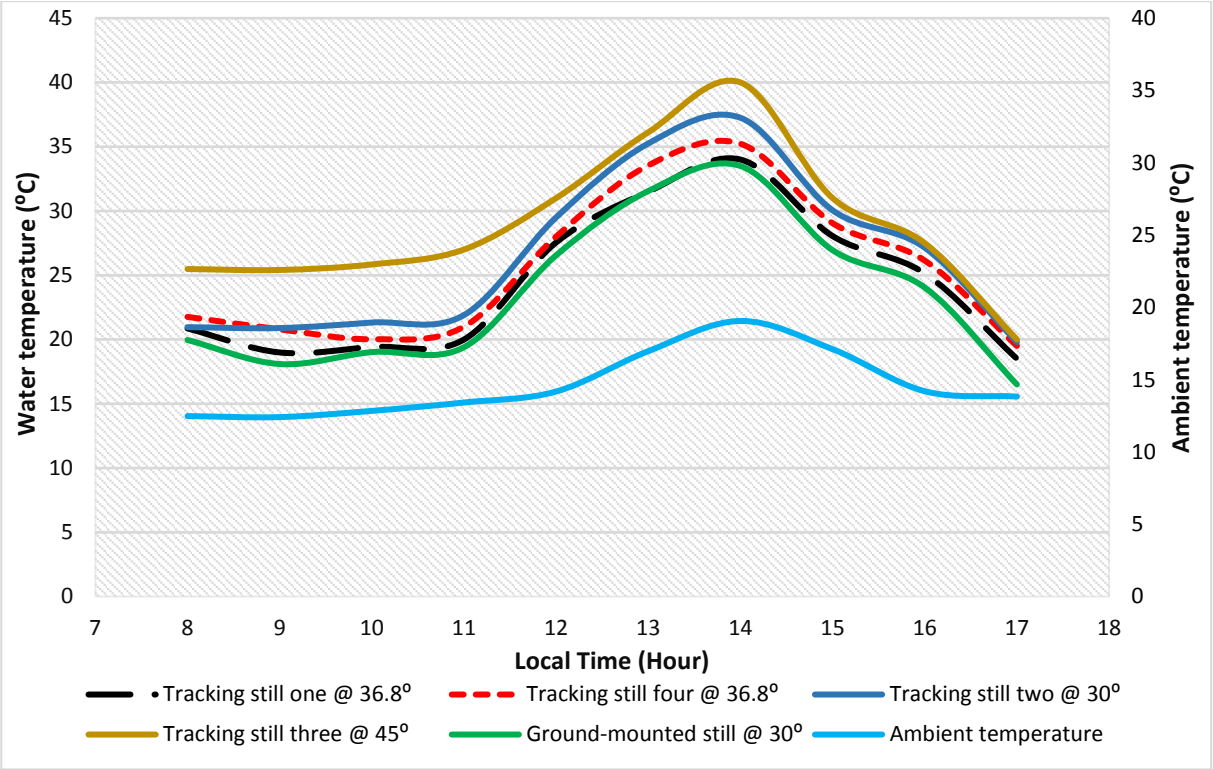

Figure 5.3: Variation of hourly water and ambient temperature obtained on 31 May 2018

The distillate yield was recorded on the hourly basis shown in figure 5.4 which shows the variation of the weather conditions and the distillate yield with respect to time. It can be seen from figure 5.4 that the distillate yield increases with the horizontal solar radiation and the ambient temperature with the highest peak obtained at 14:00. This is due to solar radiation and ambient temperature that are the driving force that increases the condensation of the still which then leads to high water yield production. The ground-mounted still obtained low distillate yield from 8:00 in the morning to 15:00 in the afternoon when compared to the tracking stills whereby it only outperformed still no. one & four after 15:00 in the afternoon. All the tracking stills distillate yield had the same trend as can be seen in figure 5.4 with its highest daily peak recorded at 14:00. The following distillate yield output were recorded for the day; ground-mounted 680 ml still, still no. three with 730 ml, still no. two 730 ml and still no. one 900 ml and still no. four 900 ml. This also shows a good agreement with the literature review in chapter two that solar tracking does increase the production yield of solar stills.

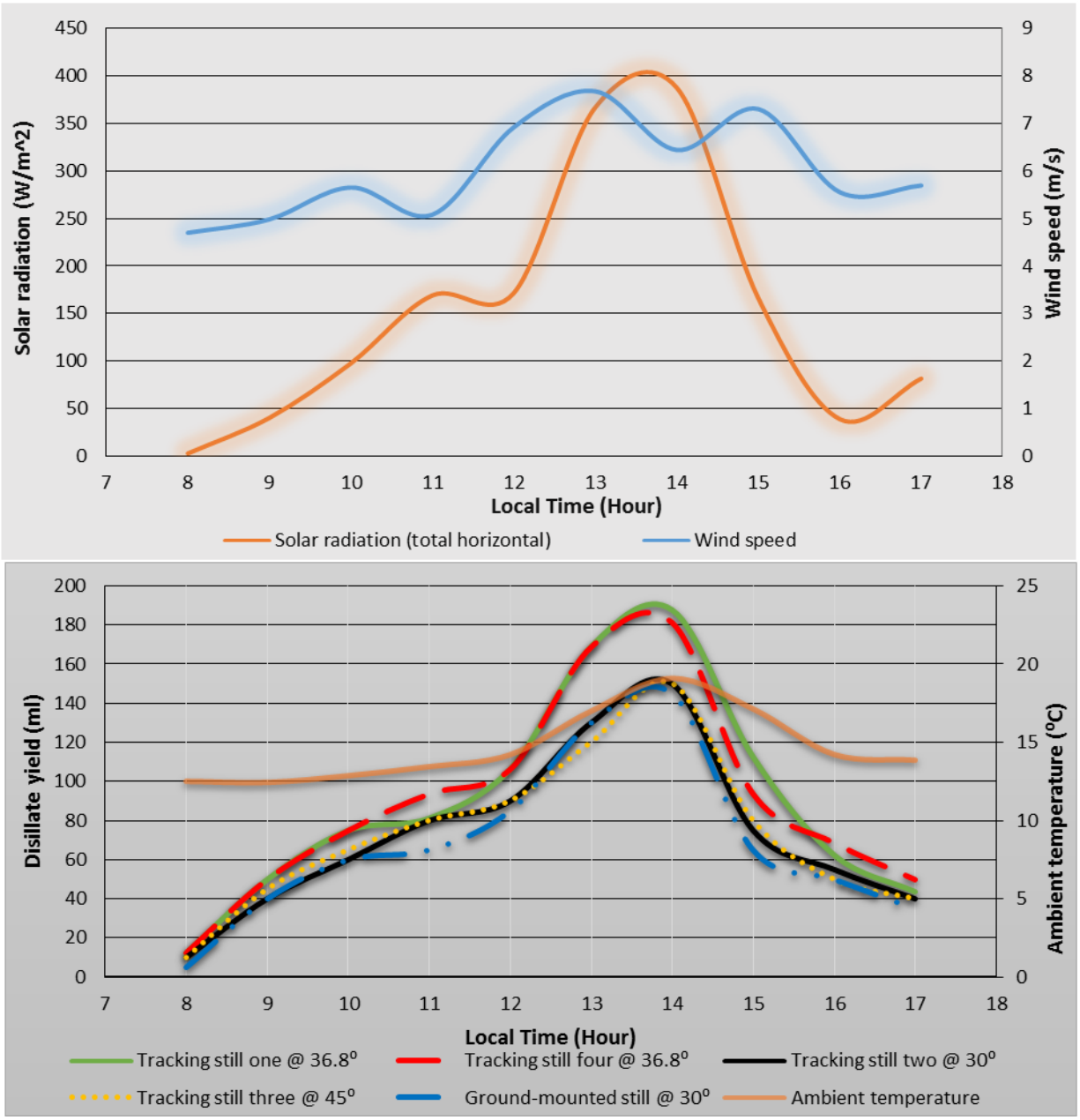

Figure 5.4: Variation of hourly weather parameters and distillate yields on 31 May 2018

The optical efficiencies of the stills obtained on 31 May 2018 where calculated by using the optical efficiency equation 4.18 in chapter four. It can be seen in figure 5.5 that the tracking stills had higher optical efficiency throughout the day when compared to the ground-mounted still. It can further be observed between the hours of 10:00 to 16:00 that the ground-mounted still, still no. three, and two had constant optical efficiencies throughout the stated time.

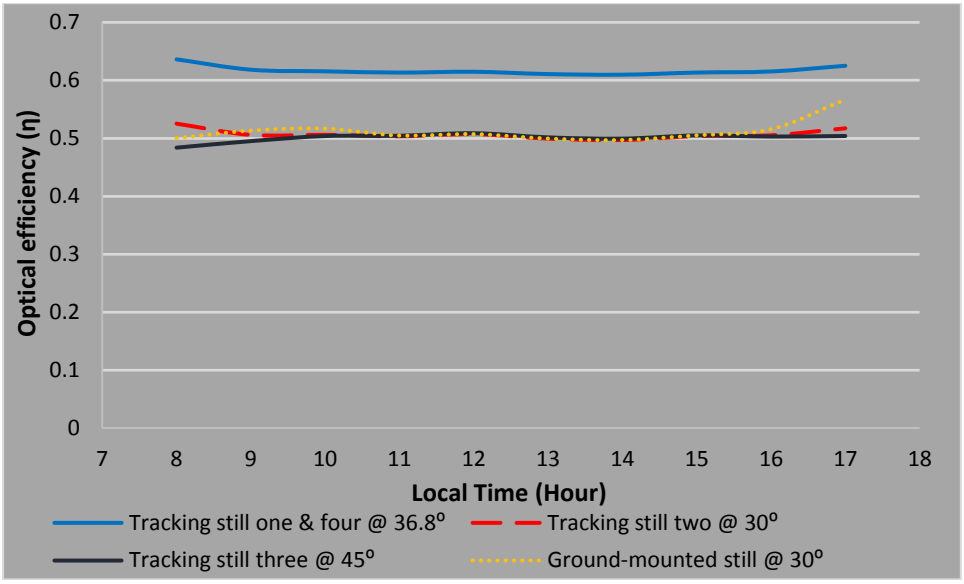

Figure 5.5: Variation of hourly stills optical efficiencies on 31 May 2018

Figure 5.6 shows the sensible heat efficiency obtained on 31 May 2018 it can be seen that the tracking stills had high sensible heat efficiency compared to the ground-mounted still. Tracking still two & four obtained the highest sensible heat efficiency for the day followed by tracking still one and three. Ground-mounted still obtained sensible heat efficacy of 38%. Hence, it can be said that tracking did increase the sensible heat efficiency of the tracking stills.

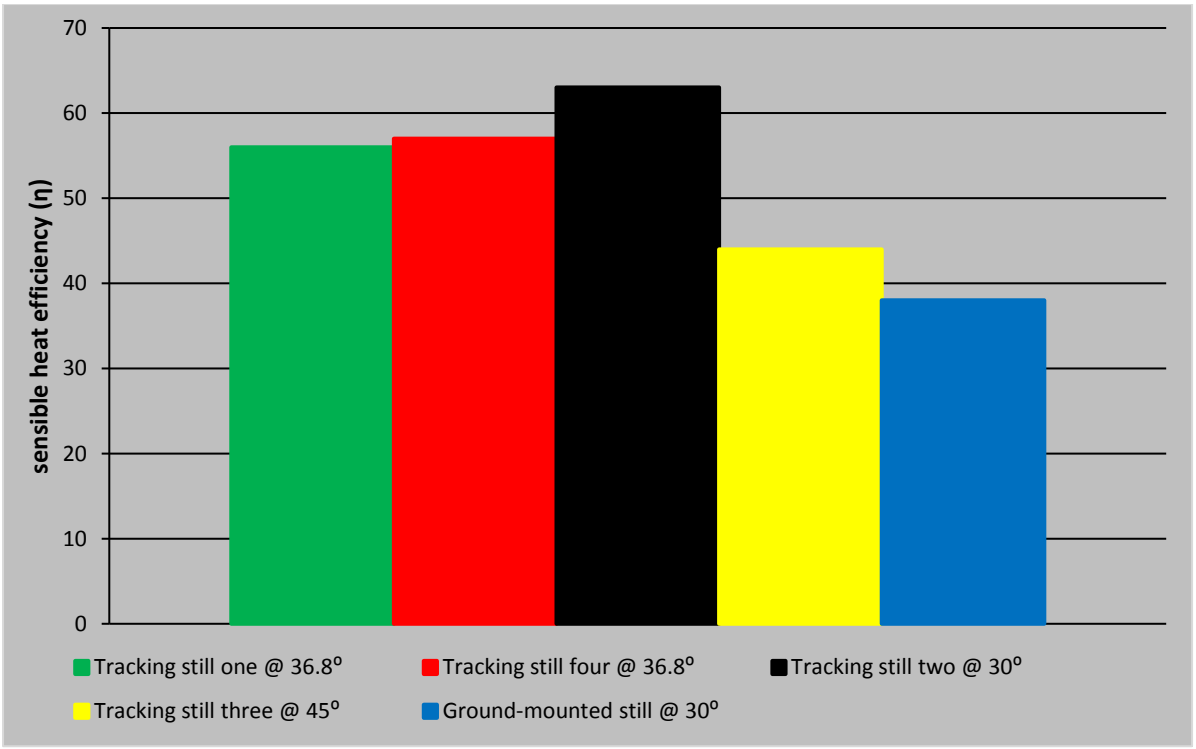

Figure 5.6: Variation stills sensible heat efficiency for the day 31 May 2018

The still efficiency is the energy used to heat and evaporate collected water divided by the total energy on the glazing which was found by using equation 4.20 in chapter four. It can be noticed that still no. 2 had a high distillate efficiency peak for the day compared to the other stills. Tracking still one & four had obtained a cumulative distillate efficiency of 20.2%, 20.4%, tracking still two with 21.8%, tracking still three 19.7% and the ground-mounted still with 20.9% distillate efficiency.

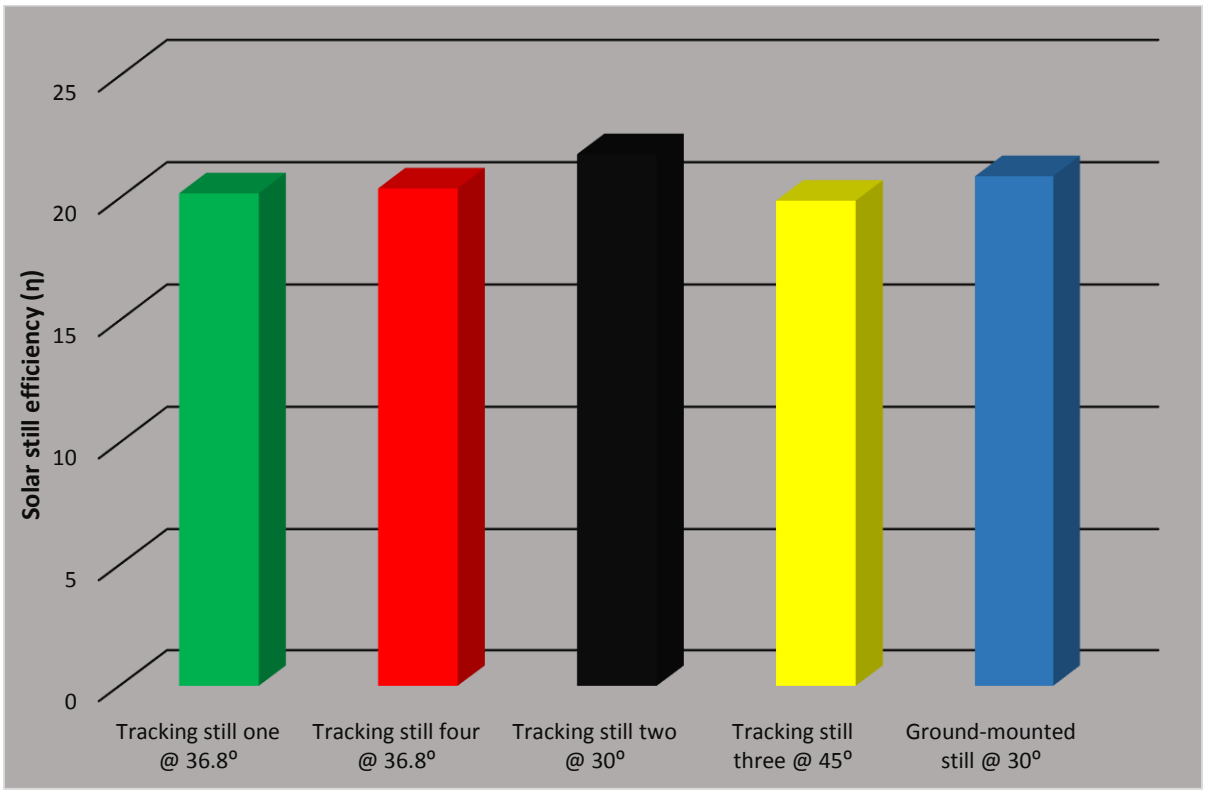

Figure 5.7: Variation stills distillate efficiency for the day 31 May 2018

5.2.2 Measured data on 3 June 2018

5.2.2.1 Meteorological conditions

The 3rd June 2018 was typical a good day during the experimental period taking into consideration that the experiments were performed during winter. The total solar radiation started peaking from 12:00 reaching a maximum of 583.8 W/m^2 at 13:00 and the beam solar radiation of 552.3 W/m^2 a high diffuse solar radiation of 105 W/m^2 was recorded in the evening at 17:00 this is usually because of cloudy conditions. It can also be observed in figure 5.8 that the ambient temperature of the day was relatively fair for the good typical winter day. The wind speed had the same trend as the ambient temperature and total solar radiation from morning 8:00 to 11:00 after then it was fluctuating throughout the day were by it reached its maximum speed of 5 m/s at 13:00. The diffuse solar radiation recorded for the day was relatively low when compared to the diffuse solar radiation recorded on day 3 in figure 5.1. See appendix C day 6 for the weather condition data of the day.

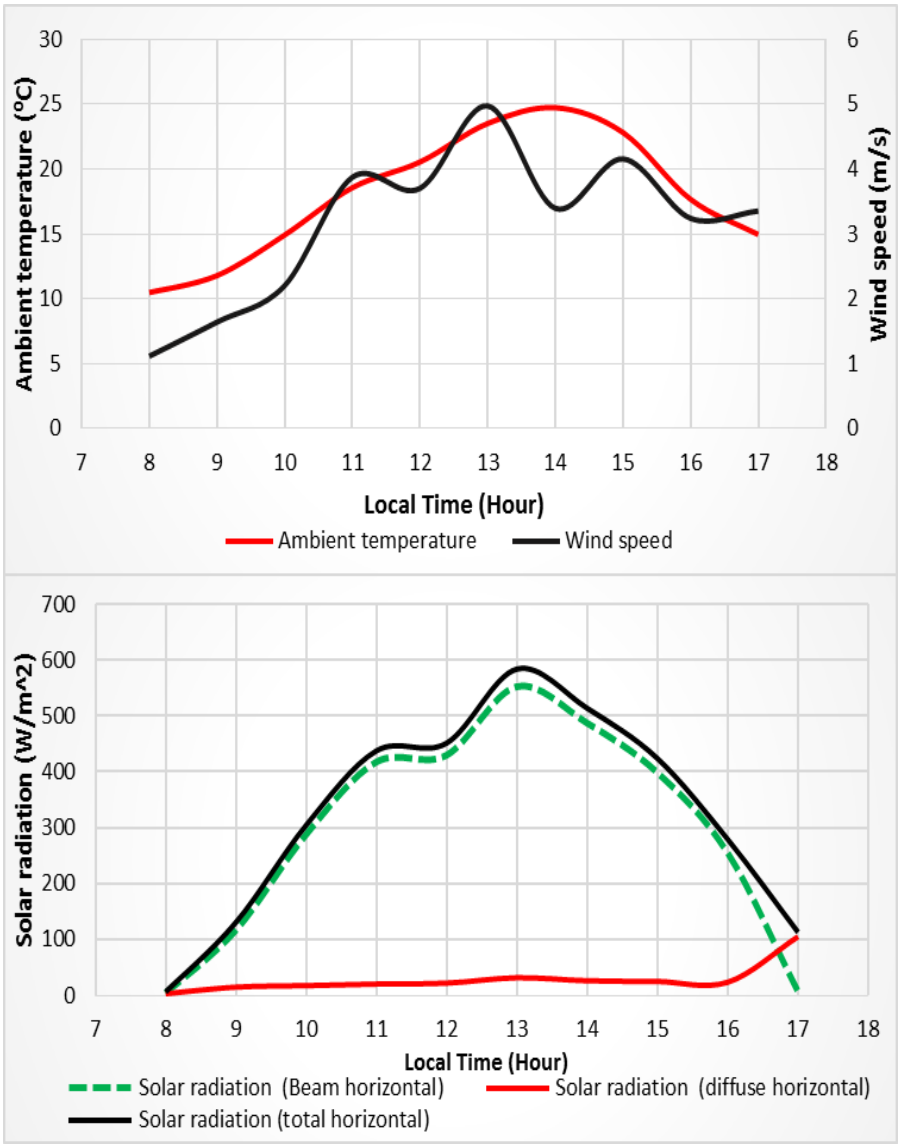

Figure 5.8: Variation of weather condition on 3 June 2018 at Cape Peninsula University of Technology, Bellville, Cape Town South Africa

5.2.2.2 Solar stills performance

Figure 5.9 shows the variation of solar radiation incidence on the ground mounted still and on the tracking still. All the total solar radiations were increasing sharply. It can be noticed that all the stills peaked at 13:00 during noon with the ground-mounted still with 945.72 W/m^2, still no. 1 & 4 with 997.4 W/m^2, still no. 2 945.72 W/m^2 and still no.3 with 1042.2 W/m^2. It can also be observed that throughout day 6 that the tracking stills obtained higher radiation then the ground mounted still.

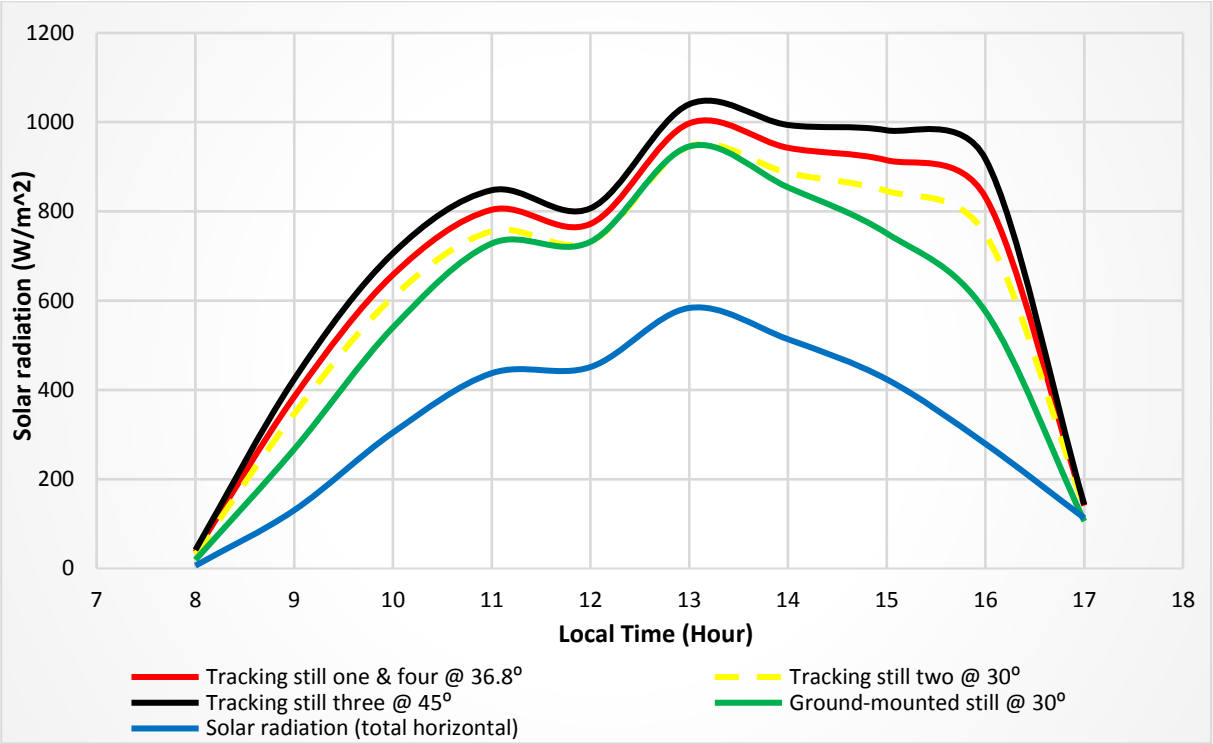

Figure 5.9: Variation of ground-mounted still total solar radiation and tracking stills on 3 June 2018

The variation of the water temperature of the stills and the ambient temperature is shown on figure 5.10 with still no. 2 attaining the maximum water temperature compared to all other stills. It can also be seen that the ground-mounted still had low water temperature throughout the day compared to the other stills.

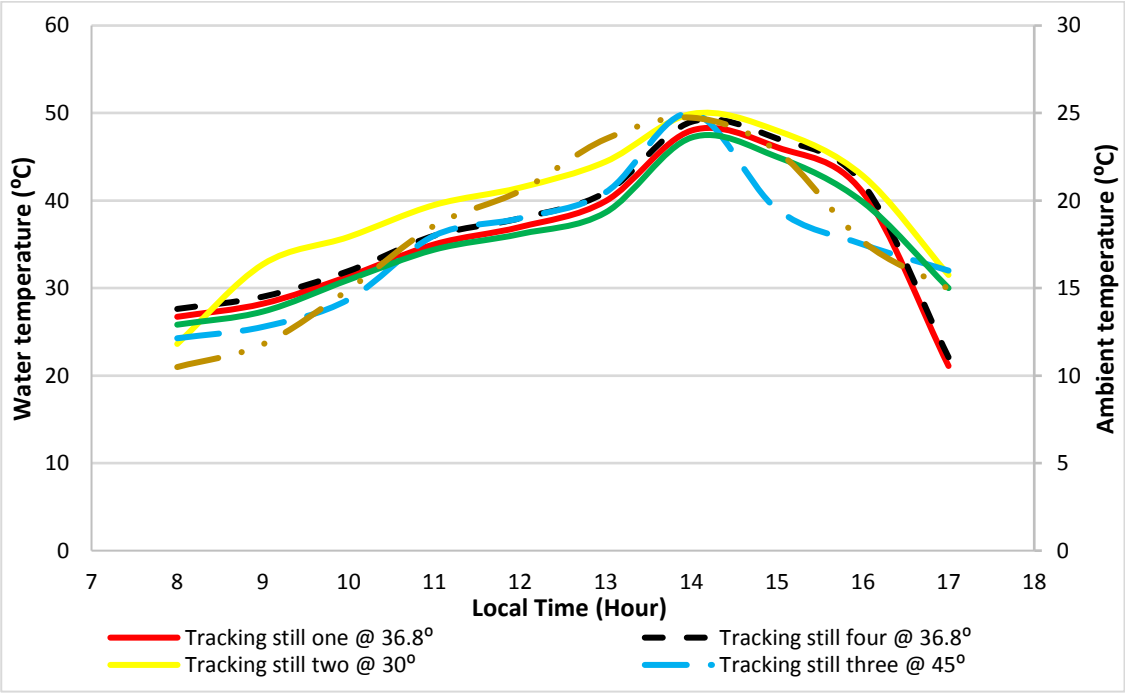

Figure 5.10: Variation of ground-mounted still total solar radiation and tracking stills on 3 June 2018

Figure 5.11 shows the climatic condition and the distillate yield with respect to time it can be observed that the distillate yield is proportional to the solar radiation. The day peaked with solar radiation maximum obtained at 14:00 with 544 W/m^2 and the maximum distillate yield of 3275 ml obtained from still no. 3 at the end of the day. It can also be seen that minimum distillate yield occurred in the morning and the evening hours where the solar radiation and the ambient temperature where low. The wind speed for the day was proportional to the distillate yield from the morning hours to 11:00 whereby the wind started to fluctuate until forenoon. The solar tracking stills had a high distillate yield throughout the day compared to the ground-mounted still this can only be true because the tracking stills where following the sun, all the solar stills peaked at 14:00.The following distillate yields were obtained for the day from each of the tracking stills, still no. 2 & 3 with 790 ml, still no. 1 with 1038 ml, still no. 4 with 3200 ml and ground-mounted still 1870 ml.

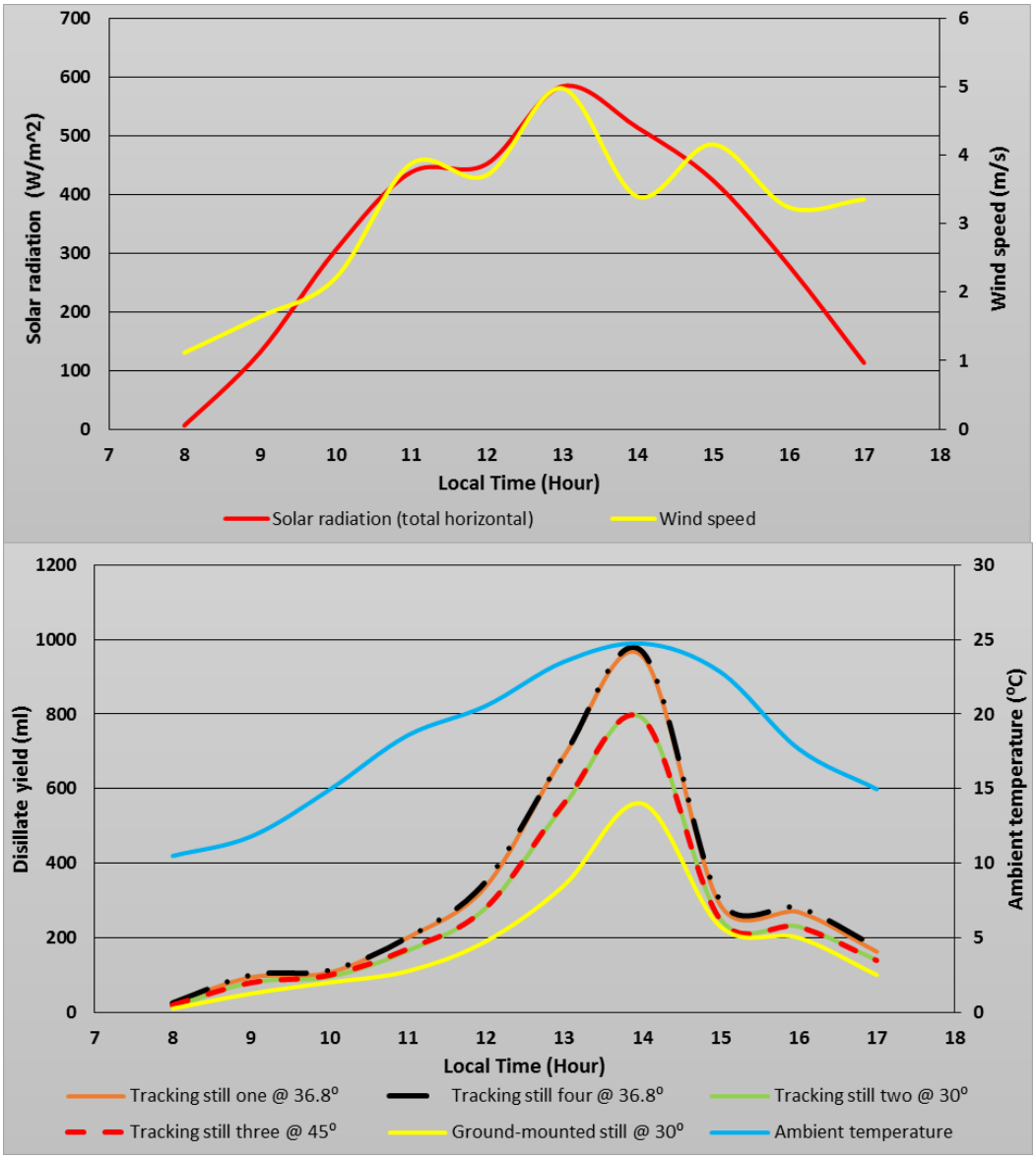

Figure 5.11: Variation of the hourly climatic condition and distillate yield on 03 June 2018

Figure 5.12 shows the variation of optical efficiencies on 03 June 2018. It can be seen that tracking still no. 1 & 2 had a high optical efficiency throughout the day compared to all the stills. Between 10:00 in the morning to 15:00 in the afternoon the optical efficiency was constant, and the highest peaks of the efficiency observed in the early morning and far noon.

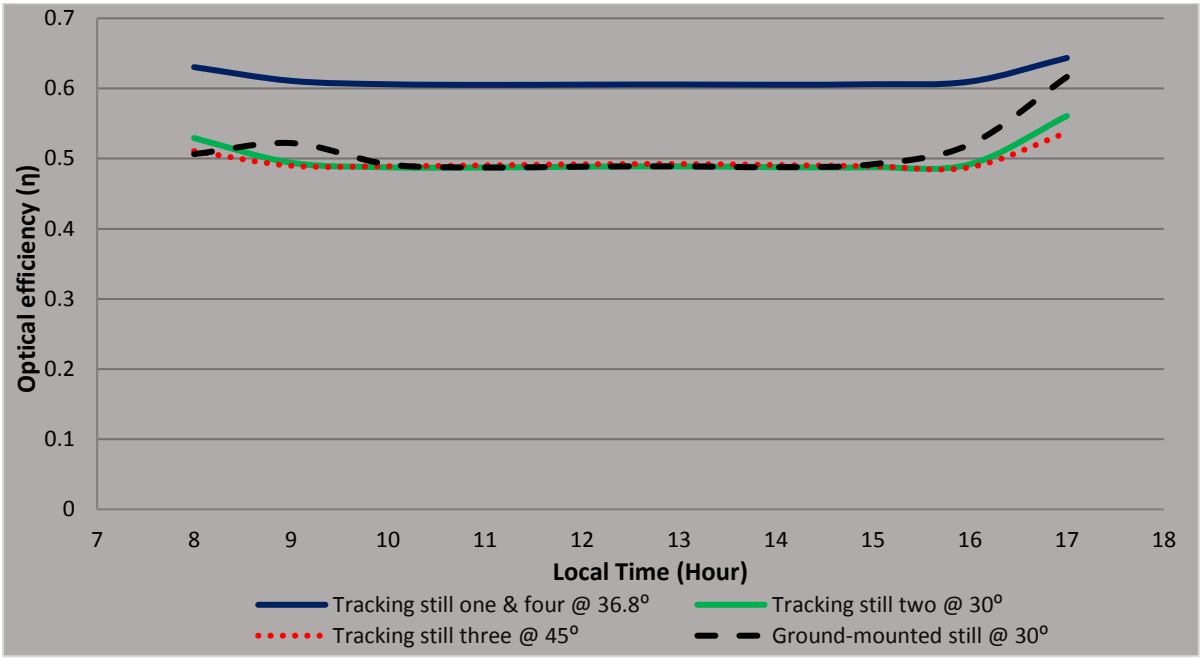

Figure 5.12: Variation stills optical efficiency for the day 03 June 2018

The figure 5.13 shows the variation of the stills sensible heat efficiency of 03 June 2018. It can be observed that the tracking stills had outperformed the ground-mounted. The still no. 1 & 4 had higher efficiency compared to all the other stills followed by still no. 3. This also shows that tracking has improved the efficiency of the tracking units.

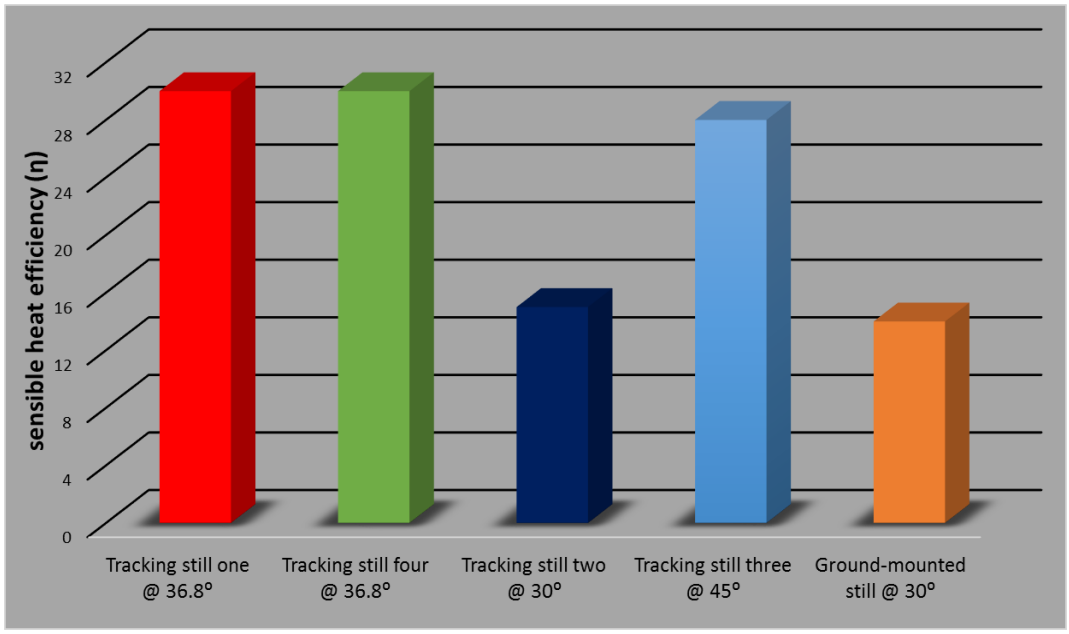

Figure 5.13: Variation stills sensible heat efficiency for the day 03 June 2018

The highest distillate efficiency was obtained from tracking still two with the numerical efficiency of 53.33%. The ground-mounted still had the lowest distillate efficiency for the day with 37.86%. See figure 5.14 for the variation of the distillate efficiency for day 6 (03 June 2018).

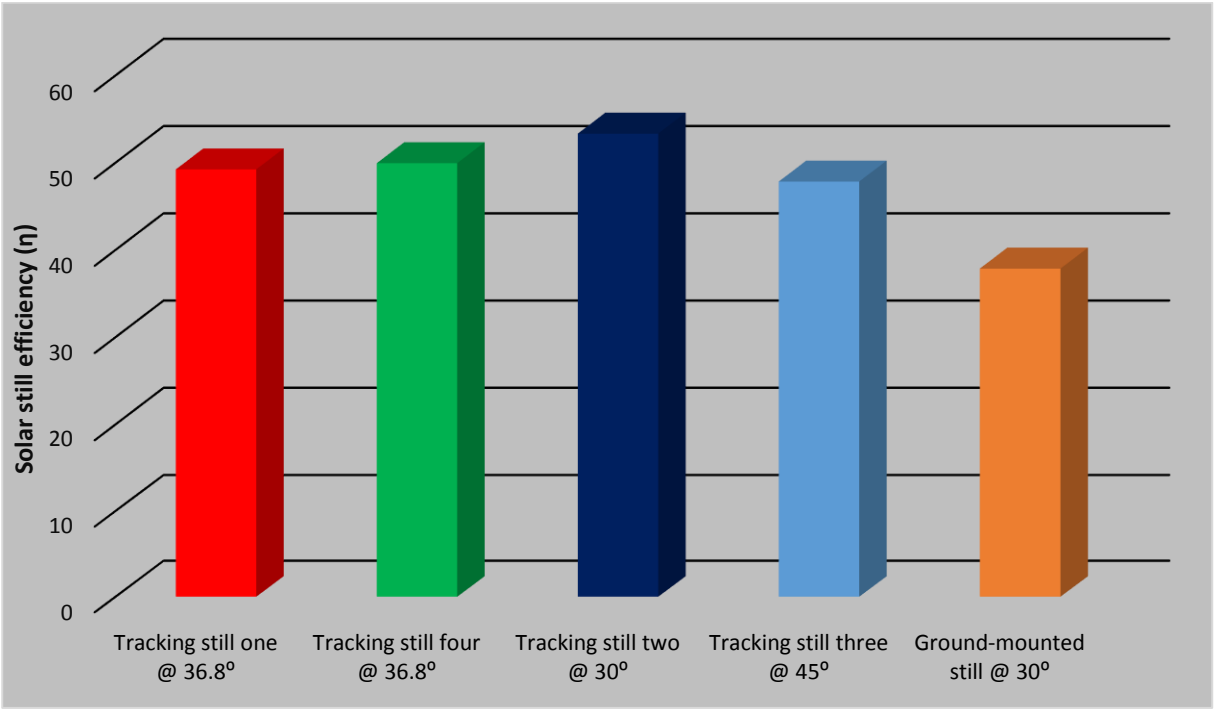

Figure 5.14: Variation stills distillate efficiency for the day 03 June 2018

5.2.3 Experimental data for the 10 days period

5.2.3.1 Meteorological conditions

The variation of the 10 days climatic conditions data were plotted on 3D Matlab® graphs. Figure 5.15 shows the total horizontal solar radiation and the diffuse horizontal solar radiation that was recorded during the experimental period. It can be seen from both graphs that the first 5 days had t fluctuating solar diffuse radiation and total horizontal solar radiation. High horizontal total solar radiation was obtained between day 6 and 7. It can also be seen that total horizontal solar radiation had a high peak yield between the hours of 12:00 to 14:00 of day 6 to 9. Minimum diffuse solar radiation can be observed to have occurred during the period when the maximum total horizontal solar radiation was obtained this was because of the clear sky during that period. Maximum diffuse solar radiation can be seen on the 3D graph to have occurred in the evenings (18:00) during the period of the experiment with a high peak yield recorded on day 1 and between days 5 to day 9. The high solar diffuse radiation was caused by cloudy conditions and also because of the sunset in the evenings. Refer to Appendix C for the total horizontal solar radiation and diffuse solar radiation data obtained during the experimental period.

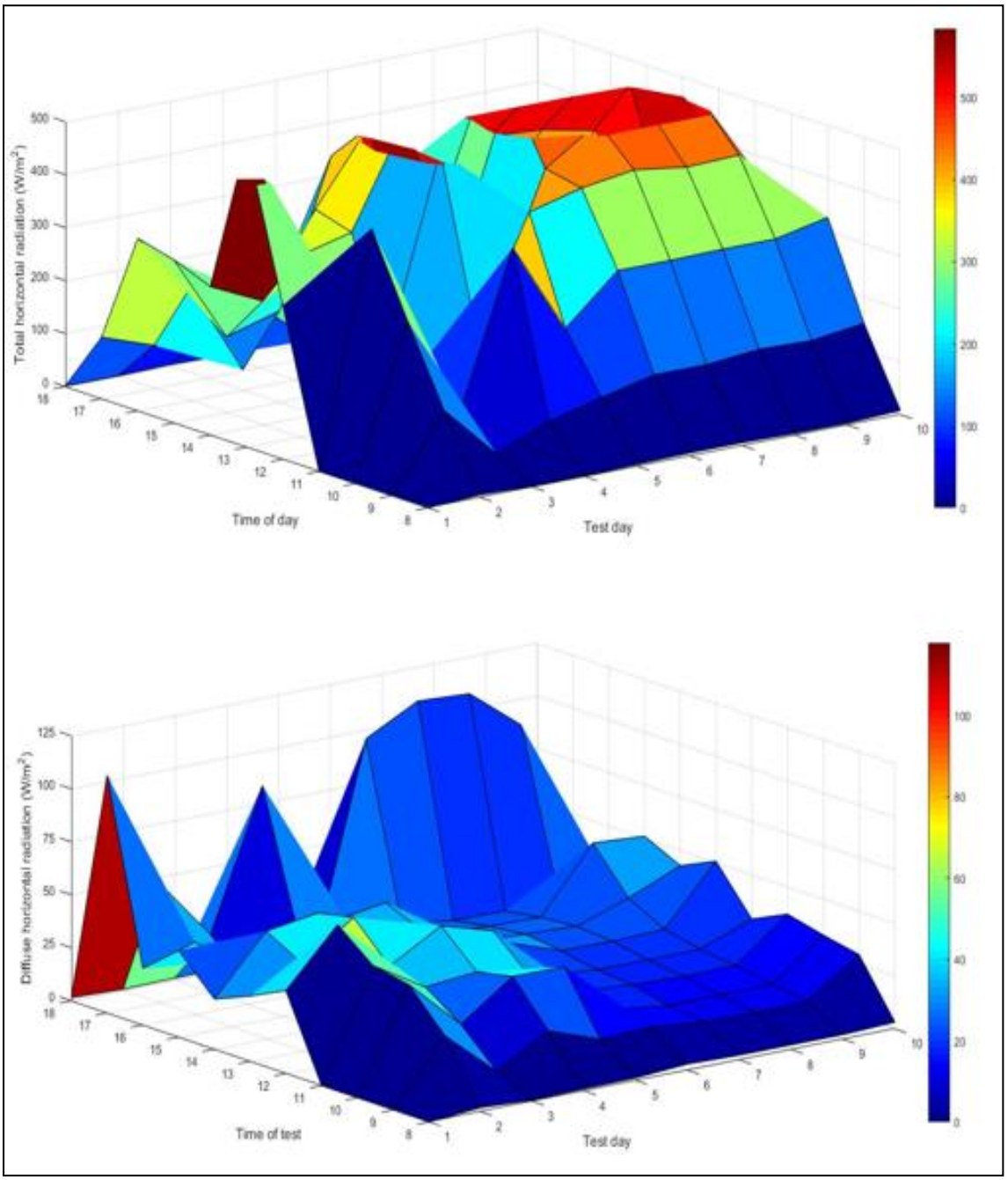

Figure 5.15: Variation of total horizontal solar radiation and diffuse solar radiation of test days

The wind speed, ambient temperature with respect to time and days is shown in figure 5.16. It can be observed that the wind speed was fluctuating during the duration of the experimental period between the speeds of 0.27 m/s to 8.77 m/s and the ambient temperature fluctuated between days 1 to 7 between 10.49 ºC to 30.26 ºC temperature. It can be seen that the wind speed was low between days 8 to 10 whereby the ambient temperature was high and the peak yield observed between 12:00 to 14:00 during the period of noon. The minimum peak yield of the ambient temperature occurred during the morning and evening hours. Maximum wind speed peak yield can be observed to have occurred on day 6 from forenoon to the evening. See Appendix C for the detail wind speed and ambient temperature.

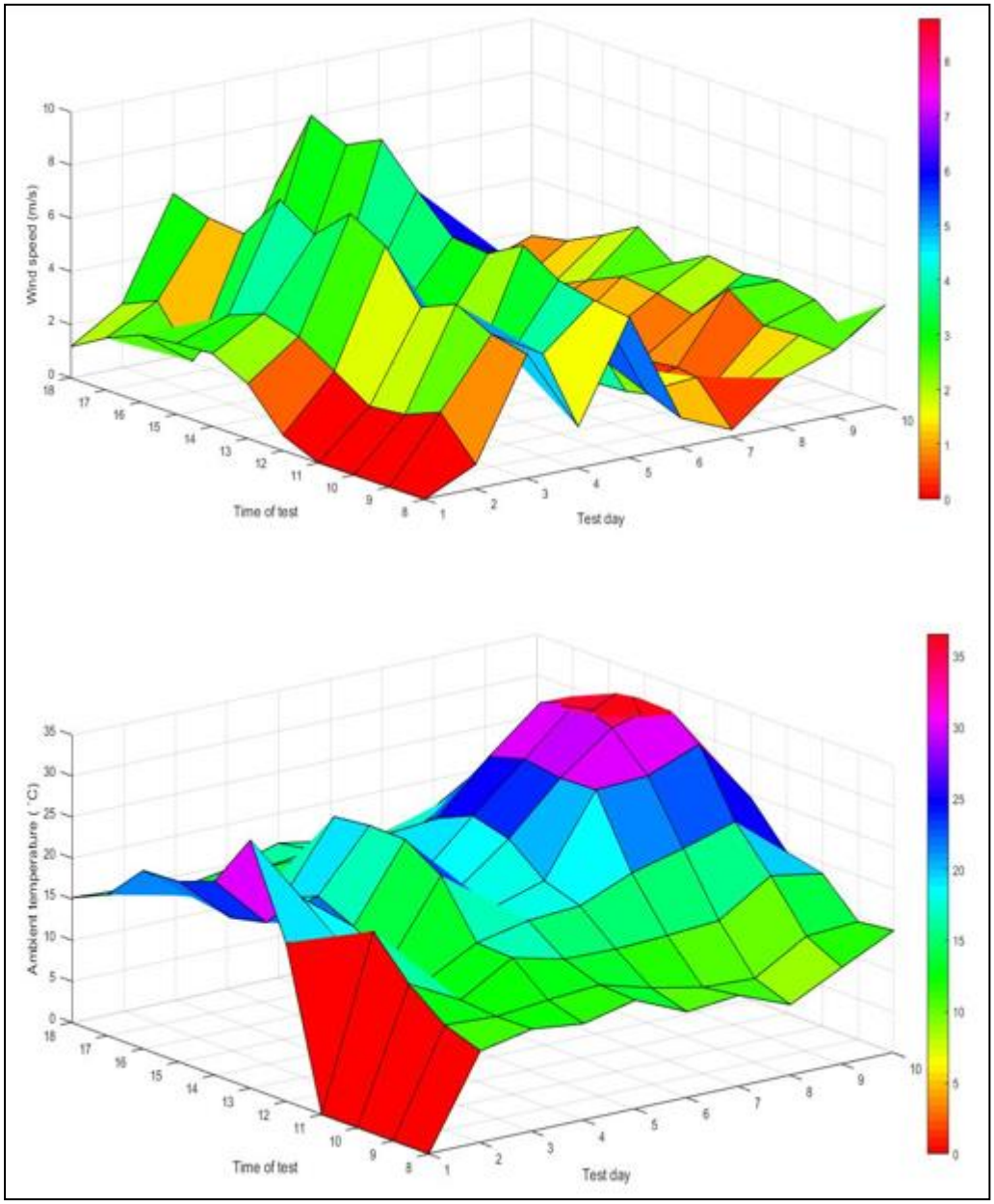

Figure 5.16: Variation of wind speed and ambient temperature of test days

5.2.3.2 Solar stills performance

The distillate yields obtained during the experimental period were plotted on the bar graph and the line graph shown in figure 5.17. Day seven can be seen to have high distillate yield with the still no. 2 peak output of 2920 ml compared to the ground-mounted still with the peak out of 2260 ml. The four tracking units together gave a daily average of 8149 ml as opposed to the 5540 ml of the four non-tracking ones, each performing like a non-tracking unit on day seven. On ten days period, winter experiment values of 4 tracking purifiers gave an average of 8.149 L/day, giving an average glazing productivity of rate of 2.102 L/m^2.day. It can, however, be seen that on very cloudy days production will be very low affecting the drinking water supplies for households for the next day which is however less consequential because the need of

drinking water on such days would be low. Clearly, it can be said that tracking has improved the yields of the tracking units, and this is likely to meet the requirements of a large household.

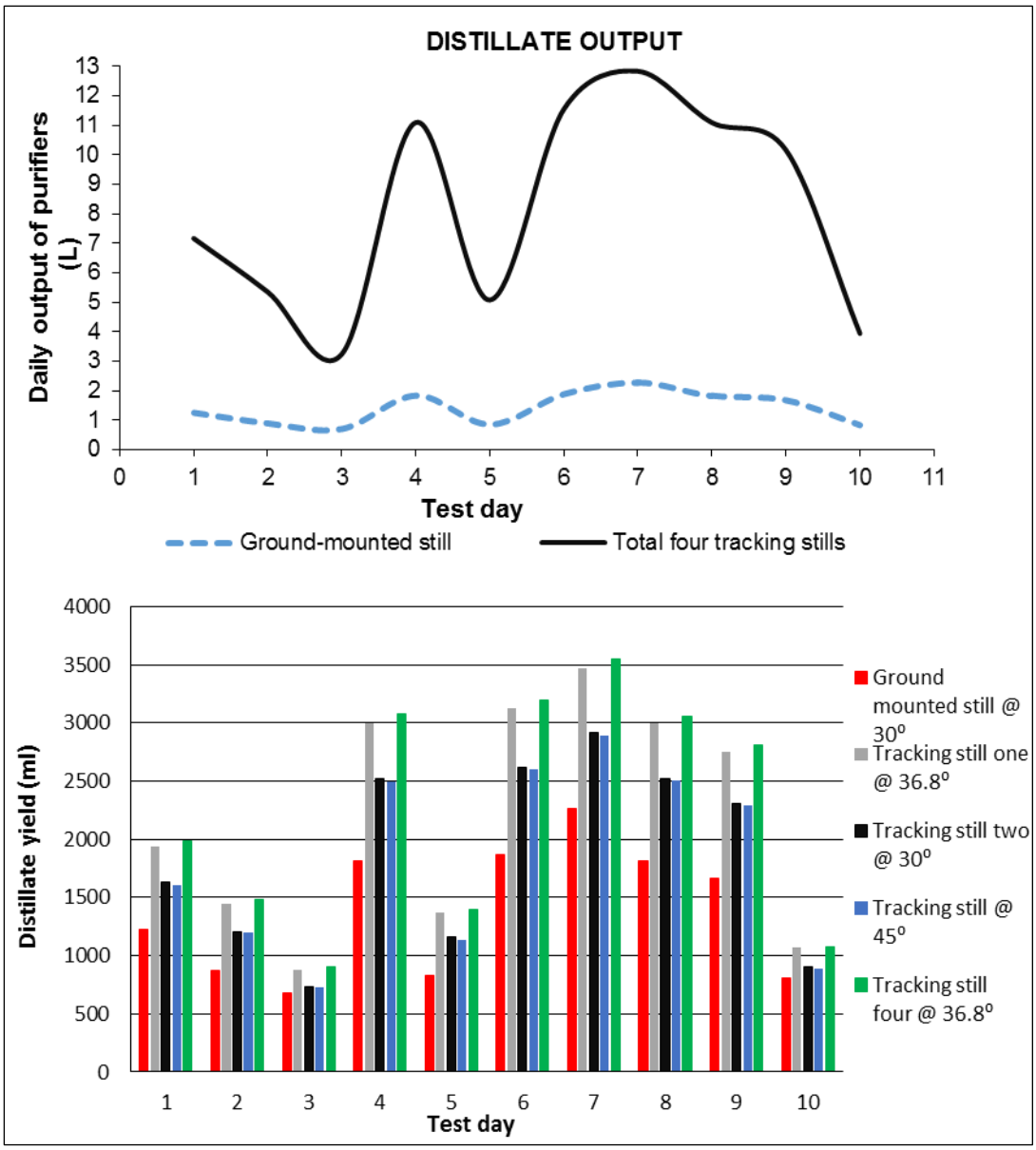

Figure 5.17: 10 days test period distillate yields

Figure 5.18 shows the optical efficiency over the 10 days period. The angle of inclination had a high effect on the optical efficiency of tracking still nos. one and four. It can be stated that 36.8º is suitable angle for Cape Town winter season. The ground-mounted still optical efficiency can be observed to be fluctuating from day one to day eight while the other stills were not fluctuating. The tracking stills' optical efficiency were not fluctuating because they followed the sun, thus keeping the sun`s radiation perpendicular to the solar water purifiers.

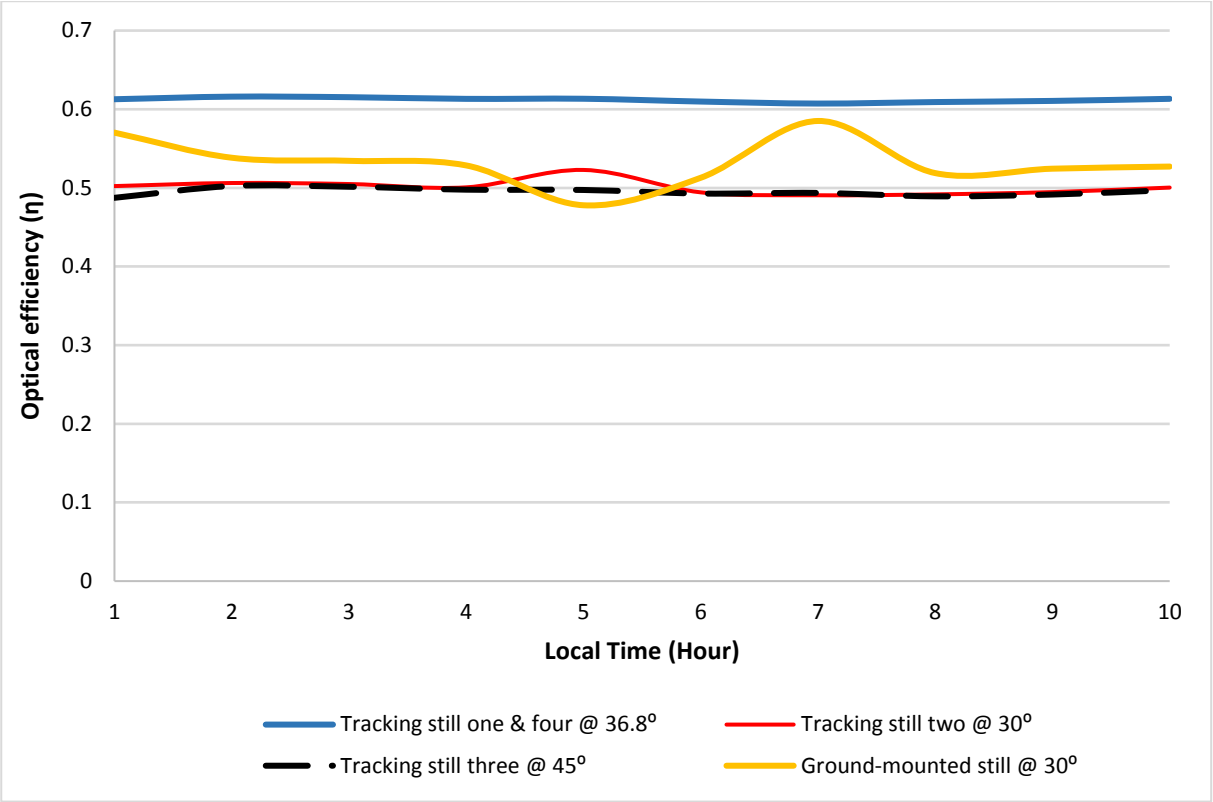

Figure 5.18: 10 days period variation stills optical efficiency

The tracking stills can be seen to have obtained a high sensible heat efficiency on most of the days during the experimental period see figure 5.19. It can further be observed that sensible heat efficiency was fluctuating throughout the experimental period. Day 7 can be observed to have higher sensible heat efficiency with tracking stills out performing the ground-mounted still, with tracking still three with 63% and while the ground-mounted had 49.5%.

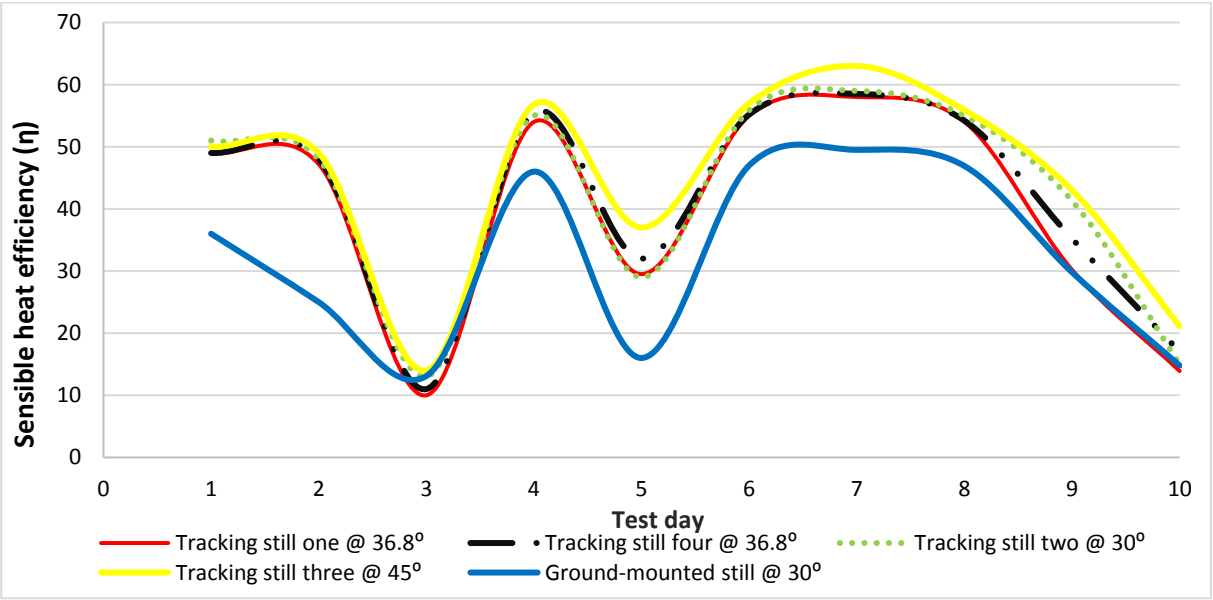

Figure 5.19: 10 days period variation stills sensible heat efficiency

CHAPTER SIX

CONCLUSION AND RECOMMENDATIONS

6.1 CONCLUSION

This study was conducted to find the solution of water problems that are encounted by large households especially in sub-Sharan African countries and developing countres. In the literature (chapter two), it was found that about 2 billion people still lack clean water for drinking whereby the most affected areas are the rural areas. There, water is collected from open sources. At one university of Technololgy in South Africa, several solar water purifiers had been designed to address the problem on hand. Although there are different methods of water purification, Engohang and Kanyarusoke used the distillation method to purify water which is the natural way of making water pure and safe for human consumption. Engohang and Kanyarusoke designed 1.5 m^2 glazing solar-water purifiers which cost ZAR 3000 each to build which can produce up to 5 litres pure water in summer months for domestic use. However, the designed solar-water purifiers would occupy high amounts of space in compunds because of large numbers required to provide the increased potable water demand. The work in this thesis addressed this very problem. It tackled the ground space used per purifier with a need to minimize it while also increasing the daily production of the solar-water purifiers.

A new design (solar tracking system) which cost ZAR 4963.55 was introduced successfully after a carefull consideration of three different designs for the solar-water purifiers in chapter 3. Space was also saved, and it was computed in chapter 3 that on full loading, the purifiers would need only about a seventh of that required by identical fixed ones. When 4 purifiers were mounted, the saving in footprint area was less, at 20.5 m^2, which was 3.7 times the new footprint. This is still very significant for a large household. The purifiers are mounted at different heights, as limited by ability to manually fill them up. This gave 3 levels with the highest at about 2.1 m, in the upper range of a human being's outreach. If six solar prurifier units are to be mounted on the ground, an area of 39 m^2 would be required , or nearly 7 times as much as that with the pillar when fully utilised.

Experiments were performed for 10 days from 31 May 2018 to 07 June 2018 time 8:00 to 17:00. The variations of the weather conditions the ambient temperature, wind speed and the incident solar radiation had a substantial effect on the solar water purifier's performance. Solar tracking had been shown to have a high influence on the solar radiation which affects the distillate out-put yields of the solar water purifiers. The solar tracking stills were observed to have a higher water temperature compared to the ground-mounted still. Validation of thermodynamic and optical analysis through experiments showed that the solar tracking stills had higher performance with comparison to none tracking unit. Tracking increased water

production by up to 31% in Cape Town's winter season. The daily water production was increased appreciably, making the design suitable for larger homesteads.

Experiments were done in winter, giving the lowest yields possible in the year. It is expected that actual yields would be much higher in other seasons and sufficient drinking water could most probably be availed for bigger families. A peer reviewed conference paper was published from this work in 2019 at International Conference Domestic Use of Energy (DUE) as a research contribution to the literature in chapter 3 from this work (Peter & Kanyarusoke, 2019).

6.2 RECOMMENDATIONS

A small dc run water pump could be used to fill up the purifiers, where homesteads can afford it, as it was time-consuming during the experimental period to refill the purifiers every morning. Standard size six solar units (2mX1m glazing) should be used to untilse the full potential of the solar tracking system to gain high amount of yields. Furthermore, a small PV solar panel could be mounted on the pillar for charging of the batteries. This system has good advantages as it saves up high amount of space that would have been taken up by the still units in compounds. The saved up area can be used to grow crops and other purposes, including playing space for small children who would otherwise dirten the glazings of the purifiers if they were ground-mounted. It further provides enough water for large households. It is therefore strongly recommended that the full potential of the tracking system should be utlised to harvest more water for unelectrified, unpiped water supply households that can afford it.

BIBLIOGRAPHY

Al-harahsheh, M., Abu-Arabi, M., Mousa, H. & Alzghoul, Z. 2018. Solar desalination using solar still enhanced by external solar collector and PCM. *Applied Thermal Engineering*, 128: 1030–1040. https://doi.org/10.1016/j.applthermaleng.2017.09.073.

AL-Rousan, N., Isa, N.A.M. & Desa, M.K.M. 2018. Advances in solar photovoltaic tracking systems: A review. *Renewable and Sustainable Energy Reviews*, 82(October 2017): 2548–2569. https://doi.org/10.1016/j.rser.2017.09.077.

Aybar, H.Ş. 2006. Mathematical modeling of an inclined solar water distillation system. *Desalination*, 190(1–3): 63–70.

Carielo, G., Calazans, G., Lima, G. & Tiba, C. 2017. Solar water pasteurizer: Productivity and treatment efficiency in microbial decontamination. *Renewable Energy*, 105: 257–269. http://dx.doi.org/10.1016/j.renene.2016.12.042.

Chafidz, A., Kerme, E.D., Wazeer, I., Khalid, Y., Ajbar, A. & Al-Zahrani, S.M. 2016. Design and fabrication of a portable and hybrid solar-powered membrane distillation system. *Journal of Cleaner Production*, 133: 631–647.

DH, T., SV, D. & GM, S. 2016. Household drinking water: Assessment of microbiological contamination between source and point of use. *Bioscience Discovery*, 7(2): 152–157. http://jbsd.in/Vol 7 No 2/Tambekar152-157.pdf.

Duffie, J. & Beckman, W. 2013. *Solar Engineering of Thermal Processes, 4th ed.* Fourth. New Jersey: John Wiley & Sons, Inc. http://books.google.com/books?hl=en&lr=&id=qkaWBrOuAEgC&pgis=1.

Eldin, S.A.S., Abd-Elhady, M.S. & Kandil, H.A. 2016. Feasibility of solar tracking systems for PV panels in hot and cold regions. *Renewable Energy*, 85: 228–233. http://dx.doi.org/10.1016/j.renene.2015.06.051.

Engohang, A.D. & Kanyarusoke, K.E. 2018. Solar water purification : How helpful is double glazing ? In Cape Town: 8.

File, W.W. 2018. Wwf`s wednesday water file. , (January): 5–7.

Flendrig, L.M., Shah, B., Subrahmaniam, N. & Ramakrishnan, V. 2009. Low cost thermoformed solar still water purifier for D&E countries. *Physics and Chemistry of the Earth*, 34(1–2): 50–54. http://dx.doi.org/10.1016/j.pce.2008.03.007.

Hafez, A.Z., Yousef, A.M. & Harag, N.M. 2018. Solar tracking systems: Technologies and trackers drive types – A review. *Renewable and Sustainable Energy Reviews*, 91(June 2017): 754–782. https://doi.org/10.1016/j.rser.2018.03.094.

Helali, S., Polo-López, M.I., Fernández-Ibáñez, P., Ohtani, B., Amano, F., Malato, S. & Guillard, C. 2013. Solar photocatalysis: A green technology for E. coli contaminated water disinfection. Effect of concentration and different types of suspended catalyst. *Journal of Photochemistry and Photobiology A: Chemistry*, 276: 31–40.

Joyce, A., Loureiro, D., Rodrigues, C. & Castro, S. 2001. Small reverse osmosis units using PV systems for water purification in rural places. *Desalination*, 137(1–3): 39–44.

Kanyarusoke, K., Gryzagoridis, J. & Oliver, G. 2015. Are solar tracking technologies feasible for domestic applications in rural tropical Africa ? *Journal of Energy in Southern Africa*,

26(1): 86–95.

Kanyarusoke, K., Jasson, G. & Graeme, O. 2015. Are solar tracking technologies feasible for domestic applications in rural tropical Africa ? *Journal of Energy in Southern Africa*, 26(1): 86–95. http://www.scielo.org.za/scielo.php?script=sci_arttext&pid=S1021-447X2015000100010.

Kanyarusoke, K.E. 2017a. *Novel approaches to improving domestic solar panel energy yields in sub-sahara Africa*. Cape Peninsula University of Technology. http://etd.cput.ac.za/handle/20.500.11838/2520.

Kanyarusoke, K.E. 2017b. *NOVEL APPROACHES TO IMPROVING DOMESTIC SOLAR PANEL ENERGY YIELDS IN SUB-SAHARA AFRICA*. Cape Peninsula University of Technology. http://hdl.handle.net/20.500.11838/2520.

Leadshine Technology. 2012. Dm542. , (86): 17. http://robokits.download/datasheets/Leadshine DM542.pdf.

Mac Mahon, J. & Gill, L.W. 2018. Sustainability of novel water treatment technologies in developing countries: Lessons learned from research trials on a pilot continuous flow solar water disinfection system in rural Kenya. *Development Engineering*, 3(January): 47–59. https://doi.org/10.1016/j.deveng.2018.01.003.

Mustafa, R. 2015. acidrain1. http://www.odec.ca/projects/2005/must5r0/public_html/purpose.html 3 April 2018.

Nsengiyumva, W., Chen, S.G., Hu, L. & Chen, X. 2018. Recent advancements and challenges in Solar Tracking Systems (STS): A review. *Renewable and Sustainable Energy Reviews*, 81(April 2017): 250–279.

Orisaleye, J.I., Ismail, S.O., Ogbonnaya, M. & Ogundare, A.A. 2018. Development and performance evaluation of a solar water still 1. 2.

Pauline Joella Koura Mbadinga. 2015. *A solar water purification system for rural areas*. Cape Peninsula University of Technology. http://hdl.handle.net/20.500.11838/2612.

Peter, J.. & Kanyarusoke, K.E. 2019. Design optimisation of pillar-mounted sun tracking solar-water purifiers for large households. In *2019 International Conference on the Domestic Use of Energy (DUE)*. Wellington, South Africa, South Africa: IEEE: 8. https://ieeexplore.ieee.org/abstract/document/8734289.

Reyneke, B., Cloete, T.E., Khan, S. & Khan, W. 2018. Rainwater harvesting solar pasteurization treatment systems for the provision of an alternative water source in peri-urban informal settlements. *Environmental Science: Water Research and Technology*, 4(2). http://dx.doi.org/10.1039/C7EW00392G.

Reyneke, B., Dobrowsky, P.H., Ndlovu, T., Khan, S. & Khan, W. 2016. EMA-qPCR to monitor the efficiency of a closed-coupled solar pasteurization system in reducing Legionella contamination of roof-harvested rainwater. *Science of the Total Environment*, 553: 662–670. http://dx.doi.org/10.1016/j.scitotenv.2016.02.108.

Samrath, M. 2011. Solar water Disinfection. , (May).

Shaaban, S. & Yahya, H. 2017. Detailed analysis of reverse osmosis systems in hot climate conditions. *Desalination*, 423(August): 41–51. http://dx.doi.org/10.1016/j.desal.2017.09.002.

Shatat, M., Worall, M. & Riffat, S. 2013. Opportunities for solar water desalination worldwide: Review. *Sustainable Cities and Society*, 9: 67–80. http://dx.doi.org/10.1016/j.scs.2013.03.004.

Sumathi, V., Jayapragash, R., Bakshi, A. & Kumar Akella, P. 2017. Solar tracking methods to maximize PV system output – A review of the methods adopted in recent decade. *Renewable and Sustainable Energy Reviews*, 74(December 2016): 130–138. https://www.sciencedirect.com/science/article/pii/S1364032117302162.

Water, D. 2017. *Progress on Drinking Water , Sanitation and Hygiene*.

Wind, R.M.Y., Set, S., Wind, R.M.Y., Anemometer, S., Wind, R.M.Y. & Vane, S. 2017. 03001 R.M. Young Wind Sentry Set 03101 R.M. Young Wind Sentry Anemometer 03301 R.M. Young Wind Sentry Vane.

Wright, M.A. & Grab, S.W. 2017. Wind speed characteristics and implications for wind power generation : Cape regions , South Africa. *South African Journal of Science*, 113(7): 1–8. https://www.sajs.co.za/article/view/3989/5734.

Zarzo, D. & Prats, D. 2018. Desalination and energy consumption. What can we expect in the near future? *Desalination*, 427(August 2017): 1–9. http://dx.doi.org/10.1016/j.desal.2017.10.046.

Zhang, Y., Sivakumar, M., Yang, S., Enever, K. & Ramezanianpour, M. 2018a. Application of solar energy in water treatment processes: A review. *Desalination*, 428(November 2016): 116–145. https://doi.org/10.1016/j.desal.2017.11.020.

Zhang, Y., Sivakumar, M., Yang, S., Enever, K. & Ramezanianpour, M. 2018b. Application of solar energy in water treatment processes: A review. *Desalination*, 428(November 2017): 116–145. https://doi.org/10.1016/j.desal.2017.11.020.

APPENDICES

APPENDIX A: TECHNICAL DRAWINGS

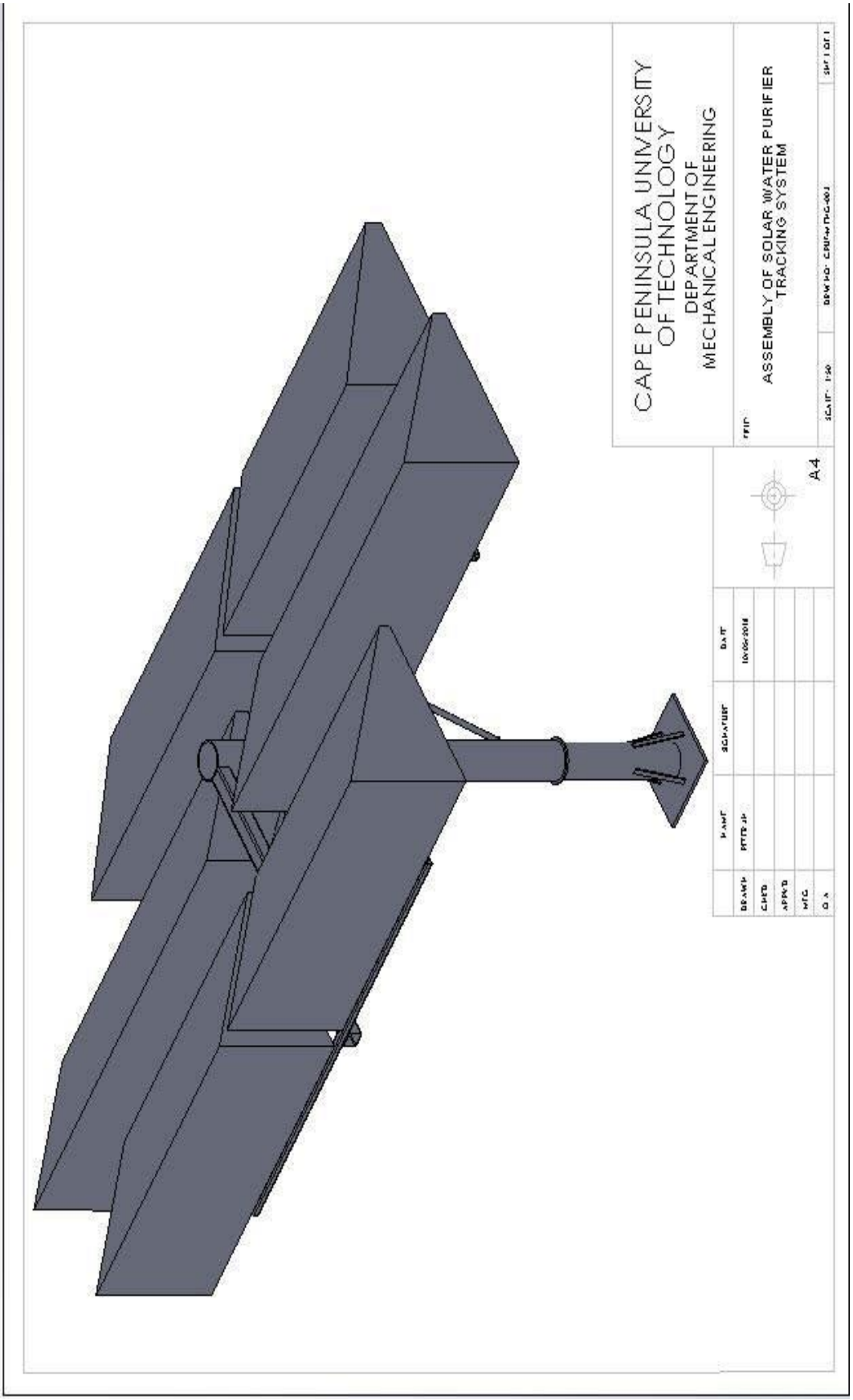

Figure A1: 3D assembly structure with solar water purifiers mounted on the pillar

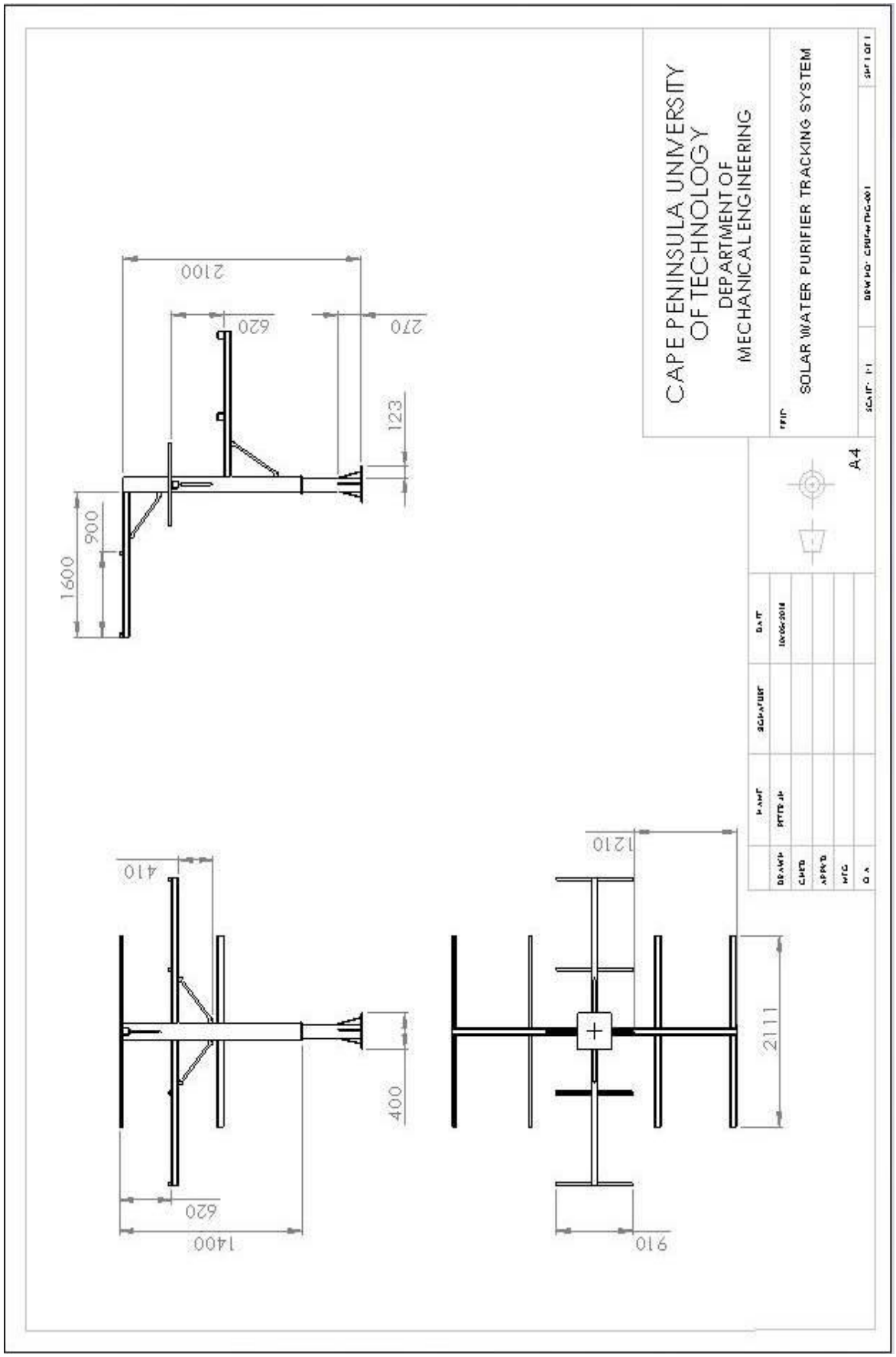

Figure A2: Orthographic drawing structure

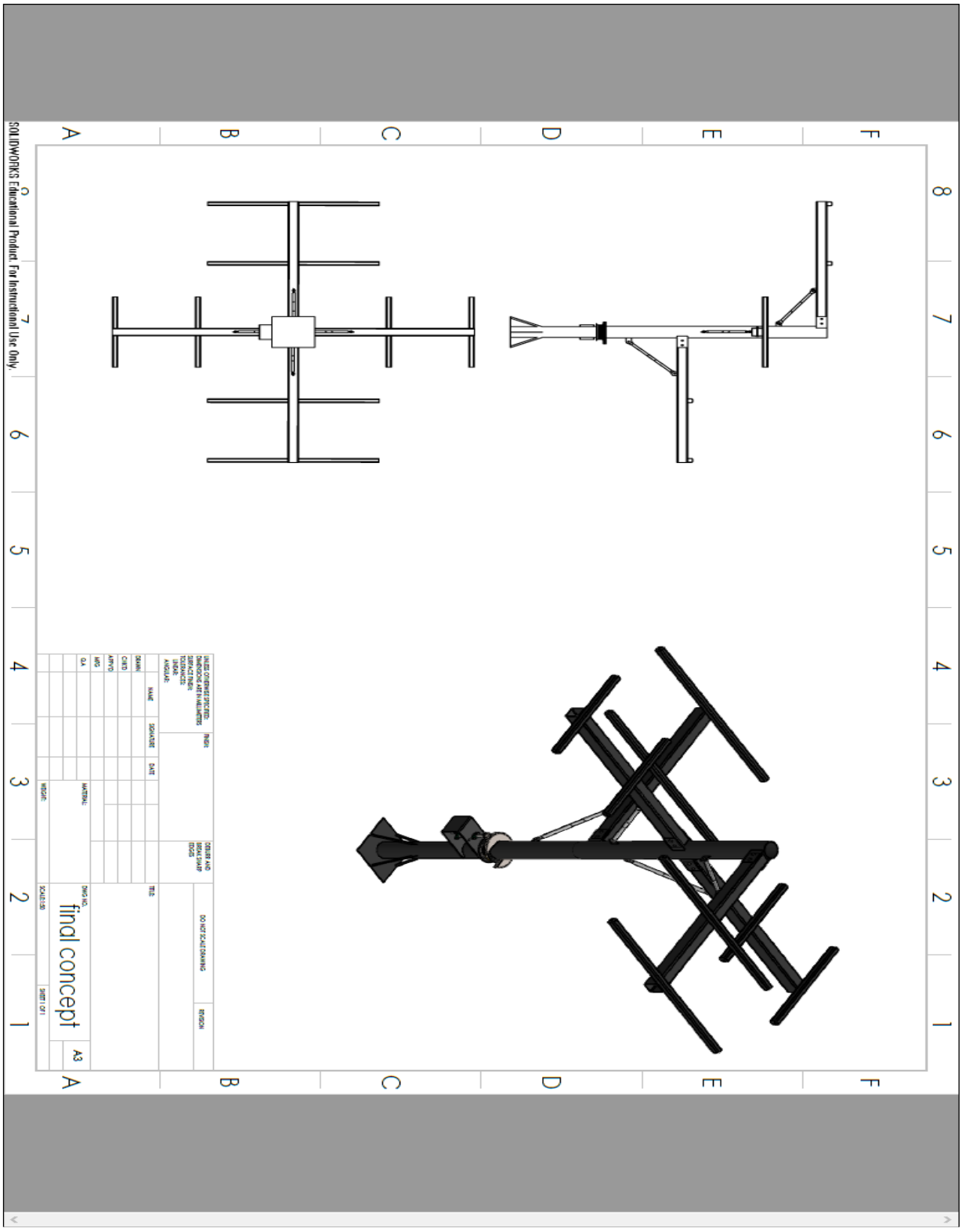

Figure A3: Isometric structure projection with gearing system

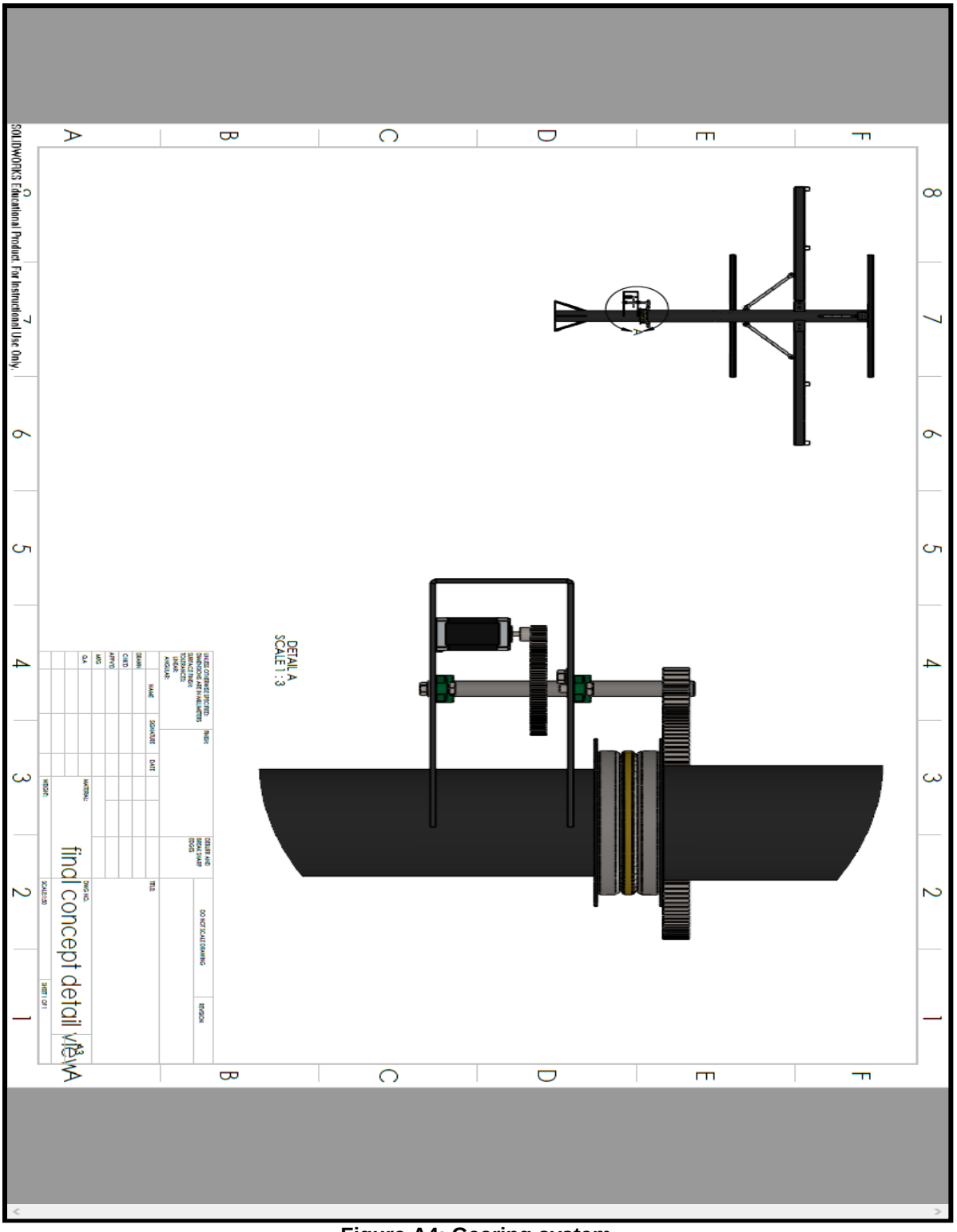

Figure A4: Gearing system

SPUR GEARSET DESIGN SPREAD SHEET

Part A: Input information - from specifics of the problem: Fill into shaded cells.					
Power, P (kW)	4,07567E-07	Pinion speed, N_p (rpm)	0,025	Appr. Gear speed $N_{g\text{-}est}$ (rpm)	0,004166667
Overload factor K_o	1,5	Quality Number A_v	6	Appr. Centre distance, C_{est} (mm	70
Number of years of service required x		8 hour Shifts per day x_{shift}		Working days in year x_{year}	
Part B: Trial variables - from suppliers' catalogues: Fill into shaded cells.					
Module, m (mm)	1	Width, w (mm)	15		
Part C: Geometrical design:					
Select pinion number of teeth, z_p	20	Select pressure angle ϕ (use standard 20°)	20		
Estimate gear ratio, $r_{est} = N_p/N_q$	6				
Compute gear teeth, $z_g = r_{est}z_p$	120				
Recompute gear ratio, $r = z_g/z_p$	6	Recompute output speed $N_q = N_p/r$ (rpm)	0,004166667		
Compute pinion pitch diameter, $d_p = mz_p$ (mm)	20	Compute gear pitch diameter, $d_g = mz_g$ (mm)	120		
Compute centre distance $C = 0.5m(z_p+z_g)$ (mm)	70				
Compute pitchline speed, $V = \pi N_p d_p/60000$ (m/s)	2,61799E-05				
Compute K_v as follows:					
$B = 0.25(A_v - 5)^{0.667}$	0,25	$C' = 3.5627 + 3.9914(1 - B)$	6,55625	$K_v = (C'/C' + \sqrt{V})^{-B}$	1,000195048
Read off manufacturing and assembly factor, K_m (Tab	1,6	Read off pinion geometry factor, J_p (Figure 3.	0,34	Read offgear geometry factor, J	0,43
Compute pitting geometry factor $I = z_g \sin 2\phi/4(z_g +$	0,137740202				
Part D: Forces and stress analysis:					
Overload power demand $P_d = K_o P$ (kW)	6,11351E-07	Design transmitted torque $T_d = 30000P_d/\pi N$	0,233518875	Design transmitted force, $F_t = 2$	23,3518875
ion bending stress, $\sigma_{bendp} = K_v K_m F_{td}/wmJ_p$ (MPa)	7,327511291	ling stress, $\sigma_{bendg} = K_v K_m F_{td}/wmJ_g$ (MPa)	5,793846137		
Part E: Materials selection					
Select a material for the PINION and its hardness from Eqns. 3.1.8 - 3.1.11 or from Tables 3.1.5-3.1.6					
Material	C45	Young modulus, E (MPa)	205000	Poisson ratio ν_p	0,3
Hardness Treatment	Grade 1	Hardness HB	255	Tensile strength S_{utp} (MPa)	585
		Working tensile strength S_{tp} (MPa)	224,175	rking contact strength S_{cp} (MPa)	766,7
		Young modulus, E (MPa)	205000	Poisson ratio ν_g	0,3
Material	C45	Hardness HB	255	Tensile strength S_{utg} (MPa)	585
Hardness Treatment	Grade 1	Working tensile strength S_{tg} (MPa)	224,175	rking contact strength S_{cg} (MPa)	766,7
Compute elastic constant $C_p = 0.5642[E_p E_g/\{(E_g(1-\nu_p^2)+E_p(1$	189,3539279				
Part F: Design for fatigue					
Number of running hours $x_{hours} = 8x*x_{year}*x_{shift}$	0	Number of cycles for pinion, $L_p = 60N_p x_{hours}$	0	Number of cycles forgear, $L_g =$	0
Bending stress fatigue factor for pinion k_{Ntp} (Figure 3.	1,060219114	Bending stress fatigue factor for gear k_{Ntg} (Fig	1,060219	Reliability factor k_R (Table 3.1.7	1
Pinion bending fatigue strength $S_{tep} = k_{Np}k_R S_{tp}$ (MPa	237,6746199	Gear bending fatigue strength $S_{teg} = k_{Ng}k_R S_{tg}$	237,6745943		
Pinion bending safety factor $n_{tp} = S_{tep}/\sigma_{bendp}$	32,4359268	Gear bending safety factor $n_{tg} = S_{teg}/\sigma_{bendg}$	41,02190302		
Pitting stress fatigue factor for pinion k_{Ncp} (Figure 3.1	1,054407381	Pitting stress fatigue factor for gear k_{Ncg} (Figu	1,054407381		
Pinion pitting fatigue strength $S_{cep} = k_{Np}k_R S_{cp}$ (MPa)	808,414139	Gear pitting fatigue strength $S_{ceg} = k_{Ng}k_R S_{cg}$	808,414139		
Pinion pitting stress $\sigma_{cp} = C_p(K_m K_v F_{td}/wId_p)^{0.5}$ (M	180,0721995	Gear pitting stress = Pinion contact stress, σ_{cg}	180,0721995		
Pinion pitting safety factor $n_{cp} = S_{cep}/\sigma_{cp}$	4,48938893	Gear pitting safety factor $n_{cg} = S_{ceg}/\sigma_{cg}$	4,48938893		

Figure A5: Gear design for gears 1&2

SPUR GEARSET DESIGN SPREAD SHEET

Part A: Input information - from specifics of the problem: Fill into shaded cells.					
Power, P (kW)	4,07567E-07	Pinion speed, N_p (rpm)	0,004166667	Appr. Gear speed $N_{g\text{-}est}$ (rpm)	0,000694444
Overload factor K_o	1,5	Quality Number A_v	6	Appr. Centre distance, C_{est} (mm)	175
Number of years of service required x		8 hour Shifts per day x_{shift}		Working days in year x_{year}	
Part B: Trial variables - from suppliers' catalogues: Fill into shaded cells.					
Module, m (mm)	2,5	Width, w (mm)	25		
Part C: Geometrical design:					
Select pinion number of teeth, z_p	20	pressure angle $\emptyset$ (use standard 20°)	20		
Estimate gear ratio, $r_{est} = N_p/N_g$	6				
Compute gear teeth, $z_g = r_{est}z_p$	120				
Recompute gear ratio, $r = z_g/z_p$	6	Recompute output speed $N_g = N_p/r$	0,000694444		
Compute pinion pitch diameter, $d_p = mz_p$ (mm)	50	Compute gear pitch diameter, $d_g =$	300		
Compute centre distance $C = 0.5m(z_p+z_g)$ (mm)	175				
Check close agreement with approximate speed and centre distance requirements:					
Compute pitchline speed, $V = \pi N_p d_p/60000$ (m/s)	1,09083E-05				
Compute K_v as follows:					
$B = 0.25(A_v - 5)^{0.667}$	0,25	$C' = 3.5627 + 3.9914(1 - B)$	6,55625	$K_v = (C'/C' + \sqrt{V})^{-B}$	1,000125916
Read off manufacturing and assembly factor, K_m (Table 3.1.	1,6	Read off pinion geometry factor, J_p	0,34	Read offgear geometry factor, J_g (F	0,43
Compute pitting geometry factor $I = z_g \sin 2\emptyset/4(z_g + z_p)$	0,137740202				
Part D: Forces and stress analysis:					
Overload power demand $P_d = K_oP$ (kW)	6,11351E-07	Design transmitted torque $T_d = 300$	1,40111325	Design transmitted force, $F_t = 2000$	56,04453
Pinion bending stress, $\sigma_{bendp} = K_vK_mF_{td}/wmJ_p$ (MPa)	4,220354779	$\sigma_{bendg} = K_vK_mF_{td}/wmJ_g$ (MPa)	3,337024709		
Part E: Materials selection					
Material		Young modulus, E (MPa)	205000	Poisson ratio ν_p	0,3
Hardness Treatment		Hardness HB	255	Tensile strength S_{utp} (MPa)	585
		Working tensile strength S_{tp} (MPa)	224,175	Working contact strength S_{cp} (MPa)	766,7
		Young modulus, E (MPa)	205000	Poisson ratio ν_g	0,3
Material		Hardness HB	255	Tensile strength S_{utg} (MPa)	585
Hardness Treatment		Working tensile strength S_{tg} (MPa)	224,175	Working contact strength S_{cg} (MPa)	766,7
Compute elastic constant $C_p = 0.5642[E_pE_g/\{(E_g(1-\nu_p^2)+E_p(1-\nu_g^2)\}$	189,3539279				
Part F: Design for fatigue					
Number of running hours $x_{hours} = 8x*x_{year}*x_{shift}$	0	Number of cycles for pinion, $L_p = 6$	0	Number of cycles forgear, $L_g = 60N$	0
Bending stress fatigue factor for pinion k_{Ntp} (Figure 3.1.2)	1,060219114	Bending stress fatigue factor for gea	1,060219	Reliability factor k_R (Table 3.1.7)	1
Pinion bending fatigue strength $S_{tep} = k_{Np}k_RS_{tp}$ (MPa)	237,6746199	Gear bending fatigue strength $S_{teg} =$	237,6745943		
Pinion bending safety factor $n_{tp} = S_{tep}/\sigma_{bendp}$	56,31626542	Gear bending safety factor $n_{tg} = S_{te}$	71,22350449		
Pitting stress fatigue factor for pinion k_{Ncp} (Figure 3.1.3)	1,054407381	Pitting stress fatigue factor for gear	1,054407381		
Pinion pitting fatigue strength $S_{cep} = k_{Np}k_RS_{cp}$ (MPa)	808,414139	Gear pitting fatigue strength $S_{ceg} = k$	808,414139		
Pinion pitting stress $\sigma_{cp} = C_p(K_mK_vF_{td}/wId_p)^{0.5}$ (MPa)	136,6604674	Gear pitting stress = Pinion contact s	136,6604674		
Pinion pitting safety factor $n_{cp} = S_{cep}/\sigma_{cp}$	5,915493739	Gear pitting safety factor $n_{cg} = S_{ceg}$	5,915493739		

Figure A6: Gear design for gears 3&4

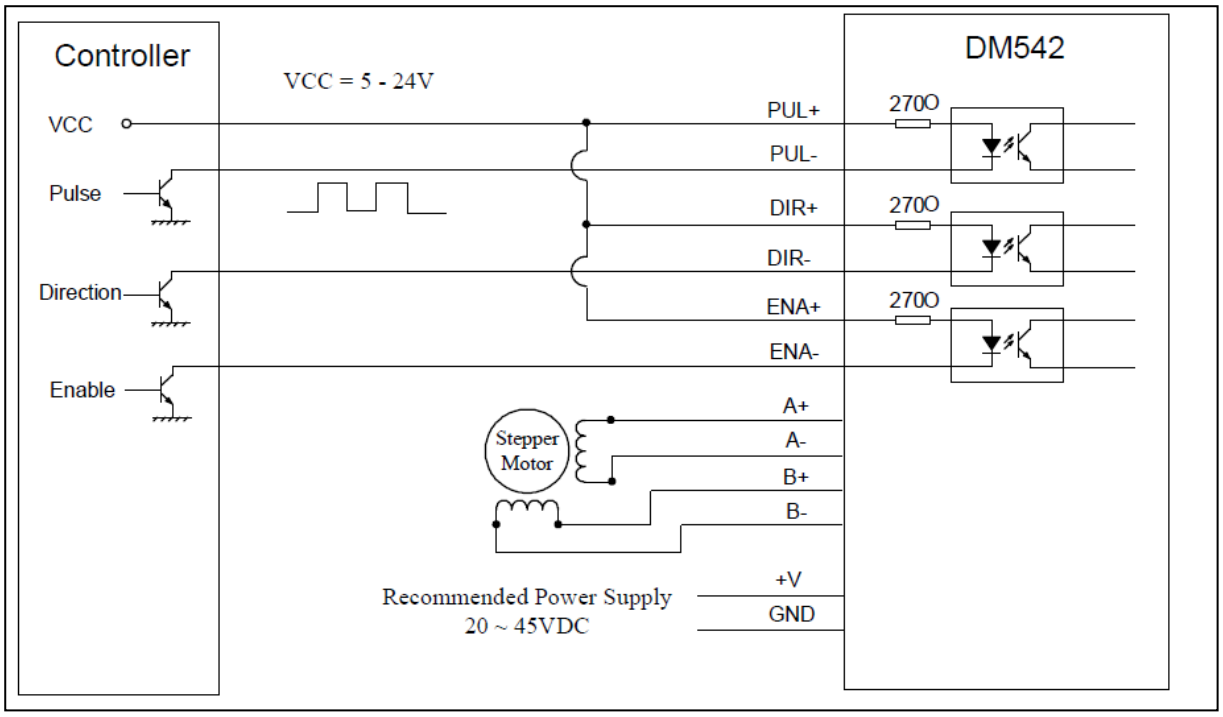

Figure A7: Stepper motor typical wiring connection

(Leadshine Technology, 2012)

Appendix A8: Arduino (Stepper motor) code

```
#include <time.h>
#include <Stepper.h> //Arduino Library added in order to interface with Stepper motors and to
//communicate with the H-Bridge

int i; //These are two constants used as variables to be able to count down the loops and
measure
//the right amount of time that the panel needs to move

long start_time = 0;
long current_time = 0;


// ================================= CHANGE THIS!!!!!!
==========================================

//change this to fit the number of steps per revolution for your motor
//const int stepsPerRevolution = 2500; //PROJECT
const int stepsPerRevolution = 10000; //DEMO

// Change from DEMO to PROJECT
bool project = false; // "true" = PROJECT ; "false" = DEMO

//
=========================================================================
=========================

// initialize the stepper library on pins 8 through 11:
Stepper myStepper(stepsPerRevolution, 8, 9, 10, 11); //Selecting the Digital Output pins we
want to
//use for the Arduino and the H-Bridge

/*
 * Setup method, run first by the arduino
 */
void setup() {

  // Initialise speed of motor
  if(project){
    myStepper.setSpeed(1); //PROJECT
  }
  else{
    myStepper.setSpeed(60); //DEMO
  }

  // Initialize the serial port:
  Serial.begin(9600); //Serial Port is monitoring system used for debugging and also to see
what the
  //code is doing and what the variables's values are

}

//================================= START OF MAIN LOOP
====================================
void loop() {
  Serial.print("Initialising clock... time:");
```

```
  Serial.println(millis());
  start_time = millis();

//================================== COUNTER CLOCKWISE
====================================
  Serial.println("Counter clockwise");
  if(project){
    myStepper.setSpeed(1); //PROJECT
  }
  else{
    myStepper.setSpeed(200); //DEMO
  }

  if(project){
    for(i=0; i<5*720; i++) { //PROJECT (5*720)
      myStepper.step(-stepsPerRevolution); //Actual function that makes the motor move
counter clockwise
    }
  }
  else{
    for(j=0; j<12; j++) {
       for(i=0; i<5*36/12; i++) { //DEMO (5*36)
    //     start_time = millis();
         myStepper.step(-stepsPerRevolution); //Actual function that makes the motor move
counter clockwise
    //     current_time = millis();
    //     Serial.print(current_time - start_time);
    //     Serial.println(" ms");
       }
       my_delay(5);
    }
  }

//================================== DELAY BEFORE ROTATING BACK
====================================
  if(project){
    my_delay(10); //PROJECT
  }
  else{
    my_delay(10); //DEMO
  }

//================================== CLOCKWISE
====================================
  Serial.println("Clockwise");
  if(project){
    myStepper.setSpeed(60); //PROJECT
  }
  else{
    myStepper.setSpeed(200); //DEMO
  }

  if(project){
    for(i=0; i<5*720; i++) { //PROJECT (5*720)
//     start_time = millis();
      myStepper.step(stepsPerRevolution);
//     current_time = millis();
```

```
//      Serial.print(current_time - start_time);
//      Serial.println(" ms!!!");
    }
  }
  else{
    for(i=0; i<5*36; i++) { //DEMO (5*36)
      myStepper.step(stepsPerRevolution);
    }
  }

//================================== "12 HOUR DELAY"
====================================
  if(project){
    my_delay(60*60 - (10 + 5*144)); //PROJECT (12 hour delay)
    my_delay(60*60);
    my_delay(60*60);
    my_delay(60*60);
    my_delay(60*60);
    my_delay(60*60);
    my_delay(60*60);
    my_delay(60*60);
    my_delay(60*60);
    my_delay(60*60);
    my_delay(60*60);
    my_delay(60*60);
  }
  else{
    my_delay(20); //DEMO
  }
}
//================================== END OF MAIN LOOP
====================================

/*
 * My delay function
 */
void my_delay(long d){
  Serial.print(d, DEC);
  Serial.println(" second delay");
  start_time = millis();
  current_time = millis();

  while(current_time - start_time <= d*1000){
    current_time = millis();
  }
}
```

APPENDIX B: TECHNICAL SPECIFICATIONS

Wind Speed (Anemometer) Specifications	
Range:	0 to 50 m s-1 (112 mph), gust survival 60 m s-1 (134 mph)
Sensor:	12 cm diameter cup wheel assembly, 40 mm diameter hemispherical cups
Accuracy:	±0.5 m s-1 (1.1 mph)
Turning Factor:	75 cm (2.5 ft)
Distance Constant (63% recovery):	2.3 m (7.5 ft)
Threshold:	0.5 m s-1 (1.1 mph)
Transducer:	Stationary coil, 1350 ohm nominal resistance
Transducer Output:	AC sine wave signal induced by rotating magnet on cup wheel shaft 100 mV peak-to-peak at 60 rpm; 6 V peak-to-peak at 3600 rpm
Output Frequency:	1 cycle per cup wheel revolution; 0.75 m s-1 per Hz
Cup Wheel Diameter:	12 cm (4.7 in)
Weight:	113 g (4 oz)

Figure B1: 03101 R.M Young Anemometer

https://s.campbellsci.com/documents/au/manuals/smp-series_man.pdf

Specifications	
Classification to ISO 9060:1990	First Class
Sensitivity	5 to 20 µV/W/m²
Impedance	20 to 200 Ω
Expected output range (0 to 1500 W/m²)	0 to 30 mV
Maximum operational irradiance	2000 W/m²
Response time (63 %)	< 6 s
Response time (95 %)	< 18 s
Spectral range (20% points)	270 to 3000 nm
Spectral range (50 % points)	285 to 2800 nm
Zero offsets (unventilated) (a) thermal radiation (at 200 W/m²) (b) temperature change (5 K/h)	 < 10 W/m² < 4 W/m²
Non-stability (change/year)	< 1 %
Non-linearity (100 to 1000 W/m²)	< 1 %
Directional response (up to 80° with 1000 W/m² beam)	< 15 W/m²
Spectral selectivity (350 to 1500 nm)	< 1 %
Tilt response (0° to 90° at 1000 W/m²)	< 1 %
Temperature response	< 4 % (-10 °C to +40 °C)
Field of view	180 °
Accuracy of bubble level	< 0.1 °
Temperature sensor output	
Detector type	Thermopile
Operating temperature range	-40 °C to +80 °C
Storage temperature range	-40 °C to +80 °C
Humidity range	0 to 100 %
MTBF (Mean Time Between Failures)	> 10 years
Ingress Protection (IP) rating	67

Figure B2: Kipp & Zonen SP-LITE Silcon pyranometer

https://s.campbellsci.com/documents/eu/manuals/sp-lite.pdf

Specifications	
Spectral range (overall)	400 to 1100 nm
Sensitivity Sensitivity (10 µV/W/m² version)	60 to 100 µV/W/m² 10 ±0.5 µV/W/m²
Impedance Impedance (10 µV/W/m² version)	50 Ω < 10 Ω
Expected output range (0 to 1500 W/m²) Expected output range (10 µV/W/m² version)	0 to 150 mV 0 to 15 mV
Maximum operational irradiance	2000 W/m²
Response time (95 %)	< 500 ns
Non-stability (change/year)	< 2 %
Non-linearity (100 to 1000 W/m²)	< 2.5 %
Directional response (up to 80 ° with 1000 W/m² beam)	< 10 W/m²
Temperature response	- 0.15 %/°C
Field of view	180 °
Accuracy of bubble level	< 0.2 °
Detector type	Photo-diode
Operational temperature range	-40 °C to +80 °C
Storage temperature range	-40 °C to +80 °C
Humidity range	0 to 100 % non-condensing
Ingress Protection (IP) rating	67

Figure B3: Kipp & Zonen CMP6 Pyranometer

https://s.campbellsci.com/documents/ca/product.../cmp6-cmp11-cmp21_br.pdf

Appendix C: Weather condition
Table C-1: 29 May 2018 measured data

TIMESTAMP	Solar radiation (Beam horizontal) Ib [W/m^2]	Solar radiation (diffuse horizontal) Id [W/m^2]	Solar radiation (total horizontal) Ih [W/m^2]	Wind speed [m/s]	Ambient temperature [`C]
2018-05-29 11:30	200.81	29.49	230.3	2.6	17.05
2018-05-29 11:45	218.29	36.01	254.3	1.45	17.68
2018-05-29 12:00	251.36	39.14	290.5	0.577	19.3
2018-05-29 12:15	374.35	39.75	414.1	1.233	23.17
2018-05-29 12:30	540.45	37.35	577.8	2.093	28.08
2018-05-29 12:45	497.01	27.39	524.4	1.949	28.42
2018-05-29 13:00	546.77	30.83	577.6	2.064	30.22
2018-05-29 13:15	463.5	31.5	495	2.608	27.89
2018-05-29 13:30	440.9	29.5	470.4	2.983	28.04
2018-05-29 13:45	501.94	34.36	536.3	2.439	28.57
2018-05-29 14:00	256.63	23.67	280.3	2.742	23.61
2018-05-29 14:15	181.08	27.72	208.8	2.289	20.29
2018-05-29 14:30	237.32	35.68	273	1.837	20.84
2018-05-29 14:45	299.91	42.39	342.3	2.617	22.21
2018-05-29 15:00	266.71	40.89	307.6	2.664	21.95
2018-05-29 15:15	254.09	31.61	285.7	1.662	21.54
2018-05-29 15:30	355.12	35.98	391.1	2.162	21.02
2018-05-29 15:45	199.15	24.85	224	1.745	19.27
2018-05-29 16:00	298.65	26.75	325.4	2.527	21.7
2018-05-29 16:15	230.23	30.87	261.1	2.302	18.93
2018-05-29 16:30	102.5	99.4	201.9	2.268	18.08
2018-05-29 16:45	6.8	151	157.8	2.075	17.5
2018-05-29 17:00	3.8	112.1	115.9	1.948	17.13
2018-05-29 17:15	0.81	76.97	77.78	1.601	16.57
2018-05-29 17:30	-0.88	43.35	42.47	1.858	16.22
2018-05-29 17:45	-0.69	14.44	13.75	1.012	15.65
2018-05-29 18:00	-0.407	1.434	1.027	1.166	15.18

Table C-2: 30 May 2018 measured data

TIMESTAMP	Solar radiation (Beam horizontal) Ib [W/m^2]	Solar radiation (diffuse horizontal) Id [W/m^2]	Solar radiation (total horizontal) Ih [W/m^2]	Wind speed [m/s]	Ambient temperature [`C]
2018-05-30 08:00	3.33	1.935	5.265	0.923	11.18
2018-05-30 08:15	19.445	7.155	26.6	1.816	11.83
2018-05-30 08:30	35.48	13.08	48.56	1.293	12.25
2018-05-30 08:45	68.4	21.3	89.7	0.971	12.62
2018-05-30 09:00	111.46	30.04	141.5	2.431	12.74
2018-05-30 09:15	162.19	35.91	198.1	2.858	12.92
2018-05-30 09:30	151.04	41.26	192.3	1.878	13.94
2018-05-30 09:45	236.69	47.61	284.3	1.655	15.65
2018-05-30 10:00	237.57	48.43	286	1.889	16.13
2018-05-30 10:15	150.04	44.86	194.9	1.724	16.26
2018-05-30 10:30	140.57	41.03	181.6	2.071	16.2
2018-05-30 10:45	189.69	46.11	235.8	0.504	17.52
2018-05-30 11:00	387.75	51.65	439.4	1.738	20.94
2018-05-30 11:15	332.66	60.24	392.9	3.05	20.25
2018-05-30 11:30	233.66	61.64	295.3	2.246	19.24
2018-05-30 11:45	216.39	57.31	273.7	2.681	18.85
2018-05-30 12:00	226.88	65.32	292.2	2.608	18.35
2018-05-30 12:15	260.51	63.59	324.1	2.539	19.25
2018-05-30 12:30	422.41	57.49	479.9	3.042	22.61
2018-05-30 12:45	420.98	59.22	480.2	3.075	24.36
2018-05-30 13:00	300.07	41.33	341.4	3.448	21.79
2018-05-30 13:15	216.24	56.46	272.7	3.642	19.01
2018-05-30 13:30	232.15	59.25	291.4	4.042	18.77
2018-05-30 13:45	204.01	58.59	262.6	3.673	18.29
2018-05-30 14:00	182.63	50.87	233.5	3.858	17.2
2018-05-30 14:15	212.07	54.73	266.8	3.042	17.46
2018-05-30 14:30	153.21	42.09	195.3	4.192	16.8
2018-05-30 14:45	192.28	42.62	234.9	3.133	17.7
2018-05-30 15:00	111.69	31.11	142.8	3.325	16.17
2018-05-30 15:15	180.53	40.87	221.4	3.389	15.9
2018-05-30 15:30	261.85	47.95	309.8	2.804	16.95
2018-05-30 15:45	142.99	36.21	179.2	1.504	16.5
2018-05-30 16:00	179.04	34.06	213.1	1.149	17.27
2018-05-30 16:15	202.28	36.32	238.6	0.726	16.86
2018-05-30 16:30	120.3	95.8	216.1	2.668	17.28
2018-05-30 16:45	34	143.2	177.2	2.933	17.04
2018-05-30 17:00	24.31	56.69	81	2.967	16.34
2018-05-30 17:15	25.65	26.62	52.27	2.933	15.85
2018-05-30 17:30	19.75	9.01	28.76	2.392	15.56
2018-05-30 17:45	6.448	2.842	9.29	2.742	15.15
2018-05-30 18:00	-0.121	0.58	0.459	2.375	14.78

Table C-3: 31 May 2018 measured data

TIMESTAMP	Solar radiation (Beam horizontal) Ib [W/m^2]	Solar radiation (diffuse horizontal) Id [W/m^2]	Solar radiation (total horizontal) Ih [W/m^2]	Wind speed [m/s]	Ambient temperature [`C]
2018-05-31 08:00	1.638	0.672	2.31	4.692	12.48
2018-05-31 08:15	6.229	2.101	8.33	4.283	12.44
2018-05-31 08:30	11.823	3.397	15.22	4.567	12.49
2018-05-31 08:45	21.871	6.079	27.95	4.758	12.52
2018-05-31 09:00	31.36	8.44	39.8	4.975	12.41
2018-05-31 09:15	46.8	11.64	58.44	4.792	12.45
2018-05-31 09:30	56.75	17.16	73.91	4.875	12.6
2018-05-31 09:45	106.56	30.84	137.4	4.792	12.88
2018-05-31 10:00	72.25	24.95	97.2	5.65	12.84
2018-05-31 10:15	66.13	22.77	88.9	5.533	12.87
2018-05-31 10:30	88.57	25.13	113.7	5.375	13.01
2018-05-31 10:45	89.7	27.6	117.3	5.733	13.17
2018-05-31 11:00	131.9	36.8	168.7	5.075	13.42
2018-05-31 11:15	180.73	41.37	222.1	5.292	13.82
2018-05-31 11:30	252.26	49.04	301.3	5.233	14.48
2018-05-31 11:45	206.69	52.31	259	5.925	14.71
2018-05-31 12:00	130.34	40.96	171.3	6.925	14.18
2018-05-31 12:15	173.22	50.88	224.1	6.642	14.43
2018-05-31 12:30	372.53	57.17	429.7	7.308	15.9
2018-05-31 12:45	202.29	47.21	249.5	7.158	16.03
2018-05-31 13:00	308.41	58.19	366.6	7.683	16.97
2018-05-31 13:15	184.4	49.9	234.3	6.958	16.84
2018-05-31 13:30	182.3	46.1	228.4	7.442	16.79
2018-05-31 13:45	242.97	51.53	294.5	6.833	17.55
2018-05-31 14:00	332.59	54.61	387.2	6.442	19.06
2018-05-31 14:15	228.06	40.04	268.1	6.933	18.08
2018-05-31 14:30	88.44	28.76	117.2	7.292	16.63
2018-05-31 14:45	161.58	39.82	201.4	6.092	17.34
2018-05-31 15:00	128.78	36.92	165.7	7.308	17.11
2018-05-31 15:15	139.05	32.25	171.3	7.767	16.74
2018-05-31 15:30	59.43	19.04	78.47	6.567	16.52
2018-05-31 15:45	32.69	10.5	43.19	7.083	15.15
2018-05-31 16:00	29.15	9.27	38.42	5.55	14.2
2018-05-31 16:15	30.57	9.27	39.84	6.008	13.91
2018-05-31 16:30	30.22	9.06	39.28	5.558	13.77
2018-05-31 16:45	21.993	6.077	28.07	6.3	13.76
2018-05-31 17:00	53.94	27.16	81.1	5.692	13.83
2018-05-31 17:15	24.498	7.512	32.01	5.817	13.74
2018-05-31 17:30	23.62	8.15	31.77	5.842	13.69
2018-05-31 17:45	12.357	5.813	18.17	6.192	13.62
2018-05-31 18:00	1.561	0.951	2.512	6.15	13.48

Table C-4: 01 June 2018 measured data

TIMESTAMP	Solar radiation (Beam horizontal) Ib [W/m^2]	Solar radiation (diffuse horizontal) Id [W/m^2]	Solar radiation (total horizontal) Ih [W/m^2]	Wind speed [m/s]	Ambient temperature [`C]
2018-06-01 08:00	1.169	1.064	2.233	1.553	11.78
2018-06-01 08:15	8.052	3.708	11.76	2.099	11.96
2018-06-01 08:30	41.08	16.89	57.97	1.879	12.35
2018-06-01 08:45	47.59	15.91	63.5	3.975	12.81
2018-06-01 09:00	58.95	22.65	81.6	3.85	13.06
2018-06-01 09:15	141.07	27.53	168.6	3.858	13.58
2018-06-01 09:30	216.01	26.89	242.9	3.083	14.61
2018-06-01 09:45	290.36	45.54	335.9	4.342	15.77
2018-06-01 10:00	343.97	42.63	386.6	3.229	16.58
2018-06-01 10:15	334.22	33.98	368.2	2.47	18.63
2018-06-01 10:30	191.13	23.37	214.5	2.26	17.77
2018-06-01 10:45	173.88	23.32	197.2	2.514	17.24
2018-06-01 11:00	159.67	39.03	198.7	2.186	16.8
2018-06-01 11:15	155.41	39.69	195.1	1.667	16.69
2018-06-01 11:30	361.72	48.78	410.5	2.209	19.69
2018-06-01 11:45	464.39	59.71	524.1	3.3	23.2
2018-06-01 12:00	468.33	55.07	523.4	3.092	23.37
2018-06-01 12:15	424.65	38.55	463.2	2.946	23.39
2018-06-01 12:30	570.17	49.13	619.3	3.692	26.28
2018-06-01 12:45	516.55	52.15	568.7	3.875	25.49
2018-06-01 13:00	514.92	41.68	556.6	3.692	26.17
2018-06-01 13:15	495.53	39.37	534.9	3.733	25.92
2018-06-01 13:30	469.94	34.46	504.4	3.833	25.29
2018-06-01 13:45	502.27	32.73	535	3.842	26.13
2018-06-01 14:00	487.71	33.79	521.5	3.817	26.27
2018-06-01 14:15	454.49	38.71	493.2	4.575	25.68
2018-06-01 14:30	429.18	40.22	469.4	4.033	25.49
2018-06-01 14:45	406.46	48.54	455	3.575	25.79
2018-06-01 15:00	406.17	40.23	446.4	2.842	25.77
2018-06-01 15:15	369.07	36.03	405.1	3.267	23.03
2018-06-01 15:30	323.29	30.01	353.3	3.058	20.34
2018-06-01 15:45	288.45	30.85	319.3	3.217	18.45
2018-06-01 16:00	232.69	28.31	261	3.133	18.96
2018-06-01 16:15	185.27	32.23	217.5	2.842	17.71
2018-06-01 16:30	90	113.4	203.4	2.892	17.18
2018-06-01 16:45	31.5	132.7	164.2	2.692	16.76
2018-06-01 17:00	23.2	92.7	115.9	2.875	16.26
2018-06-01 17:15	17.68	57.34	75.02	2.3	15.82
2018-06-01 17:30	13.24	16.27	29.51	2.618	15.32
2018-06-01 17:45	4.948	3.282	8.23	1.812	14.86
2018-06-01 18:00	-0.311	1.015	0.704	1.545	14.48

Table C-5: 02 June 2018 measured data

TIMESTAMP	Solar radiation (Beam horizontal) Ib [W/m^2]	Solar radiation (diffuse horizontal) Id [W/m^2]	Solar radiation (total horizontal) Ih [W/m^2]	Wind speed [m/s]	Ambient temperature [`C]
2018-06-02 08:00	2.994	1.344	4.338	5.292	13.27
2018-06-02 08:15	11.89	3.88	15.77	5.167	13.48
2018-06-02 08:30	22.59	8.25	30.84	5.292	13.49
2018-06-02 08:45	28.12	7.03	35.15	5.667	13.54
2018-06-02 09:00	93.19	13.81	107	5.475	13.53
2018-06-02 09:15	146.71	26.89	173.6	5.817	14.08
2018-06-02 09:30	117.59	23.91	141.5	6.242	14.12
2018-06-02 09:45	135.95	31.25	167.2	6.8	14.39
2018-06-02 10:00	172.26	42.34	214.6	5.767	15.07
2018-06-02 10:15	261.37	48.23	309.6	6.767	16.08
2018-06-02 10:30	262.21	42.09	304.3	6.95	16.55
2018-06-02 10:45	220.39	35.11	255.5	7.525	16.22
2018-06-02 11:00	378.84	32.86	411.7	6.625	18.15
2018-06-02 11:15	431.97	26.43	458.4	7.158	18.23
2018-06-02 11:30	435.95	29.85	465.8	6.35	19.55
2018-06-02 11:45	357.71	61.79	419.5	6.7	20.37
2018-06-02 12:00	157.49	47.91	205.4	5.858	18.13
2018-06-02 12:15	170.25	46.75	217	7.442	18.06
2018-06-02 12:30	152.26	40.44	192.7	6.675	17.9
2018-06-02 12:45	192.26	33.04	225.3	8.52	17.54
2018-06-02 13:00	244.69	29.81	274.5	6.017	18.71
2018-06-02 13:15	411.21	35.99	447.2	6.65	21.11
2018-06-02 13:30	365.26	33.44	398.7	6.375	21.71
2018-06-02 13:45	218.2	34.1	252.3	6.425	19.81
2018-06-02 14:00	204.25	36.55	240.8	7.317	19.01
2018-06-02 14:15	406.68	38.32	445	6.692	22.71
2018-06-02 14:30	434.45	37.45	471.9	8.29	23.62
2018-06-02 14:45	387.82	47.78	435.6	8.25	23.27
2018-06-02 15:00	335.23	44.07	379.3	8.77	22.2
2018-06-02 15:15	246.75	35.25	282	8.55	20.54
2018-06-02 15:30	102.88	29.42	132.3	9.17	18.35
2018-06-02 15:45	93.6	30.6	124.2	7.317	18.15
2018-06-02 16:00	69.66	27.04	96.7	8.12	17.87
2018-06-02 16:15	58.89	22.71	81.6	8.7	17.58
2018-06-02 16:30	41.37	18.49	59.86	8.74	17.46
2018-06-02 16:45	28.58	13.28	41.86	7.833	17.3
2018-06-02 17:00	24.64	8.26	32.9	8.77	17.1
2018-06-02 17:15	18.015	6.215	24.23	7.925	16.91
2018-06-02 17:30	12.27	5.63	17.9	8.82	16.79
2018-06-02 17:45	4.738	2.299	7.037	7.825	16.62
2018-06-02 18:00	0.528	0.628	1.156	5.683	16.37

Table C-6: 03 June 2018 measured data

TIMESTAMP	Solar radiation (Beam horizontal) Ib [W/m^2]	Solar radiation (diffuse horizontal) Id [W/m^2]	Solar radiation (total horizontal) Ih [W/m^2]	Wind speed [m/s]	Ambient temperature [`C]
2018-06-03 08:00	3.287	2.994	6.281	1.116	10.49
2018-06-03 08:15	28.54	10.28	38.82	1.378	10.86
2018-06-03 08:30	51.03	13.12	64.15	1.298	11.07
2018-06-03 08:45	82.75	14.05	96.8	1.042	11.45
2018-06-03 09:00	115.78	14.72	130.5	1.641	11.79
2018-06-03 09:15	160.36	15.64	176	2.617	12.15
2018-06-03 09:30	205.07	16.33	221.4	2.617	12.84
2018-06-03 09:45	247.82	16.98	264.8	2.139	14.88
2018-06-03 10:00	287.2	17.4	304.6	2.204	14.92
2018-06-03 10:15	323.15	18.15	341.3	2.95	16.23
2018-06-03 10:30	360.49	18.81	379.3	3.333	18.56
2018-06-03 10:45	393.28	19.32	412.6	4.067	16.84
2018-06-03 11:00	417.35	20.15	437.5	3.875	18.57
2018-06-03 11:15	434.6	21.3	455.9	3.417	18.15
2018-06-03 11:30	341.35	23.65	365	3.358	18
2018-06-03 11:45	277.33	25.97	303.3	3.75	17.94
2018-06-03 12:15	429.53	21.87	451.4	3.704	20.55
2018-06-03 12:30	511.49	28.51	540	3.833	22.5
2018-06-03 12:45	533.36	28.54	561.9	4.75	23.15
2018-06-03 13:00	552.3	31.5	583.8	4.975	23.52
2018-06-03 13:15	547.92	29.68	577.6	4.542	24.22
2018-06-03 13:30	521.75	25.95	547.7	5.125	23.62
2018-06-03 13:45	505.63	25.97	531.6	4.267	24.05
2018-06-03 14:00	487.48	26.12	513.6	3.396	24.74
2018-06-03 14:15	465.88	26.22	492.1	3.917	23.81
2018-06-03 14:30	446	26.1	472.1	3.625	24.14
2018-06-03 14:45	425.56	25.44	451	3.542	24.16
2018-06-03 15:00	398.99	24.81	423.8	4.158	22.83
2018-06-03 15:15	365.23	24.17	389.4	3.758	20.61
2018-06-03 15:30	333.1	23.7	356.8	3.95	17.93
2018-06-03 15:45	295.41	23.69	319.1	4.017	16.75
2018-06-03 16:00	255.76	23.44	279.2	3.242	17.67
2018-06-03 16:15	203.67	34.33	238	3.517	16.32
2018-06-03 16:30	62	132.5	194.5	3.392	15.91
2018-06-03 16:45	12	141.3	153.3	3.117	15.4
2018-06-03 17:00	8	105	113	3.356	14.96
2018-06-03 17:15	3.3	71.83	75.13	4.308	14.47

Table C-7: 04 June 2018 measured data

TIMESTAMP	Solar radiation (Beam horizontal) Ib [W/m^2]	Solar radiation (diffuse horizontal) Id [W/m^2]	Solar radiation (total horizontal) Ih [W/m^2]	Wind speed [m/s]	Ambient temperature [`C]
2018-06-04 11:15	433.81	18.39	452.2	0.038	21.4
2018-06-04 11:30	456.66	18.84	475.5	0.148	23.6
2018-06-04 11:45	477.36	19.14	496.5	0.438	27.25
2018-06-04 12:00	498.81	19.69	518.5	0.27	29.72
2018-06-04 12:15	509.64	20.46	530.1	0.215	31.69
2018-06-04 12:30	520.72	21.38	542.1	0.428	31.41
2018-06-04 12:45	526.99	22.21	549.2	1.053	31.51
2018-06-04 13:00	527.19	23.01	550.2	1.709	29.54
2018-06-04 13:15	519.4	23.5	542.9	1.508	29.73
2018-06-04 13:30	503.98	24.52	528.5	1.896	30.06
2018-06-04 13:45	492.58	24.92	517.5	1.584	30.5
2018-06-04 14:00	487.83	25.07	512.9	2.018	30.26
2018-06-04 14:15	474.71	24.89	499.6	1.458	30.37
2018-06-04 14:30	453.2	24.5	477.7	1.17	30.68
2018-06-04 14:45	426.75	23.95	450.7	1.032	30.82
2018-06-04 15:00	400.82	23.08	423.9	1.868	28.98
2018-06-04 15:15	371.62	22.18	393.8	1.665	25.35
2018-06-04 15:30	337.93	21.37	359.3	1.598	20.92
2018-06-04 15:45	301.38	20.62	322	1.567	19.91
2018-06-04 16:00	259.62	20.08	279.7	1.451	20.86
2018-06-04 16:15	206.83	34.97	241.8	1.245	19.62
2018-06-04 16:30	45.1	154.6	199.7	1.529	18.63
2018-06-04 16:45	-0.5	158.3	157.8	1.744	17.9
2018-06-04 17:00	-2	117.9	115.9	1.704	17.19
2018-06-04 17:15	-5.38	81.6	76.22	1.327	16.52
2018-06-04 17:30	-8.71	49.65	40.94	1.455	15.86
2018-06-04 17:45	-7.02	19.46	12.44	0.476	15.32
2018-06-04 18:00	-1.21	1.37	0.16	0.392	14.71

Table C-8: 05 June 2018 measured data

TIMESTAMP	Solar radiation (Beam horizontal) Ib [W/m^2]	Solar radiation (diffuse horizontal) Id [W/m^2]	Solar radiation (total horizontal) Ih [W/m^2]	Wind speed [m/s]	Ambient temperature [`C]
2018-06-05 08:00	1.942	2.28	4.222	1.831	8.62
2018-06-05 08:15	23.83	7.19	31.02	1.931	8.79
2018-06-05 08:30	54.79	9.5	64.29	1.867	9.14
2018-06-05 08:45	90.27	10.83	101.1	1.65	9.55
2018-06-05 09:00	127.87	11.73	139.6	1.321	10.22
2018-06-05 09:15	169.35	12.55	181.9	0.492	11.06
2018-06-05 09:30	210.22	13.18	223.4	0.127	12.42
2018-06-05 09:45	252.04	13.66	265.7	0.378	15.38
2018-06-05 10:00	291.55	14.35	305.9	0.645	15.66
2018-06-05 10:15	329.13	15.27	344.4	1.008	17.37
2018-06-05 10:30	362.1	16.1	378.2	0.742	22.06
2018-06-05 10:45	393	16.7	409.7	0.857	19.68
2018-06-05 11:00	420.58	17.42	438	0.863	22.84
2018-06-05 11:15	443.71	17.99	461.7	0.691	22.39
2018-06-05 11:30	466.11	18.59	484.7	0.708	24.18
2018-06-05 11:45	483.31	18.99	502.3	0.584	28.67
2018-06-05 12:00	499.31	19.49	518.8	0.703	30.06
2018-06-05 12:15	510.96	20.14	531.1	1.148	30.88
2018-06-05 12:30	519.07	21.03	540.1	1.077	31.89
2018-06-05 12:45	523.14	21.86	545	1.156	33.33
2018-06-05 13:00	521.83	22.57	544.4	1.192	34.31
2018-06-05 13:15	517.63	23.27	540.9	1.167	33.83
2018-06-05 13:30	510.99	23.81	534.8	1.204	34.95
2018-06-05 13:45	501.35	24.15	525.5	1.229	35.63
2018-06-05 14:00	488.02	23.88	511.9	0.998	35.87
2018-06-05 14:15	468.13	23.67	491.8	1.15	35.12
2018-06-05 14:30	446.03	23.57	469.6	1.115	35.39
2018-06-05 14:45	422.29	23.01	445.3	1.156	35.59
2018-06-05 15:00	394.6	22.4	417	1.014	34.2
2018-06-05 15:15	364.83	21.57	386.4	1.303	26.14
2018-06-05 15:30	332.01	20.99	353	1.326	23.88
2018-06-05 15:45	295.8	20.5	316.3	1.066	23.24
2018-06-05 16:00	258.52	19.68	278.2	1.244	24.18
2018-06-05 16:15	200.02	37.28	237.3	1.141	23.1
2018-06-05 16:30	38.1	158	196.1	1.568	22.06
2018-06-05 16:45	-2	155.9	153.9	1.163	21.32
2018-06-05 17:00	-2.8	116.5	113.7	1.316	20.65
2018-06-05 17:15	-5.91	80.3	74.39	1.018	19.97
2018-06-05 17:30	-9.23	48.81	39.58	1.006	19.14
2018-06-05 17:45	-6.86	18.87	12.01	1.117	18.2
2018-06-05 18:00	-0.963	1.385	0.422	0.586	17.27

Table C-9: 06 June 2018 measured data

TIMESTAMP	Solar radiation (Beam horizontal) Ib [W/m^2]	Solar radiation (diffuse horizontal) Id [W/m^2]	Solar radiation (total horizontal) Ih [W/m^2]	Wind speed [m/s]	Ambient temperature [`C]
2018-06-06 08:00	1.722	2.231	3.953	2.5	11.8
2018-06-06 08:15	21.224	6.886	28.11	2.423	11.9
2018-06-06 08:30	51.01	9.68	60.69	2.077	12.42
2018-06-06 08:45	85.38	11.12	96.5	2.392	13.09
2018-06-06 09:00	124.34	12.26	136.6	2.6	13.99
2018-06-06 09:15	164.48	13.02	177.5	2.192	14.78
2018-06-06 09:30	207.71	13.59	221.3	2.375	15.88
2018-06-06 09:45	250.49	14.11	264.6	2.448	18.92
2018-06-06 10:00	290.79	14.71	305.5	2.5	19.74
2018-06-06 10:15	330.22	15.58	345.8	3.367	21.27
2018-06-06 10:30	364.88	16.32	381.2	3.3	23.81
2018-06-06 10:45	395.32	17.18	412.5	2.673	22.67
2018-06-06 11:00	423.61	17.69	441.3	3.417	24.72
2018-06-06 11:15	451.01	18.19	469.2	3.223	24.87
2018-06-06 11:30	470.76	18.74	489.5	3.05	26.2
2018-06-06 11:45	485.77	19.13	504.9	3.017	30.33
2018-06-06 12:00	499.82	19.68	519.5	1.998	32.55
2018-06-06 12:15	510.93	20.47	531.4	3.399	32.43
2018-06-06 12:30	518.13	21.47	539.6	3.289	32.2
2018-06-06 12:45	518.42	22.68	541.1	2.685	33.95
2018-06-06 13:00	513.78	23.32	537.1	2.346	36.03
2018-06-06 13:15	507.79	24.31	532.1	1.684	36.96
2018-06-06 13:30	500.21	25.89	526.1	1.666	37.51
2018-06-06 13:45	483.48	28.02	511.5	1.402	37.83
2018-06-06 14:00	472.67	32.33	505	2.521	36.55
2018-06-06 14:15	419.83	34.27	454.1	2.906	33.91
2018-06-06 14:30	317.65	36.55	354.2	1.822	31.66
2018-06-06 14:45	338.85	42.05	380.9	1.384	31.59
2018-06-06 15:00	343.37	52.63	396	1.902	31.9
2018-06-06 15:15	245.04	48.36	293.4	2.006	27.07
2018-06-06 15:30	270.24	48.66	318.9	1.678	26.25
2018-06-06 15:45	268.72	38.38	307.1	1.962	25.87
2018-06-06 16:00	178.79	24.91	203.7	1.275	25.41
2018-06-06 16:15	220.8	46.7	267.5	0.759	25.65
2018-06-06 16:30	85.7	124.6	210.3	1.157	25.04
2018-06-06 16:45	49.5	125.6	175.1	1.098	24.43
2018-06-06 17:00	46	96.8	142.8	0.824	24.03
2018-06-06 17:15	33.38	68.32	101.7	0.941	23.46
2018-06-06 17:30	15.37	19.37	34.74	1.123	22.34
2018-06-06 17:45	2.32	10.57	12.89	1.081	21.35
2018-06-06 18:00	-0.883	1.31	0.427	1.115	20.47

Table C-10: 07 June 2018 measured data

TIMESTAMP	Solar radiation (Beam horizontal) Ib [W/m^2]	Solar radiation (diffuse horizontal) Id [W/m^2]	Solar radiation (total horizontal) Ih [W/m^2]	Wind speed [m/s]	Ambient temperature [`C]
2018-06-07 08:00	4.966	3.224	8.19	3.817	14.9
2018-06-07 08:15	26.94	11.52	38.46	2.193	15.23
2018-06-07 08:30	45.26	12.64	57.9	1.982	15.15
2018-06-07 08:45	89.06	18.34	107.4	2.281	15.22
2018-06-07 09:00	120.36	29.34	149.7	2.148	14.4
2018-06-07 09:15	84.56	22.54	107.1	1.97	15.26
2018-06-07 09:30	126.24	20.36	146.6	2.95	16.66
2018-06-07 09:45	158.33	21.87	180.2	2.892	17.44
2018-06-07 10:00	294.07	32.83	326.9	3.083	18.63
2018-06-07 10:15	234.05	28.85	262.9	3.333	19.29
2018-06-07 10:30	160.34	30.76	191.1	3.623	18.54
2018-06-07 10:45	227.29	43.01	270.3	3.173	19.36
2018-06-07 11:00	226	37	263	3.35	19.65
2018-06-07 11:15	310.47	37.23	347.7	3.189	20.61
2018-06-07 11:30	462.2	31.4	493.6	4.15	23.13
2018-06-07 11:45	489.23	31.47	520.7	4.425	25.85
2018-06-07 12:00	336.78	29.02	365.8	3.15	24.62
2018-06-07 12:15	321.49	37.31	358.8	3.267	23.68
2018-06-07 12:30	223.44	34.66	258.1	2.775	22.3
2018-06-07 12:45	358.29	37.21	395.5	3.267	24.34
2018-06-07 13:00	364.74	50.56	415.3	3.368	24.37
2018-06-07 13:15	406.45	64.55	471	3.142	25.76
2018-06-07 13:30	138.08	49.72	187.8	3.35	21.24
2018-06-07 13:45	160.08	52.02	212.1	2.9	20.7
2018-06-07 14:00	102.49	42.71	145.2	2.617	20.02
2018-06-07 14:15	115.92	38.48	154.4	2.589	19.73
2018-06-07 14:30	112.87	36.03	148.9	2.606	19.7
2018-06-07 14:45	213.5	47.8	261.3	3.025	20.91
2018-06-07 15:00	319.87	50.93	370.8	3.542	24.37
2018-06-07 15:15	232.83	28.77	261.6	2.249	22.11
2018-06-07 15:30	134.18	20.92	155.1	2.358	21.06
2018-06-07 15:45	90.14	22.76	112.9	2.358	19.91
2018-06-07 16:00	87.96	24.14	112.1	2.758	19.34
2018-06-07 16:15	85.55	26.85	112.4	2.883	19.14
2018-06-07 16:30	68.99	17.51	86.5	2.487	18.92
2018-06-07 16:45	57.63	12.81	70.44	2.253	18.61
2018-06-07 17:00	21.091	5.339	26.43	2.098	18.21
2018-06-07 17:15	12.095	3.765	15.86	2.121	17.91
2018-06-07 17:30	7.723	2.497	10.22	1.93	17.73
2018-06-07 17:45	2.795	1.042	3.837	2.287	17.58
2018-06-07 18:00	0.46	0.419	0.879	1.831	17.42

Table C-11: Measured distillate yields and temperatures

29-May-18																				
	Ground-mouned still				Purifier one				Purifier two				Purifier three				Purifier four			
Local time	Yield (ml)	Temp (°C)			Yield (ml)	Temp (°C)			Yield (ml)	Temp (°C)			Yield (ml)	Temp (°C)			Yield (ml)	Temp (°C)		
		Water	Glass	Steam		Water	Glass	Steam		Water	Glass	Steam		Water	Glass	Steam		Water	Glass	Steam
8																				
9																				
10																				
11	160	27.4	32.8	27.4	250	28	33.4	28	209	31.5	33	28	210	32	35	29	250	29	34.4	29
12	280	29.45	34.85	29.45	450	30.25	35.65	30.25	370	33.75	35.25	30.25	375	34.25	37.25	31.25	460	31.25	36.65	31.25
13	650	39.87	45.27	39.87	1025	41.17	46.57	41.17	850	44.67	46.17	41.17	860	45.17	48.17	42.17	1050	42.17	47.57	42.17
14	870	32.2	37.2	29.2	1375	33	38	30	1140	37	40	33.5	1160	43.51	46.51	40.51	1410	34	39	31
15	1030	30.24	35.24	27.24	1625	31.34	36.34	28.34	1340	35.34	38.34	31.84	1360	39	44	35.2	1660	32.34	37.34	29.34
16	1160	29.99	34.99	26.99	1830	31.09	36.09	28.09	1520	35.09	38.09	31.59	1540	34.18	39.18	30.38	1875	32.09	37.09	29.09
17	1230	28	30	28.9	1940	30.2	32	29	1610	31	33	29	1630	32	34	30	1990	31.2	33	30
30-May-18																				
8	10	21	20	18	20	21.66	20.86	18.86	15	29.86	24.66	20.76	15	23.05	16.25	15.75	20	22.56	21.66	19.66
9	30	23.9	20.9	18.9	50	24.8	21.8	19.8	50	30.8	25.6	21.7	60	23.99	17.19	16.69	60	25.6	22.6	20.6
10	60	27.79	24.79	22.79	95	28.19	25.19	23.19	105	34.19	28.99	25.09	110	27.38	20.58	20.08	125	28.79	25.79	23.79
11	110	32.4	29.4	27.4	190	33	30	28	156	39	33.8	29.9	160	37	30.2	29.7	190	34	31	29
12	200	29.61	26.61	24.61	340	30.41	27.41	25.41	280	36.41	31.21	27.31	280	34.41	27.61	27.11	340	31.41	28.41	26.41
13	460	32.55	29.55	27.55	770	33.85	30.85	28.85	640	39.85	34.65	30.75	640	37.85	31.05	30.55	790	34.85	31.85	29.85
14	620	33.2	27.2	24.5	900	34	28	25.3	850	29.5	31	27.4	860	36.82	30.02	29.52	1060	35	29	26.3
15	730	31.87	25.87	23.17	1210	32.97	26.97	24.27	1000	28.47	29.97	26.37	1010	29	28.8	29	1250	33.97	27.97	25.27
16	820	32.97	26.97	24.27	1375	34.07	28.07	25.37	1130	29.57	31.07	27.47	1140	29.17	28.97	29.17	1400	35.07	29.07	26.37
17	870	19.2	19	17	1450	23	19	20	1200	20	19	17	1210	25	21	22	1490	24	20	21
31-May-18																				
8	5	20	19.2	17.7	12	20.86	20.06	18.56	10	20.96	26.06	24.16	10	25.48	21.98	21.58	10	21.76	20.86	19.36
9	45	18.09	19.09	17.59	60	18.99	19.99	18.49	50	20.89	25.99	24.09	55	25.41	21.91	21.51	60	20.79	20.79	19.29
10	105	19.02	20.02	18.52	140	19.42	20.42	18.92	110	21.32	26.42	24.52	120	25.84	22.34	21.94	140	20.02	21.02	19.52
11	170	19.4	20.4	18.9	220	20	21	19.5	190	21.9	27	25.1	200	27	23.5	23.1	230	21	22	20.5
12	255	26.55	20.96	19.46	325	20.76	21.76	20.26	280	22.66	27.76	25.86	290	27.76	24.26	23.86	340	21.76	22.76	21.26
13	385	31.55	23.25	21.75	490	31.5	24.55	23.05	410	35.25	30.55	28.65	410	36.12	27.05	26.65	510	33.55	32.55	24.05
14	530	33.5	24.2	22.2	680	34	25	23	560	37.25	30.5	27.2	560	40	28.3	24.7	690	35.23	26	24
15	595	26.95	21.95	19.95	800	28.05	23.05	21.05	635	30.05	28.55	25.25	640	31	25.1	28.3	780	29.05	24.05	22.05
16	645	24.04	19.04	17.04	860	25.14	20.14	18.14	690	27.14	25.64	22.34	690	27.5	21.82	25.02	850	26.14	21.14	19.14
17	680	16.5	22.3	20.7	900	18.5	20	19.2	730	19.8	21.3	23.8	730	20	21	24	900	19.5	21	20.2
01-Jun-18																				
8	20	22.88	22.08	20	10	23.78	22.98	20.88	5	24.88	27.28	21.58	5	25.76	24.06	23.36	10	24.68	23.78	21.68
9	55	21.36	23.36	21.26	25	22.26	24.26	22.16	20	26.16	28.56	22.86	40	27.04	25.34	24.64	25	23.06	25.06	22.96
10	120	25.38	27.38	25.28	190	25.78	27.78	25.68	50	29.68	32.08	26.38	50	30.56	28.86	28.16	60	26.38	28.38	26.28
11	230	25.4	27.4	25.3	390	26	28	25.9	325	29.9	32.3	26.6	330	31	29.3	28.6	400	27	29	26.9
12	420	31.77	33.77	31.67	690	32.57	34.57	32.47	575	36.47	38.87	33.17	580	37.57	35.87	35.17	710	33.57	35.57	33.47
13	965	34.07	36.07	33.97	1590	35.37	37.37	35.27	1325	39.27	41.67	35.97	1340	40.37	38.67	37.97	1625	36.37	38.37	36.27
14	1290	35	32.2	31.6	2130	37	33	32.4	1775	46	49.5	41.1	1780	49	49.6	37.47	2190	36	34	33.4
15	1520	31	31.4	30.8	2500	35.6	32.5	31.9	2090	45.5	49	40.6	2100	39.87	38.2	46.9	2575	38.9	33.5	32.9
16	1720	24.33	24.59	23.99	2840	25.68	25.69	25.09	2360	38.69	42.19	33.79	2380	38.55	28.69	37.39	2910	33.88	26.69	26.09
17	1820	31	33.5	25.5	3000	20.1	25	23	2500	26	30.4	24.5	2520	29	31.2	26.6	3075	21.1	26	24
02-Jun-18																				
8	10	23.02	22.22	22	30	23.92	23.12	22.42	25	33.76	36.28	27.58	25	27.96	31.96	29.86	30	24.82	23.92	23.22
9	25	22.88	22.48	21.78	90	23.78	23.38	22.68	75	35.84	37.84	29.14	20	28.22	32.22	30.12	90	24.58	24.18	23.48
10	50	24.92	24.52	23.82	90	25.32	24.92	24.22	160	38.92	40.92	32.22	160	32.84	36.84	34.74	200	25.92	25.52	24.82
11	105	27.8	27.4	26.7	175	28.4	28	27.3	148	42	44	35.3	150	39	43	40.9	190	29.4	29	28.3
12	190	27.58	27.18	26.48	310	28.38	27.98	27.28	262	41.98	43.98	35.28	280	38.98	42.98	40.88	325	29.38	28.98	28.28
13	440	30.8	27.26	26.56	725	32.5	28.56	27.86	600	42.56	44.56	35.86	615	39.56	43.56	41.46	750	31.55	29.56	28.86
14	560	29.55	28.2	27	975	30	29	27.8	810	50	43.6	35.8	820	36	45.7	38	1000	31	30	28.8
15	700	28.49	31.09	29.89	1150	29.59	32.19	30.99	950	43	46.79	38.99	970	42.75	46.75	44.65	1175	30.59	33.19	31.99
16	780	24.1	26.7	25.5	1300	25.2	27.8	26.6	1080	38.61	42.4	34.6	1100	37.65	41.65	39.55	1320	26.2	28.8	27.6
17	830	21	24.3	22.9	1375	23	19	21.3	1140	20	20.9	22.8	1160	24	20.8	21.3	1400	24	20	22.3
03-Jun-18																				
8	10	25.82	25.02	22.02	25	26.72	25.92	22.92	25	23.68	23.58	21.98	20	24.27	27.57	24.47	25	27.62	26.72	23.72
9	60	27.32	26.32	23.32	120	28.22	27.22	24.22	95	32.72	37.22	29.92	100	25.57	28.87	25.77	125	29.02	28.02	25.02
10	140	30.95	29.95	26.95	225	31.35	30.35	27.35	190	35.85	40.35	33.05	200	28.7	32	28.9	240	31.95	30.95	27.95
11	250	34.4	33.4	30.4	425	35	34	31	355	39.5	44	36.7	370	36	39.3	36.2	440	36	35	32
12	440	36.18	35.18	32.18	760	36.98	35.98	32.98	635	41.48	45.98	38.68	650	37.98	41.28	38.18	790	37.98	36.98	33.98
13	780	38.65	37.65	34.65	1450	39.95	38.95	35	1190	44.45	48.95	41.65	1210	40.95	44.25	41.15	1475	40.95	39.95	36.95
14	1340	47.2	37.6	34.2	2410	48	38.4	35	1980	49.9	54.9	45.8	2000	50	54	49.2	2440	49	39.4	36
15	1570	44.99	35.39	31.99	2690	46.09	36.49	33.09	2230	47.99	52.99	43.89	2250	39	42.3	39.2	2740	47.09	37.49	34.09
16	1770	39.83	30.23	26.83	2960	40.93	31.33	27.93	2460	42.83	47.83	38.73	2480	35	35	31.33	3025	41.93	32.33	28.93
17	1870	30	32.7	29.9	3125	21.1	22	23.8	2600	31.5	33	28.6	2620	32	36.7	32.3	3200	22.1	23	24.8
04-Jun-18																				
8	20	31.32	30.15	29.6	30	32.22	31.05	30.5	25	23.68	23.58	21.98	25	19.28	30.58	24.48	30	30.5	27	23.25
9	70	28.42	37.92	32.92	90	29.32	38.82	33.82	80	34.88	34.78	33.18	35	27.28	38.58	32.48	100	30.12	39.62	34.62
10	150	34.36	43.86	38.86	225	34.76	44.26	39.26	170	45.76	45.66	44.06	170	32.72	44.02	37.92	210	35.36	44.86	39.86
11	290	39.9	49.4	44.4	450	40.5	50	45	376	51.5	51.4	49.8	380	44.2	55.5	49.4	470	41.5	51	46
12	520	48.02	57.52	52.52	800	48.82	58.32	53.32	665	59.82	59.72	58.12	670	52.52	63.82	57.72	810	49.82	59.32	54.32
13	1120	47.34	56.84	51.84	1840	48.64	58.14	53.14	1530	59.64	59.54	57.94	1550	52.34	63.64	57.54	1890	49.64	59.14	54.14
14	1605	51.2	52.2	47.2	2460	52	53	48	2050	60	53.6	48.3	2070	55	62.36	56.26	2525	53	54	49
15	1890	49.62	50.62	45.62	2900	50.72	51.72	46.72	2410	52	52.32	47.02	2440	51	57.8	49.6	2975	51.72	52.72	47.72
16	2140	41.5	42.5	37.5	3290	42.6	43.6	38.6	2730	43.88	44.2	38.9	2780	39.21	46.01	37.81	3350	43.6	44.6	39.6
17	2260	22.5	31.9	24.4	3475	19.9	18.8	17.5	2890	19	18.7	17.8	2920	20	21	20.3	3550	20.9	19.8	18.5

05-Jun-18																				
8	10	25.82	25.02	22.02	30	17.22	16.42	21.42	30	26.64	26.14	21.54	30	26.76	28.46	13.96	40	25.55	24	20.65
9	60	27.32	26.32	23.32	100	31.02	18.02	23.02	90	37.84	37.34	32.74	80	34.76	36.46	21.96	110	31.82	18.82	23.82
10	140	30.95	29.95	26.95	190	36.46	23.46	28.46	190	48.72	48.22	43.62	190	45.64	47.34	32.84	230	37.06	24.06	29.06
11	250	34.4	33.4	30.4	390	58	45	50	326	55.9	55.4	50.8	330	60	61.7	47.2	400	59	46	51
12	440	36.18	35.18	32.18	690	65.22	52.22	57.22	577	63.12	45.56	27.96	580	67.22	68.92	54.42	700	66.22	53.22	58.22
13	780	38.65	37.65	34.65	1590	69.47	56.47	61.47	1330	67.37	49.81	36.46	1340	71.47	73.17	58.67	1625	70.47	57.47	62.47
14	1340	47.2	37.6	34.2	2125	71	60	50	1780	69	62.1	50.3	1790	73	71.5	57	2170	71.9	60	51
15	1570	44.99	35.39	31.99	2510	58.33	57.33	48.33	2100	59.33	60.43	48.63	2100	62	62.4	52.8	2560	59.33	58.33	49.33
16	1770	39.83	30.23	26.83	2840	48.31	47.31	38.31	2370	49.31	50.41	38.61	2380	48.45	48.85	39.25	2900	49.31	48.31	39.31
17	1870	30	32.7	29.9	3000	30	33	31	2510	32.5	34.5	29.2	2520	39	38.9	36.4	3060	31	34	32
06-Jun-18																				
8	15	26.02	25.22	22.22	25	26.92	26.12	23.12	25	20.19	22.79	14.39	25	19.59	23.39	17.29	30	27.82	26.92	23.92
9	50	28.41	27.41	24.41	90	29.31	28.31	25.31	75	35.52	38.12	29.72	90	30.54	34.34	28.24	90	30.11	29.11	26.11
10	110	34.66	33.66	30.66	175	35.06	34.06	31.06	160	47.02	49.62	41.22	160	42.04	45.84	39.74	200	35.66	34.66	31.66
11	215	49.4	48.4	45.4	350	50	49	46	298	52	54.6	46.2	300	52	55.8	49.7	260	51	50	47
12	380	57.03	56.03	53.03	630	57.83	56.83	53.83	527	59.83	62.43	54.03	530	59.83	63.63	57.53	650	58.83	57.83	54.83
13	880	60.01	59.01	56.01	1460	61.31	60.31	57.31	1210	63.31	65.91	57.51	1220	63.31	67.11	61.01	1490	62.31	61.31	58.31
14	1180	65.8	49.2	42.2	1950	66	50	43	1630	67	50.9	44.5	1640	69	62.46	56.36	2000	67.88	51	44
15	1340	40.25	44.25	37.25	2300	41.35	45.35	38.35	1910	41	46.25	39.85	1930	49	48.9	46.6	2350	42.35	46.35	39.35
16	1570	33.76	37.76	30.76	2600	34.86	38.86	31.86	2160	34.51	39.76	33.36	2180	41.13	41.03	38.73	2660	35.86	39.86	32.86
17	1660	26	27.5	26.6	2750	30	27.5	26	2290	30	27	26	2310	32	28.2	27.6	2810	31	28.5	27
07-Jun-18																				
8	10	26.5	28.45	25.35	25	27	29.35	26.25	20	27.92	28.92	25.02	20	28.53	28.53	25.33	25	30.2	30.15	27.05
9	20	27.85	27.95	24.85	90	28.75	28.85	25.75	70	24.42	25.42	21.52	80	28.03	28.03	24.83	90	29.55	29.65	26.55
10	50	32.58	32.68	29.58	60	32.98	33.08	29.98	150	32.88	33.88	29.98	150	32.26	32.26	29.06	190	33.58	33.68	30.58
11	105	33.4	33.5	30.4	140	34	34.1	31	116	33.9	34.9	31	120	34.3	34.3	31.1	140	35	35.1	32
12	190	38.17	38.27	35.17	250	38.97	39.07	35.97	205	38.87	39.87	35.97	210	39.27	39.27	36.07	250	39.97	40.07	36.97
13	430	37.42	37.52	34.42	575	38.72	38.82	35.72	480	38.62	39.62	35.72	580	39.02	39.02	35.82	200	39.72	39.82	36.72
14	575	29.2	26.2	25.2	760	30	27	26	630	28	27.6	26.2	640	29	25.8	26.1	760	31	28	27
15	680	33.25	30.25	29.25	8975	34.35	31.35	30.35	740	30.25	31.95	30.55	750	43.37	43.37	40.17	900	35.35	32.35	31.35
16	765	28.22	25.22	24.22	1010	29.32	26.32	25.32	840	25.22	26.92	25.52	850	28	25	19.94	1010	30.32	27.32	26.32
17	810	26	27	27.9	1075	27	28	28.5	890	24	27.1	25.9	900	26.2	24.8	25.9	1075	28	29	29.5